

Distributed Control of Battery Energy Storage Systems for Voltage Support in PV Rich Low-Voltage Distribution Network

Master Thesis

Bagas Ihsan Priambodo

Distributed Control of Battery Energy Storage Systems for Voltage Support in PV Rich Low-Voltage Distribution Network

by

Bagas Ihsan Priambodo

to obtain the degree of Master of Science
at the Delft University of Technology,
to be defended publicly on Wednesday August 23, 2023 at 09:00 AM.

Student number: 5628903
Project duration: January 23, 2023 – August 23, 2023
Thesis committee: Prof. Dr. ir. Pavol Bauer, DCE&S
Dr. ir. Laura Ramirez Elizondo, DCE&S (Main supervisor)
Dr. Mohamad Ghaffarian Niasar, HVDC
Daily Supervisor: Joel Alpizar Castillo, DCE&S

Cover: Image by Mrillustration from Pixabay

An electronic version of this thesis is available at <http://repository.tudelft.nl/>.

Preface

As renewable energy technologies become more popular, there is a noticeable shift toward distributed and environmentally-friendly power systems. One of the main challenges of this change is controlling the voltage distribution networks. This master thesis explores voltage control in low-voltage distribution networks using battery energy storage systems. It was written as part of the graduation requirement at TU Delft and is aimed towards academics as well as practitioners in the domain of power systems, renewable energy integration, and controls alike.

The chapters in this report can be read in full or as stand-alone, should the reader have prior knowledge of voltage regulation techniques, especially in low voltage distribution networks. Readers interested in the current state of voltage control technology can refer to Chapter 2. To understand the method and model used in this work, readers can consult Chapter 4. The important findings of this work can be found in Chapter 5. Finally, the conclusion and recommendations for future works can be found in Chapter 6.

I would like to thank my main thesis supervisor, Dr. ir. Laura Ramirez Elizondo for the opportunity to work under her guidance. Her feedback is valuable in shaping me as a better researcher. I would also like to thank Joel Alpizar Castillo for the extraordinary day-to-day advice throughout this whole master thesis creation. I am really thankful for the kind and timely responses he gave me despite his busy schedule working towards his PhD. I would also like to thank the committee members, Prof. Dr. ir. Pavol Bauer and Dr. Mohamad Ghaffarian Niasar, for agreeing to participate, as well as provide critical feedback to this work. To my family and friends, thank you for standing by my side throughout this academic journey. Your unwavering belief in me has been a source of motivation and strength.

I hope this thesis inspires further research in voltage control and battery energy storage systems integration. May its findings contribute to the collective pursuit of a sustainable energy future.

*Bagas Ihsan Priambodo
Delft, August 2023*

Abstract

As demand for clean and renewable energy around the world increases, solar photovoltaic (PV) technology becomes substantially popular, especially in low-voltage (LV) distribution networks. The integration of PV in LV distribution networks, however, requires careful planning as it introduces voltage violations. To maintain network voltage, distributed control of residential-scale battery energy storage systems (BESS) is a possible option. Previous studies considered only one-day simulations with limited testing conditions. However, it is important to evaluate voltage control capability over an extended period of time. Moreover, it is important to estimate battery lifetime for the economic feasibility evaluation of distributed control.

This work aims to present a distributed control method for BESSs at a residential scale to provide voltage support in a highly PV-penetrated LV network while providing insights into their lifetime estimation. A control method based on a consensus algorithm with the addition of SOC balancing control is proposed and tested on a modified CIGRE LV distribution network using MATLAB/Simulink. Evaluations on the voltage support capability and control behavior are performed in various testing conditions and are extended beyond one day of simulation. Moreover, a battery lifetime estimation is performed using the resulting cycling profile from the proposed control.

The proposed control strategy can provide voltage support in most case variations with the exception of cold seasons and extreme addition of PV power generation. Concerning battery lifetime, there is only a small observable capacity fade from the proposed strategy's cycling profile. It is important to investigate calendar aging as well because of the small cycling current from the operating conditions presented in this work.

Contents

Preface	i
Abstract	ii
Nomenclature	viii
1 Introduction	1
2 Literature Study	4
2.1 Undervoltage and Overvoltage In Distribution Networks	4
2.1.1 Mechanism	4
2.1.2 Voltage Limitation Standard	6
2.1.3 Impact of Over/Undervoltage	6
2.2 Techniques for Voltage Support	6
2.2.1 On-Load Tap-Changing Transformers	6
2.2.2 Smart Transformers	7
2.2.3 Reactive Power Control	7
2.2.4 Distributed Generation Curtailment	8
2.2.5 Active Power Control: Battery Energy Storage Systems	8
2.3 Lithium-Ion Battery Degradation	12
2.3.1 Components of Lithium-Ion Battery	12
2.3.2 Battery Degradation Mechanism and Influencing Factors	13
2.3.3 Battery Degradation Model	14
3 Coordinated Control of Multiple Distributed BESSs	16
3.1 Information Consensus	16
3.1.1 Multi-Agent System and Graph Theory	16
3.1.2 Degree Matrix, Adjacency Matrix, Laplacian Matrix	17
3.1.3 Consensus Algorithm	17
3.2 Control Algorithm for Voltage Support	19
3.2.1 Local Voltage Controller	20
3.2.2 Consensus Controller	21
3.2.3 SOC Controller	21
4 Simulation Setup of Low Voltage Distribution Network	23
4.1 Voltage Control Strategy Evaluation Method	23
4.2 CIGRE LV Distribution Test Feeder Specification	23
4.2.1 MV Grid and Transformer Specification	24
4.2.2 Line Specification	24
4.2.3 Battery Energy Storage Units Specification	24
4.2.4 Controller Parameter	25
4.3 Power Profile	25
4.3.1 Synthetic Demand Profile	25
4.3.2 PV Power Profile	26
4.3.3 Mismatch Profile	27
4.4 LV Network Model MATLAB/Simulink	27
4.5 Communication Network	28
4.6 Battery Lifetime Evaluation Model	28
5 Simulation results and discussion	31
5.1 Voltage behavior and BESS participation	31
5.1.1 Base Case	31

5.1.2	BESS Under Varying initial SOC	34
5.1.3	BESS Under Seasonal Change	36
5.1.4	BESS Under Varying PV Penetration	38
5.2	Battery Lifetime Estimation	40
5.3	Results Summary	42
6	Conclusion	43
6.1	Future Works	44
	References	45
A	Utilization Factor Calculation	51
B	Simulation Parameters	55
C	Cell Specification	56

List of Figures

1.1	Net renewable electricity capacity additions by technology, historical, main and accelerated cases.	1
1.2	EU capacity additions in 2023-2024 (left) and average household electricity prices for selected capital cities (right).	2
2.1	Line diagram and circuit representation of a radial feeder bus.	4
2.2	Schematic of an On-load tap-changing transformer.	7
2.3	Effect of PV with curtailment and without curtailment on (a) Feed-in power (b) Voltage.	8
2.4	Lithium-ion battery price outlook from 2010 to 2018 with prediction until 2030 in terms of real price with respect to the year 2018.	9
2.5	Schematic of decentralized control.	10
2.6	Schematic of centralized control.	10
2.7	Schematic of distributed control.	11
2.8	Schematic of a lithium-ion battery.	13
3.1	Multi-agent system with four agents.	16
3.2	five-agent system with a line configuration.	18
3.3	Convergence of a five-agent system: (a) $\epsilon = 0.125$ and (b) $\epsilon = 0.25$	19
3.4	Proposed coordinated control strategy for the i^{th} bus.	20
4.1	General overview of information flow and simulation sequence.	24
4.2	Single line diagram of the modified CIGRE LV distribution network.	25
4.3	Demand profile for a small apartment building containing four households: (a) Day profile and (b) Week profile.	26
4.4	Irradiance profile in Delft during mid-July 2005: (a) Day profile and (b) Week profile.	26
4.5	One-day mismatch profile taken from the 15 th day of July 2005.	27
4.6	One-week mismatch profiles of two different seasons: (a) Summer (mid-July) and (b) Winter (mid-January).	27
4.7	Simulink model segment of the modified CIGRE LV network	28
4.8	Communication network of the modified CIGRE LV distribution network	29
4.9	Synthetic regular cycling profile based on worst operating conditions of BESSs	30
5.1	One-day voltage profiles of the buses in the modified CIGRE LV network: (a) Without BESS and (b) With BESS and proposed control.	32
5.2	Utilization factor of the BESSs in the modified CIGRE LV network.	32
5.3	Seven-day bus voltage profiles in the modified CIGRE LV network: (a) Using proposed control and (b) Using decentralized control only.	33
5.4	Seven-day SOC profiles in the modified CIGRE LV network: (a) Using proposed control and (b) Using decentralized control only.	34
5.5	Proposed control under slight initial SOC difference - Variation A: (a) Voltage, (b) Power, and (c) SOC profiles.	35
5.6	Proposed control under extreme initial SOC difference (variation B): (a) Voltage, (b) Power, and (c) SOC profiles.	36
5.7	Proposed control in winter period: (a) Voltage, (b) Power, and (c) SOC profiles.	37
5.8	Proposed control in autumn period: (a) Voltage, (b) Power, and (c) SOC profiles.	38
5.9	Proposed control with +10% PV w.r.t base case: (a) Voltage, (b) Power, and (c) SOC profiles.	39
5.10	Proposed control with +25% PV w.r.t base case: (a) Voltage, (b) Power, and (c) SOC profiles.	40

5.11	Maximum battery capacity in Ah (one-year simulation).	41
5.12	Battery current in C-rate (one-week simulation)	41
5.13	Number of equivalent cycles (one-year simulation).	42
A.1	Overview of the distributed control in Simulink.	52
A.2	Simulink block diagram of the local utilization factor computation.	53
A.3	Simulink block diagram of the final utilization factor computation inside the SOC controller.	54

List of Tables

2.1	Summary of distributed control for voltage support	12
3.1	Initial states of agents	19
3.2	Notation description for Equations (3.6) and (3.7)	21
3.3	Notation description for Equation (3.9).	22
4.1	Summary of case studies used to evaluate the proposed control strategy.	24
4.2	BESS specification: system level	25
4.3	Voltage controller parameters.	25
4.4	Notation summary of Equation (4.1) through (4.4)	29
4.5	Synthetic cycling profile parameters for battery lifetime estimation	30
5.1	Initial SOC of the BESSs	34
5.2	Key points of simulation results.	42
B.1	Transformer specification of the modified CIGRE LV test feeder.	55
B.2	Line parameter of the modified CIGRE LV Network.	55

Nomenclature

Abbreviations

Abbreviation	Definition
ANSI	American National Standards Institute
BESS	Battery energy storage systems
CIGRE	The International Council on Large Electric Systems
DOD	Depth of discharge
DSO	Distributed system operators
GIS	Global information system
IEEE	Institute of Electrical and Electronics Engineers
LFP	Lithium-Iron-Phosphate
LV	Low-voltage
MAS	Multi-agent system
MV	Medium-voltage
OLTC	On-load tap changer
PCC	Point of common coupling
PF	Power Factor
PV	Photo-voltaic
SEI	solid electrolyte interphase
SOC	State of charge
ST	Smart transformers
SST	Solid-state transformers

Symbols and Notations

Symbol	Definition	Unit
a	Elements of adjacency matrix	[-]
A	Adjacency matrix	[-]
d	Elements of degree matrix D	[-]
D	Degree matrix	[-]
E	Set of edges	[-]
G	Graph	[-]
\bar{I}_n	Current at bus n	[A]
L	Laplacian matrix	[-]
P_{net}	Net active power	[W]
$P_{\text{net},i}$	Net active power at bus i	[W]
$P_{\text{bat, rated}}$	Rated BESS power	[W]
$P_{\text{lim, pos}}$	Positive net power limit	[W]
$P_{\text{lim, neg}}$	Negative net power limit	[W]
P_{PV}	Active power injected from PV generation	[W]
P_{PV}	Active power drawn by load	[W]
Q_n	Reactive power at bus n	[W]
R	Line resistance	[Ω]
\bar{S}_n	Apparent power at bus n	[W]
$SOC_{\text{ESS},i}$	SOC of BESS i	[%]
$SOC_{\text{lim, charge}}$	SOC charging limit	[%]

Symbol	Definition	Unit
$SOC_{lim, discharge}$	SOC discharging limit	[%]
\bar{V}_G	Grid voltage	[V]
\bar{V}_n	Voltage at bus n	[V]
$\Delta\bar{V}_G$	Voltage deviation along a feeder line	[V]
X	Line reactance	[Ω]
U_i	Utilization factor of node i at time instance t	[-]
$U_{add,i}(t)$	Additional utilization factor	[-]
$U_{cons,i}(k)$	Estimated consensus utilization ratio at bus i and step k	[-]
$U_{final,i}(k)$	Final utilization factor of node i	[-]
\bar{Z}	Impedance	[Ω]
ϵ	Consensus step size	[-]

1

Introduction

As the demand for clean and renewable energy around the world increases, the use of solar photovoltaic (PV) technology becomes substantially popular. In 2022, the global added capacity of PV was nearly 220 GW; a record-breaking increase of 35% with respect to its previous year [1]. Moreover, PV dominates the global addition of renewable energy as shown in Figure 1.1, where the combination of distributed and utility PV takes up the largest portion of the bar graph compared to other technologies.

Global annual growth of the PV market is expected to continue in 2023 and into 2024 [1]. This growth will be driven by lower module prices, greater distributed PV system uptake (i.e., residential and commercial installations in low-voltage (LV) distribution networks) and a policy push for large-scale deployment in all major markets including China, the European Union, the United States and India [1]. In Europe, the policy push was driven by the immediate need for diversification from imported fossil fuel after Russia's recent invasion of Ukraine [1]. Following this event, Governments of European countries sought options to rapidly increase renewables in their energy mix, which can be offered by distributed PV systems. Additionally, the global increase in wholesale and retail energy prices since the invasion (Figure 1.2) has made distributed PV systems become economically attractive for customers [1].

The integration of PV in LV distribution networks, however, requires careful planning as their non-dispatchable nature creates uncertainty [2]. When only one user generates electrical energy from this source, this uncertainty would be insignificant. But, when the number of users multiplies, the associated uncertainty is going to add up and impact the grid. Some notable impacts include power fluctuation, voltage instability, and frequency deviation [3], [4], [5]. Failure to mitigate these impacts may congest

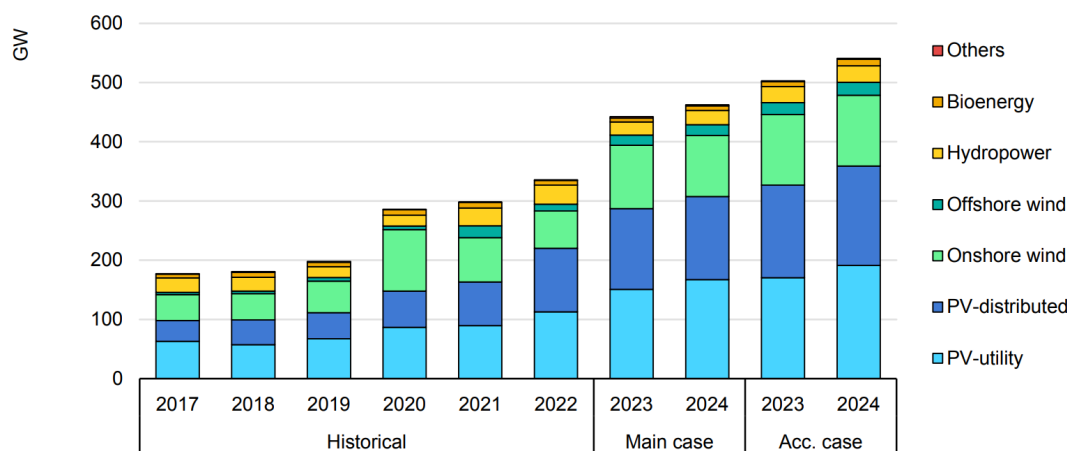


Figure 1.1: Net renewable electricity capacity additions by technology, historical, main and accelerated cases. Source: [1].

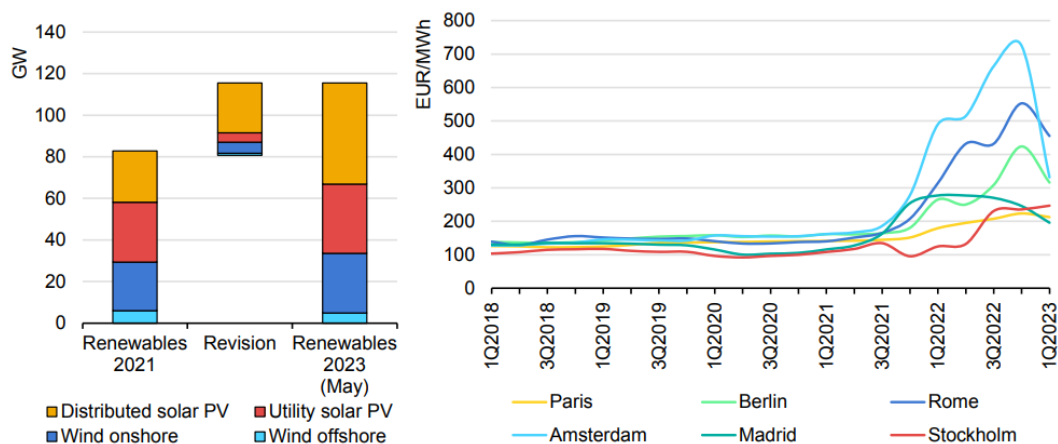


Figure 1.2: EU capacity additions in 2023-2024 (left) and average household electricity prices for selected capital cities (right). Source: [1].

distribution lines and is detrimental to grid users as their grid-connected appliances are operated outside of their specifications.

Among various impacts introduced by the integration of PV in LV distribution networks, voltage fluctuation is one of the most common, and therefore many solutions have been sought to mitigate it. The on-load tap changing (OLTC) transformer, for example, allows a low-voltage distribution network to regulate its voltage by changing the turn ratio at the transformer. This approach, however, is slow as changing the turns ratio is done mechanically and ineffective for solving voltage problems at end nodes due to its limited tap positions [6], [7], [8]. Another alternative is by injecting reactive power through the PV's inverter. This solution has a high response characteristic but is not efficient on low voltage distribution networks as voltage in these networks is less sensitive to reactive power compared to active power [9]. An option to regulate voltage using active power compensation can be done using residential-scale battery energy storage systems (BESS), which are typically installed with solar PVs. This type of solution is characterized by its fast response and high-power operation capability. Furthermore, the use of residential-scale BESSs opens the possibility for customers to participate in services aside from voltage support such as frequency regulation, peak shaving, and energy arbitrage, to name a few [10].

One challenge in utilizing residential scale BESSs to achieve network-wide voltage objectives is finding the optimal mechanism to control them. The literature generally mentions three types of control, namely decentralized, centralized, and distributed control, each with its advantages and drawbacks. In decentralized control, the monitoring and control of each BESS' charging and discharging actions are performed locally [11]. This type of control is simple but may not provide an optimal solution because batteries spread across the network work independently. In centralized control, BESSs at different locations of a network cooperate to solve voltage fluctuation under a central management system. It is generally superior to the decentralized method as the central controller can search for an alternative unit in case of a BESS being unavailable [11]. However, they require fast and uninterrupted communication [10], [12]. In distributed control, intelligent electronic devices cooperate to reach a collective decision according to the goals that have been set (e.g., voltage limits) [13]. This principle is similar to centralized control where BESSs work together, but they only have to communicate with their nearest neighbors. This allows the need for fast communication between the central management system and the BESSs to be eliminated.

Works regarding the formulation of a distributed control for voltage support have been presented in [12], [14], [15], and [16]. In addition to formulating distributed control strategies, these works evaluated the capability of the strategies in supporting network voltage by testing them under varying conditions. However, they do not provide information on the BESS and controller's performance beyond one day of simulation. Moreover, battery lifetime from the resulting cycling profile has not been investigated.

Understanding the lifetime characteristic is important to evaluate the economic feasibility of using distributed control principle.

This work aims to present a distributed control method for BESSs at a residential scale in a highly PV-penetrated LV network while providing insights into the lifetime of the batteries when using this type of control. Based on this objective, a main research question is then formulated as follows:

How can residential-scale BESSs be controlled in a distributed manner to regulate voltage in a low-voltage distribution network under high PV penetration while evaluating their battery lifetime profile?

The main research questions can be broken down into the following sub-questions:

1. **How is the voltage behavior of an LV network under high PV penetration?**
2. **How does the proposed distributed BESS control strategy affect the voltage performance of an LV network?**
3. **How is the control behavior of the proposed strategy when performing voltage support?**
4. **How does the proposed control strategy affect battery lifetime?**

To answer the research questions, a literature review is first performed to understand the voltage behavior of LV distribution networks as well as state-of-the-art voltage support techniques. Afterward, an LV distribution network under high PV penetration is modeled and simulated in MATLAB/Simulink. A proposed BESS control method is then added to the model to see how it can mitigate voltage violation. Using the battery SOC profile obtained from the control simulation, a battery lifetime estimation is then performed.

The distributed control of BESSs for voltage control is not an entirely novel discussion. However, this work differs from other work through the following contributions:

1. **A distributed control strategy aimed at voltage support for an extended period.**
2. **An insight into the network voltage behavior when using the proposed strategy.**
3. **An insight into the BESSs' voltage support capability under variations of PV generation, initial BESS SOC, and seasons when using the proposed strategy.**
4. **BESS cycling profile at an extended period and lifetime estimation when using distributed control strategy.**

Following this introduction, this work presents 5 chapters and is structured as follows: Firstly, some theoretical background on voltage mitigation in low voltage networks and state-of-the-art technologies are reviewed in Chapter 2. Afterward, Chapter 3 discusses the control strategy proposed along with detailed formulas used in achieving voltage support. In Chapter 4, the models and simulation method used to evaluate the proposed strategy in terms of voltage performance and implication on battery lifetime are discussed. Chapter 4 presents the results and discussions of the simulations described in the preceding chapter. Finally, Chapter 6 concludes this work by revisiting the research questions and providing the answers to corresponding questions.

2

Literature Study

This chapter aims to review the current state of technology used in voltage support as well as provide an introduction to battery degradation. To fully understand how voltage support is performed, a theoretical background on how the voltage drop and rise in a distribution network is first presented in Section 2.1. Afterward, the different available techniques for voltage control are explored in Section 2.2 with more focus on battery energy storage. Lastly, since this work also aims to evaluate battery degradation, the Chapter closes out with a description of Lithium-Ion degradation mechanisms and modeling techniques.

2.1. Undervoltage and Overvoltage In Distribution Networks

Voltage fluctuation is a common occurrence in distribution networks. This section describes the mechanism, governing standards and impacts related to voltage fluctuations in this type of network.

2.1.1. Mechanism

A circuit analysis of a simple distribution feeder can be performed to understand the voltage drop and rise concept in a radial LV network. Figure 2.1a. shows the single line diagram of a simple distribution feeder, while the equivalent circuit of the feeder is shown in Figure 2.1b.

The simple distribution feeder comprises a grid and a transformer, a feeder bus, and a line in which power flows. In the circuit, the grid is represented as a constant voltage source \bar{V}_G , the power line is represented by impedance \bar{Z} and the net injected power by the PV and load pair connected to the Point of Common Coupling (PCC) is considered as a current source \bar{I}_n . Lastly, the voltage measured at the PCC is $\bar{V}_n = |\bar{V}_n| \angle 0^\circ$, while the voltage deviation along the feeder is denoted in $\Delta\bar{V}$.

According to [14] the voltage deviation ($\Delta\bar{V}$) between the grid and feeder bus due to the current injection \bar{I}_n at bus n can be derived by Equations (2.1) through (2.9).

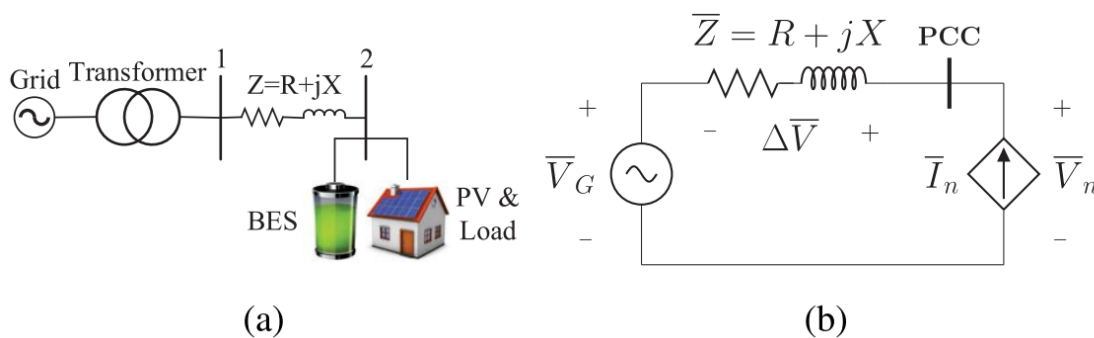


Figure 2.1: Line diagram and circuit representation of a radial feeder bus. Source: [14].

$$\Delta \bar{V} = \bar{Z} \cdot \bar{I}_n \quad (2.1)$$

$$\bar{I}_n = \left(\frac{\bar{S}_n}{\bar{V}_n} \right)^* = \left(\frac{P_{\text{net}}}{\bar{V}_n} - j \frac{Q_n}{\bar{V}_n} \right). \quad (2.2)$$

\bar{Z} in (2.1) can be broken down in terms of resistance and reactance. Therefore, by substituting (2.2) into (2.1), $\Delta \bar{V}$ can be expressed as

$$\Delta \bar{V} = \frac{R \cdot P_{\text{net}} + X \cdot Q_n}{|\bar{V}_n|} + j \frac{X \cdot P_{\text{net}} - R \cdot Q_n}{|\bar{V}_n|}, \quad (2.3)$$

where, $\Delta \bar{V}$ in can be split into V_d and V_q components as

$$\Delta V_d \triangleq \frac{R \cdot P_{\text{net}} + X \cdot Q_n}{|\bar{V}_n|} \quad (2.4)$$

and

$$\Delta V_q \triangleq \frac{X \cdot P_{\text{net}} - R \cdot Q_n}{|\bar{V}_n|}. \quad (2.5)$$

Going back to the circuit shown in Figure 2.1b, the voltage from the source can be formulated as

$$|\bar{V}_G| = \left[(|\bar{V}_n| - \Delta V_d)^2 + (\Delta V_q)^2 \right]^{\frac{1}{2}}, \quad (2.6)$$

where, ΔV_q is usually very small compared to $|\bar{V}_n| - \Delta V_d$. As a result, this term is neglected. By using that assumption $|\bar{V}_n|$ can then be approximated as

$$|\bar{V}_n| = |\bar{V}_G| + \Delta V_d. \quad (2.7)$$

When a small difference between $|\bar{V}_n|$ and $|\bar{V}_G|$ is assumed, they can be taken as similar. Therefore, Equation (2.4) can also be expressed as

$$\Delta V_d \approx \frac{R \cdot P_{\text{net}} + X \cdot Q_n}{|\bar{V}_G|}. \quad (2.8)$$

Finally, (2.8) can be substituted into (2.7) to obtain

$$|\bar{V}_n| \simeq |\bar{V}_G| + \frac{R \cdot P_{\text{net}} + X \cdot Q_n}{|\bar{V}_G|}, \quad (2.9)$$

where, P_{net} is

$$P_{\text{net}} = P_{\text{PV}} - P_{\text{Load}}. \quad (2.10)$$

In Equation (2.10), P_{net} represents net power, meaning the difference between power injected from PV, P_{PV} , and the power drawn by the load, P_{Load} .

Based on Equation (2.9) the voltage behavior in a low-voltage (LV) distribution network due to active power can be predicted. Clearly, the voltage at PCC is proportional to the net power; hence, when the net power becomes too high, voltage violation may occur. Moreover, In an LV distribution network, the short circuit ratio (i.e. X/R) is generally small. Consequently, the term $R \cdot P_n$ in Equation (2.9) becomes more dominant than $X \cdot Q_n$; thus, the net real power affects the voltage magnitude at PCC more than reactive power.

Besides the relation between active power and voltage, Equation (2.9) also describes the voltage characteristic along a line in an LV distributed network. If there is no reactive power control by the PV inverter, and the Q_n value related to load is constant, a positive P_{net} implies that the voltage increases along the feeder line due to increasing resistance magnitude. Meanwhile, if P_{net} is negative, the voltage decreases along the feeder.

2.1.2. Voltage Limitation Standard

To prevent impacts of over/undervoltage, different countries use different standards for steady-state voltage magnitude variations and unbalanced conditions. In Europe, the EN50160 standard [17] limits the voltage deviation in LV distribution networks at ± 0.1 p.u. ($230V \pm 10\%$). Moreover, the standard also limits voltage unbalance between 2 to 3% for 95% of the week. In the US, the ANSI C84.1 [18] standard sets a tighter voltage deviation limit at ± 0.05 p.u. Meanwhile, according to IEEE 1547, the maximum and minimum critical voltage are 1.1 and 0.88 p.u., respectively. Although the networks are allowed to be operated up to the critical voltages, corrective actions need to be taken to improve the network voltage profile if many points of the system violate the maximum or minimum threshold. According to [14] starting corrective actions should have limits that are lower than the critical voltage.

2.1.3. Impact of Over/Undervoltage

The voltage limitation standard applied to the distribution network described in the previous subsection serves to protect the distribution system operators and end customers from unwanted operating conditions. The impacts of violating those standards are given for each perspective as follows:

Distribution System Operators

1. **Equipment damage and maintenance cost:** Operating outside of an electrical equipment's specified range presents higher stress to the internal components. This repeated stress leads to shorter age of the equipment, thus requiring the distributed system operators (DSO) to repair or replace them sooner compared to normal condition
2. **System instability and reliability:** Severe overvoltage leads to overloading of infrastructures and consequently, network failures. Meanwhile, undervoltage poses a risk of the system collapsing. These associated risks decrease the overall reliability of the distribution system.

End Customers

1. **Shorter life of electrical appliance:** Similar to what the DSO experience, end customers may suffer from equipment damages due to over or undervoltage.
2. **Service disruption:** As the risk of instability increase, the availability of the distribution system decrease. This leads to increased downtime and productivity loss, particularly for businesses.
3. **Safety risks:** Since overvoltage or undervoltage causes damage to equipment, the risk of fire or electrical hazard may appear.
4. **Energy efficiency:** Aside from possible damages, operating equipment outside of specified window presents more losses, leading to increased energy bills

2.2. Techniques for Voltage Support

Voltage violation is undesirable for network users as previously indicated in Section 2.1.3. Thus, this section presents five commonly known voltage control techniques to mitigate violations in LV distribution networks.

2.2.1. On-Load Tap-Changing Transformers

On-load tap-changing transformers (OLTC) are transformers that can alter their secondary winding to increase or decrease output voltage by switching into different tap positions [19]. The tap-changing mechanism can be both mechanical and electronic [19]. However, their aim is the same, which is to adjust its tap according to reference voltage [20].

Figure 2.2 illustrates the working principle of OLTCs. Changing the tap position from A8 to B1 increases the number of turns on the output side of the OLTC; hence, increasing voltage on the secondary winding side. This mechanism is robust and reliable for most cases. However, it has an inherent delay to prevent arcing and minimize mechanical stress from the switching. In a network with high PV penetration, fast voltage fluctuation can happen and OLTCs may not effectively mitigate this [20]. Furthermore, they are not effective in handling voltage issues in far-end nodes because regulation only happens on the primary side of the transformer. As the nodes get further away from the transformer, the voltage difference will become too large while the number of taps in an OLTC is limited [6].

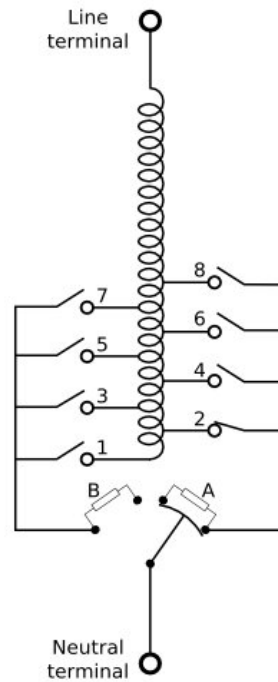


Figure 2.2: Schematic of an on-load tap-changing transformer. By switching its tap position from A8 to B1, the turn ratio of the transformer will change. Source: [21].

2.2.2. Smart Transformers

A similar alternative to OLTC is Smart Transformers (ST). ST refers to solid-state transformers (SST); a type of transformer that uses power electronics to elevate or step down voltage, that can provide ancillary services to the distribution and transmission grids to optimize their performance [22]. The advantages of SST alone include its wide range of operating voltage and enhanced efficiency, and they also allow for better integration of renewable energy as it can facilitate both AC and DC [23]. Moreover, they offer the same feature as core-type transformers (e.g., galvanic isolation and voltage matching) but with less weight and volume [24].

When SSTs are combined with information and combination technology, they become smart transformers and offer additional features. In combination with distributed generation, STs can control the downstream-connected LV grid in islanded mode because it can connect and disconnect from the main grid [24]. Furthermore, by providing a robust DC bus, any disturbance in the LV network can also be isolated from the healthy medium voltage (MV) side [25]. Another essential feature of ST is to filter out harmonics from non-linear loads; thus, relieving some stress from the high voltage to medium voltage transformer [24].

Despite the advantages, the use of SSTs and ultimately STs have yet to gain general acceptance owing to several barriers. One barrier is the cost of SSTs, which are much higher than conventional transformers [25]. Another barrier that makes them less appealing compared to conventional transformers is their robustness [25]. However, with advances in power electronics, the cost SSTs are expected to decrease while their reliability keeps improving [25].

2.2.3. Reactive Power Control

Adjusting reactive power can be done to control voltage in a network. This method is also known as volt-var control. To understand this mechanism, we refer to Equation (2.8). This equation implies that a certain amount of reactive power needs to be present to increase active power flow in a bus while keeping its voltage at the same level [7].

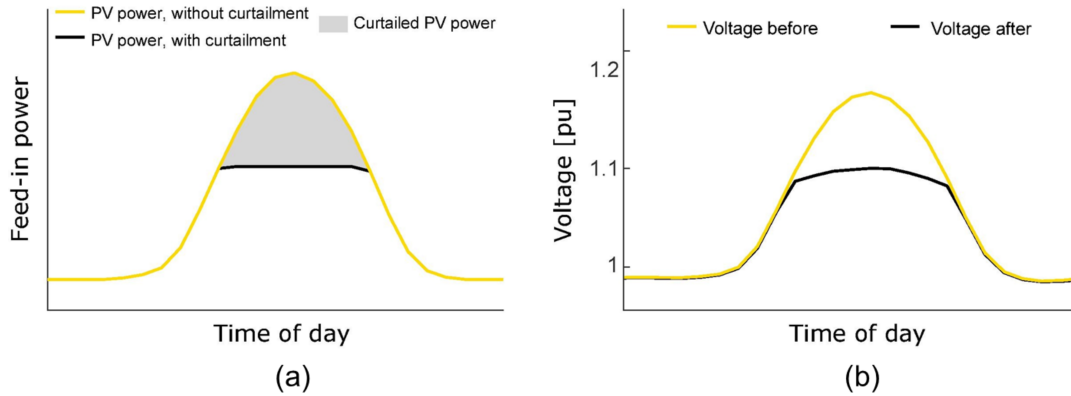


Figure 2.3: Effect of PV with curtailment and without curtailment on (a) Feed-in power (b) Voltage. Source: Adapted from [28].

According to [26], several volt-var control methods can be grouped into two categories: network side management and demand side management. The methods that fall within the former include adding fixed or switched capacitor banks and flexible AC transmission devices [19], [26]. Meanwhile, reactive power control using smart PV inverters falls within demand-side management.

In the context of LV networks with high PV penetration, volt-var control using PV inverters proved advantageous especially compared to capacitor banks. This advantage is mainly due to their flexibility and adaptability as smart inverters can absorb and inject reactive power while capacitor banks only absorb the reactive power [26], [27]. Despite this, volt-var control pales compared to active power control as the R/X ratio in distribution networks is far larger than transmission networks, leading to voltage amplitudes being more sensitive to active power than reactive power [9].

2.2.4. Distributed Generation Curtailment

One method to control voltage in a distribution network by way of active power is through the output curtailment of distributed renewable energy systems installed in it. For a solar PV-based generator, curtailment is achieved by stopping the maximum power point tracking algorithm and then limiting the active power at the PV inverter to avoid reverse power flow [19]. By injecting less active power into the grid, any predicted mismatch between generated power and load demand can be reduced or even eliminated. Consequently, the voltage peak can be reduced as depicted in Figure 2.3.

The main advantage of distributed generation curtailment is similar to reactive power control, in the sense that it can react fast to voltage changes compared to load tap changers and does not require any system upgrade [8]. In [8], a method of overvoltage regulation through PV power capping and curtailment sharing was presented with an aim for equal customer participation. [29] presented a study case of voltage regulation through solar PV active power curtailment. This study merges a droop-based inverter reactive power compensation algorithm and active power curtailment method using very short-term PV power forecasts.

Despite the possibilities presented by active power curtailment, it also presents disadvantages, primarily to owners of these generators. By curtailing the output of these generators, the revenue that owners receive is also reduced [7]; hence compromising their investment. Besides that, this method is only suitable for overvoltage issues and cannot tackle undervoltage problems [19].

2.2.5. Active Power Control: Battery Energy Storage Systems

Active power injection/absorption using battery energy storage systems (BESS) is another attractive solution for voltage control. By taking in energy when solar power production is at its highest and feeding it into the grid during peak demand, voltage fluctuations can be kept to a desired level. Similar to volt-var and curtailment-based control, BESSs have a fast response. However, it can keep losses at a

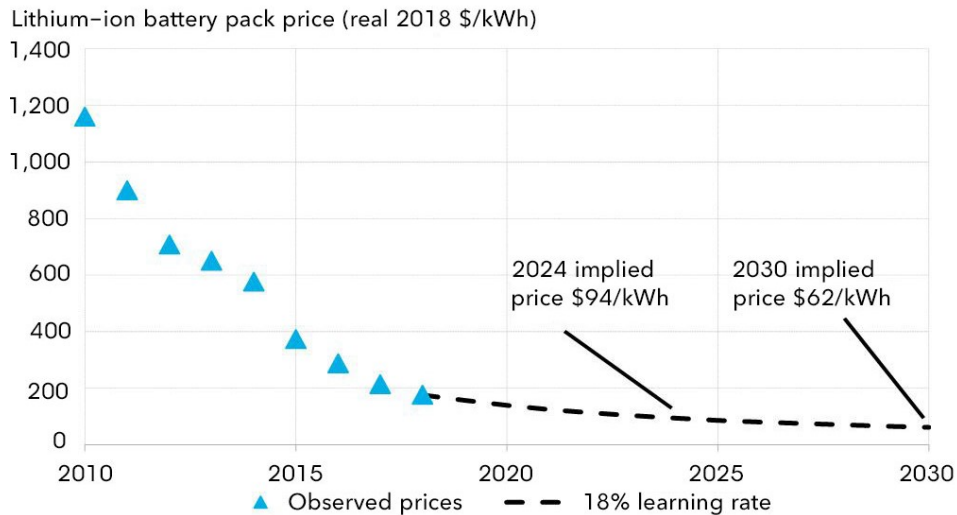


Figure 2.4: Lithium-ion battery price outlook from 2010 to 2018 with prediction until 2030 in terms of real price with respect to the year 2018 \$/kWh. Battery price is expected to reach \$62/kWh in 2030. Source: [31].

minimal [7]. Moreover, voltage control using BESSs is also effective owing to the resistive impedance (high R/X ratio) of LV feeders. A network with this characteristic has a voltage profile that is highly affected by real power flow [30]. Besides, the price of batteries is declining as depicted in Figure 2.4. According to the figure, the price for batteries can reach \$62/kWh in 2030 in terms of real price from 2018 (i.e., value adjusted for inflation relative to 2018) [31].

As the price for batteries continues to decline, BESSs become more accessible to customers, and thus the possibility of utilizing multiple BESSs in a network increase. The use of multiple BESSs in a network presents several advantages compared to a central BESS.

1. **Increased grid reliability:** Adding more BESS into a network increases its redundancy. consequently the energy not supplied due to network interruptions can be decreased [32]
2. **Grid congestion mitigation and transmission losses reduction:** By shaving generation and load peaks, the overloading of network conductors can be mitigated because less amount of power flows from or into the larger grid during peak times [33]. Besides freeing up line capacity, installation of BESS, together with distributed generation in the distribution network, can reduce line losses through optimal placement [32], [34].
3. **Customer participation in energy trade:** Customers can participate in energy trade and ancillary service provision by providing power from their battery should the DSO call for them. spreading out the cost for storage with customers.
4. **Enhanced performance compared to centralized BESS:** Distributed BESS within the power system can provide an effective solution for restoring out-of-range nodes to compliance. However, battery technology has technical and financial constraints; hence, the feasibility of this integration strategy using BESS is currently limited [35].

There are different ways to control multiple BESSs for voltage support. The following subsections describe three commonly known strategies presented in the literature: decentralized, centralized, and distributed control.

Decentralized Control

In decentralized control, the monitoring and control of each BESS' charging and discharging actions are performed locally [11]. BESSs with local control work independently of other BESSs; hence, eliminating any need for broadband and a complex communication network [14], [10], [36]. A schematic of decentralized control can be seen in Figure 2.5.

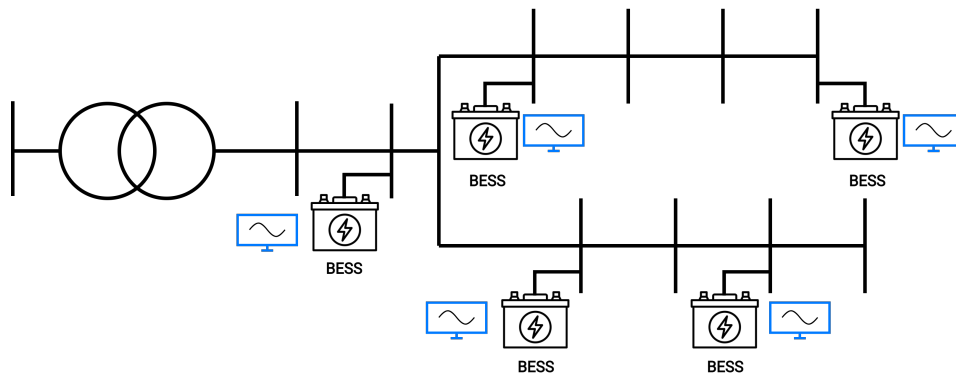


Figure 2.5: Schematic of decentralized control. The local controller in each BESS works independently from other BESS.

Several decentralized control has been proposed in the literature. [37] presented a simple decentralized control in residential BESS where excess PV power is used to charge the BESS and then utilized when PV generation is low or zero. An overvoltage mitigation technique based on voltage sensitivity analysis was proposed by [38]. In that study, the charging of BESS is triggered by a predefined PV power threshold. A strategy to adapt BESS charging power proportionally to PV generation to directly tackle PV export was proposed by [39]. Through these studies, the viability of decentralized control is proven.

While decentralized control is simple and robust, it cannot provide optimal solutions, especially for larger networks. For example, if a BESS unit is fully charged or can only provide limited power, it cannot communicate with other BESS to share its burden [11]. Besides that, it pales in comparison to centralized control when considering its effectiveness and ability to solve voltage problems comprehensively due to the lack of broader network information [36]. Moreover, with the emergence of smart grid components, controlling BESSs in a decentralized manner presents wasted potential and thus leads to a sub-optimal solution [13].

Centralized Control

The centralized control strategy utilizes a central management system that is in charge of making decisions regarding the contribution of each BESS. In the context of voltage support, decisions are based on the voltage magnitude fluctuation. Figure 2.5 illustrates the general schematic of a centralized control strategy.

In principle, a centralized controller works in the following order. First, each storage system sends local measurements to the central controller and the central controller. Afterward, the central controller

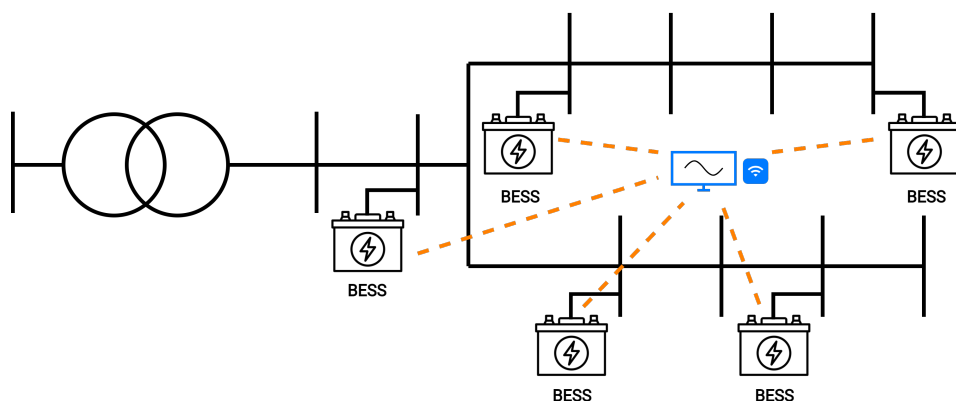


Figure 2.6: Schematic of centralized control. A central management system coordinates BESSs to perform cooperation and provide network support.

aggregates measurements from the entire network and calculates the solution to the control problem. The solution is communicated to the local controller and serves as a set point.

Several works have investigated centralized control for voltage support. A strategy to centrally control multiple BESSs by determining their dynamic operation points through linear optimization is proposed in [36]. In that work, the reactive power absorbed by the inverter is considered when determining the set points. [40] proposed a centralized control strategy that determines BESS participation based on the voltage sensitivity factor and aging characteristic of the BESSs. Another example is a coordinated control between BESS and OLTC for voltage regulation [41].

The centralized control strategy is generally superior compared to decentralized control. In the event of the unavailability of a particular BESS unit, the central controller can search for an alternative unit and resolve the problem [11]. Besides that, centralized control is more efficient than decentralized control, as it is based on the current information about the entire network [11]. Aside from controlling BESSs, the centralized controller can also send commands to PVs, smart loads, and other controllable units and perform coordination.

One major drawback of centralized controllers, however, is their need for fast and uninterrupted communication between central and BESS controller [10], [12]. Consequently, this will lead to high investment costs. Aside from that, an error in the central controller may compromise the network. In such a case, the system may become unstable [11].

Distributed Control

From the previous subsections, it is known that centralized control requires expensive computation and network infrastructure, while decentralized control cannot provide a globally optimal solution for the network. Distributed control strategy serves as a middle ground between them because BESSs can still coordinate with each other and share their burdens without the need for a high-speed central controller.

In distributed control, intelligent electronic devices cooperate to reach a collective decision according to the goals set (e.g., voltage limits) [13]. Each device only has to communicate with nearby devices, as illustrated in Figure 2.7. In more detail, the communication works by the principle of consensus algorithm where variables of interest are shared among the agents and synchronized to achieve a common state. In the context of this work, the variable of interest is the ratio between the BESSs' required power and their rated power.

By taking a coordinated approach while keeping information sharing only between neighbors BESS, distributed control avoids the drawbacks of centralized and decentralized control. According to [13], distributed control can deal with limited communication and low bandwidth, is less affected by faults in the communication lines, and have plug and play capability.

There are some variations to the distributed control strategy for voltage support in the literature. A leader-follower consensus algorithm to coordinate distributed BESS for voltage regulation is presented

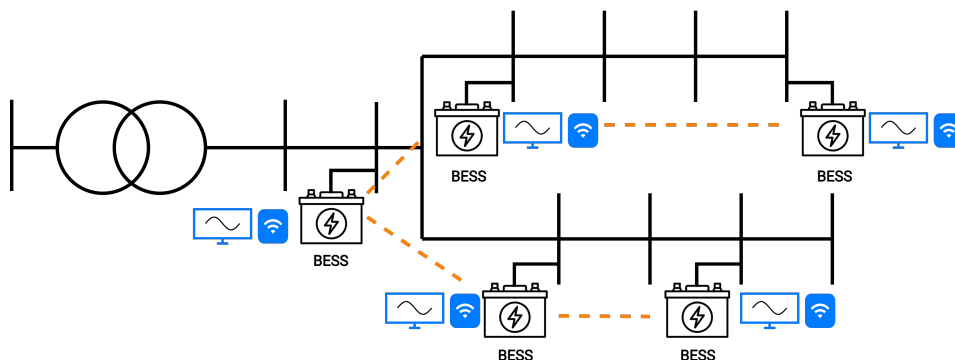


Figure 2.7: Schematic of distributed control. The BESSs cooperate with each other in the absence of a central management system. Information is only shared among neighboring BESS.

Table 2.1: Summary of distributed control for voltage support

No.	Ref.	Contribution	Limitation
1	[12]	Distributed control strategy based on leader-follower consensus combined with local SOC controller based on a predefined SOC reference.	Requires determining edge nodes as virtual leaders. Meanwhile, the extension of nodes can happen at any moment; therefore, the need to evaluate the network from time to time. Additionally, there is no evaluation of the battery degradation.
2	[14]	Distributed control strategy based on the installed capacity of BESSs and SOC balancing strategy to equalize SOC values.	The simulation was limited to 24 hours and cannot demonstrate voltage support readiness over an extended period of time. Moreover, battery degradation is not investigated.
3	[15], [42]	Distributed control strategy considering time-varying communication network and communication link failures.	Limited simulation time demonstration and does not include battery degradation analysis.
4	[43]	Distributed control strategy considering communication delays.	Does not present battery SOC and its degradation analysis.

in [12]. A combination of two weighted consensus algorithms is presented in [14] with aims to distribute power burden equalizing SOC of heterogeneous BESS capacity. In [15] and [42], event-triggered distributed control to further minimize communication burden is proposed. Additionally, distributed control under communication delay is demonstrated in [43]. Nonetheless, all of the above results do not consider the cycling effects of distributed control on battery degradation. To summarize the recent research direction in the domain of distributed control, Table 5.2 is presented.

2.3. Lithium-Ion Battery Degradation

Batteries with lithium-ion chemistry are popular for grid applications due to their high power density, high energy density, and long lifetime [33]. This section presents a short description of the components in a lithium-ion battery, several degradation mechanisms, as well as degradation modeling techniques.

2.3.1. Components of Lithium-Ion Battery

There are three main components in a Li-ion battery: electrodes (anode and cathode), electrolyte, and separator (Figure 2.8). The cell performance, power and energy capacity, cycle life, safety behavior, and operating temperatures are influenced by the interaction of these components. The following text describes the components according to the definition in [44].

Electrodes

The electrodes are composite structures made of active materials, additives, and binders. The positive electrodes (cathode) generally have metal oxides as their active materials, whereas negative electrodes (anode) are usually made of carbon. The primary function of the active components is to securely store Lithium over extended periods of time. Li-ions undergo intercalation and de-intercalation as they move back and forth between the cathode and anode during battery operation. To improve the electronic conductivity within the composite electrode, carbon-based additives are usually included. Finally, the binders act as a "glue" to keep the current collector and the active ingredients together [44].

Electrolyte

Electrolyte is a medium that facilitates the Li-ion diffusion between the electrodes during charging and discharging cycles. In Lithium-Ion batteries, the electrolyte is constituted of one or more liquid solvents along with lithium salts, for example, Lithium- Hexafluoro-phosphate (LiPF_6). A good electrolyte should have the following characteristics [44],[46]:

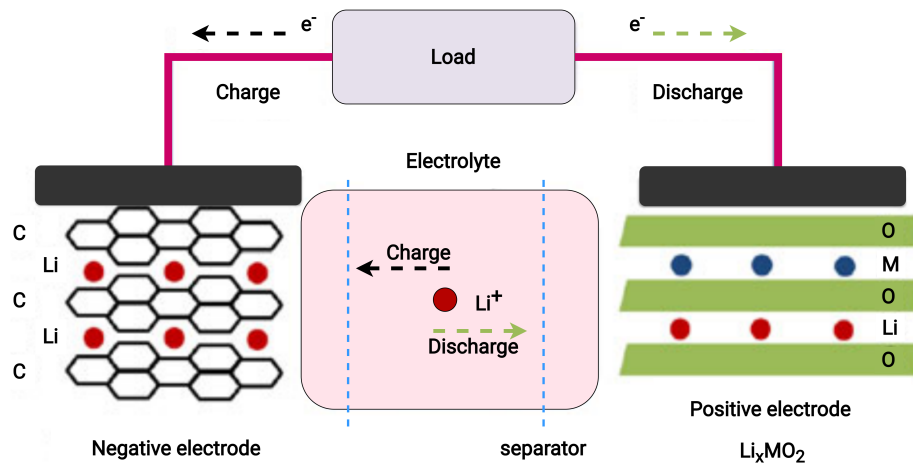


Figure 2.8: Schematic of a lithium-ion battery. Source: Adapted from [45].

1. Has a good ionic conductivity.
2. Electrochemically inert with the electrodes' surfaces in the cell's operating voltage range.
3. Chemically stable.
4. Does not react with the other components of the battery, for example, the current collector and separator.
5. Does not harm the environment.

Separator

The separator is a porous membrane placed between the anode and cathode to physically separate them both. Although a separator prevents the anode and cathode from coming into contact, it should be porous to allow the diffusion of lithium. According to [47], the ideal characteristic of separators are as follows:

1. A good electric insulation.
2. Minimal resistance in ion transport.
3. Appropriate dimensional and mechanical stability with adequate physical strength.
4. Uniform thickness.
5. Good chemical and thermal stability.
6. Easily wettable by typical electrolytes.

2.3.2. Battery Degradation Mechanism and Influencing Factors

There are three common degradation mechanisms often mentioned in the literature. Most of which are influenced by operating temperature, charging/discharging rate, and battery SOC. The following text discusses these mechanisms and their influencing factors in more detail.

Solid Electrolyte Interphase (SEI) Growth

A solid electrolyte interphase (SEI) is a semi-permeable layer formed at the interphase between the anode and electrolyte due to their different electrochemical stability window [48]. The process is driven by operating temperature and also by the battery's state of charge (SOC) at idle condition [48]. Furthermore, high current also leads to accelerated SEI growth through an electrode particle cracking mechanism [49]. SEI growth decreases the battery's state of health by preventing lithium from participating in charge storage and by increasing internal impedance [50].

Lithium Plating

Besides SEI growth, lithium plating on the graphite surface of the electrode can also occur [50]. Instead of intercalating into the graphite bulk, Li^+ ions from the electrolyte form lithium metal [50]. [51] mentions three conditions that promote lithium plating, high charging C-rate, high SOC, and low temperature. Lithium plating leads to capacity loss as it consumes cyclable lithium [52], [53], [54].

Particle Fracture

Particle fracture refers to the cracking of an electrode due to the volume changes of the electrode during cycling, (i.e., expansion on lithiation and contraction on delithiation) [50]. It affects degradation in three ways: revealing additional surface area for SEI growth, detachment of conductive additives from the electrode particles during delithiation, and complete detachment of particles from the binder, making them electrically isolated [55], [56], [57], [58]. In terms of influencing factors, cracking becomes more severe at higher currents and for larger particle sizes of the electrode material [59].

Other Degradation Mechanism

There are several other mechanisms less known than the three common ones described in the previous subsections. However, this work will not describe these other mechanisms in detail since it focuses on the implication of a control algorithm toward battery lifetime rather than the study of battery degradation itself. These mechanisms, to name a few, are salt precipitation, current collector corrosion, binder decomposition, separator pore blockage, electrode-current collector delamination, and electrolyte evaporation [60].

2.3.3. Battery Degradation Model

Battery degradation models can generally be categorized into four: physics-based models, equivalent circuit models, machine learning models, and empirical and semi-empirical models. Each method is a compromise of accuracy and computational speed, and their use depends highly on the situation.

Physics-Based Model

In physics-based models, partial differential equations are used to represent the actual physical behavior of batteries and their chemical reactions (e.g., SEI growth) [60]. From this type of modeling, an accurate insight into the degradation mechanism is obtained. Since it requires a series of partial differential equations, it presents a major drawback in terms of computing efficiency; therefore, making it unsuitable for real-time predictions [61].

Equivalent Circuit Model

In contrast to the physics-based model, equivalent circuit models use electrical components such as resistances, capacitances, and inductances to mimic the battery behavior instead of electrochemical reactions [48],[62]. The main advantage is their mathematical simplicity compared to physics-based models, which makes them suitable for real-time applications, such as battery state estimations [48],[63]. However, equivalent circuit models cannot be extrapolated to conditions such as when the battery is pushed toward its operating limits [64]. Therefore, it is not suitable for applications that demand high current rates or are run at very low temperatures [64].

Machine Learning Methods

In general, machine learning methods use support vector machines or neural networks to predict the battery's state of health. A few examples of this method are to train the machine learning algorithm to estimate the state of health from the differential voltage curve or incremental capacity curve of the battery, as shown in [65] and [66]. The advantages of machine learning approaches are that the required parameters (e.g., voltage, current, and temperature) are easily obtained [48] high accuracy can be achieved. However, aiming for a high accuracy requires large data sets to train the algorithms [67], [68].

Empirical and Semi-empirical Model

Empirical modeling involves testing and measurement of batteries under accelerated aging conditions and fitting the obtained data into a curve [60]. Furthermore, the underlying equations simply try to emulate the behavior of the battery as a black box without providing any physical insight [60]. Given this characteristic, empirical models can provide fast results; Hence, making them suitable for control designs such as battery management systems, optimization models, and system-level design problems [48]. However, they may exhibit poor generality because they are limited to the testing data [69].

To work around the drawbacks of empirical models, semi-empirical models were introduced. In semi-empirical models, physical insights into the model as opposed to only curve fitting are incorporated as

analytical formulas. The formulas provided in these models give an intuitive feel to the effect of various stress factors [48]. For example, four stress factors, namely depth of discharge (DOD), average charging current, average discharging current, and operating temperature, are presented in [70]. By incorporating physical insights, the semi-empirical models can make more accurate estimations compared to purely empirical models. However, it is important to note the added complexity of the physical equations, which may add some time to the development of these types of models. Moreover, large test matrices are required to accurately decouple the impacts of these stress factors [48].

3

Coordinated Control of Multiple Distributed BESSs

In this chapter, the distributed control strategy aimed at voltage support is described. Section 3.1 opens this chapter with a background to multi-agent systems, graph theory, and the consensus algorithm used as the basis for the control. The chapter then describes how the control is sequenced in Section 3.2.

3.1. Information Consensus

The distributed control presented in this work refers to the coordination of agents among nearby neighbors in the absence of a centralized controller. The basis of distributed control is the information consensus of agents; therefore, some basic principles are presented in the following text.

3.1.1. Multi-Agent System and Graph Theory

In this work, the BESSs coordinating with each other in a distributed manner can be analyzed as a multi-agent system (MAS). From a MAS perspective, BESSs are agents which can exchange information with their neighbors. This information exchange can be done either in a unidirectional or bidirectional way. Furthermore, the links in which the agents communicate can be represented in a graph. A graph representation of a simple multi-agent system is illustrated in Figure 3.1.

A graph comprises a set of vertices that represent the agents and a set of edges that represent the communication links in a MAS. A graph can be written in the form of $G = (V, E)$, where V indicates a set of vertices and E denotes a set of edges [71]. Furthermore, [71] describes that for a Multi-agent

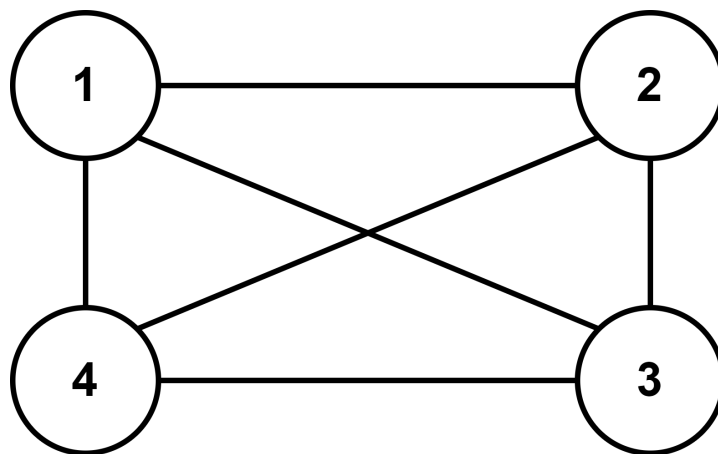


Figure 3.1: Multi-agent system with four agents. The agents are connected to each other forming a complete graph.

system consisting of n agents, the corresponding graph will be in the form of $G = (V, E)$, where $V = 1, 2, 3, \dots, n$ and $E \subseteq V \times V$. An edge represented as $(i, j) \in E$ means that agent j has a relationship with agent i (i.e., both agents have access to each other's information [71]). Besides, it also means that agent i is a neighbor of agent j . Looking at Figure 3.1 as an example, the MAS has four agents with each connected to every other agent. Therefore, this example MAS has 6 edges.

3.1.2. Degree Matrix, Adjacency Matrix, Laplacian Matrix

To describe the number of neighbors that each agent has in a graph, a degree matrix D is used. A degree matrix is represented as a diagonal matrix with a size of $V \times V$ where V is the number of vertices in a graph (the agents). The degree matrix of a graph follows a general form below:

$$D = \begin{bmatrix} d_{11} & 0 & \dots & 0 \\ 0 & d_{22} & 0 & \dots \\ \dots & 0 & \dots & 0 \\ 0 & \dots & 0 & d_{ij} \end{bmatrix}$$

The values assigned to elements d_{ij} , where $j=i$, are the number of neighbors that agent i has. For example, if agent 1 has three neighbors, then $d_{11} = 3$. To give a much clearer example, the degree matrix of the graph illustrated in Figure 3.1 is presented as follows:

$$D = \begin{bmatrix} 3 & 0 & 0 & 0 \\ 0 & 3 & 0 & 0 \\ 0 & 0 & 3 & 0 \\ 0 & 0 & 0 & 3 \end{bmatrix}$$

Besides the degree matrix, another important component in a graph is its adjacency matrix. The adjacency matrix of a graph, denoted in $A = [a_{ij}]$ describes which agents are neighbors. Similar to a degree matrix, an adjacency matrix also has a size of $V \times V$. In general, the following rules apply to the elements of the adjacency matrix (a_{ij}):

$$a_{ij} = a_{ji} = \begin{cases} 1, & \text{if agent } i \text{ and } j \text{ are connected and } i \neq j \\ 0, & \text{Otherwise} \end{cases} \quad (3.1)$$

The rule means that if agent i and agent j are neighbors, a value of 1 is assigned to element row i , column j as well as row j , column i in the matrix. The adjacency matrix of Figure 3.1 can be used as an example. In Figure 3.1, agent 1 and 4 are neighbors; thus, $A(1, 4)$ and $A(4, 1)$ have 1 assigned to them.

$$A = \begin{bmatrix} 0 & 1 & 1 & 1 \\ 1 & 0 & 1 & 1 \\ 1 & 1 & 0 & 1 \\ 1 & 1 & 1 & 0 \end{bmatrix}$$

The last important component of a graph is its Laplacian matrix. The Laplacian matrix is vital when describing a graph's global dynamics. The general form of a Laplacian matrix is given by $L = D - A$; hence, the graph in Figure 3.1 has the following Laplacian matrix.

$$L = \begin{bmatrix} 3 & 0 & 0 & 0 \\ 0 & 3 & 0 & 0 \\ 0 & 0 & 3 & 0 \\ 0 & 0 & 0 & 3 \end{bmatrix} - \begin{bmatrix} 0 & 1 & 1 & 1 \\ 1 & 0 & 1 & 1 \\ 1 & 1 & 0 & 1 \\ 1 & 1 & 1 & 0 \end{bmatrix} = \begin{bmatrix} 3 & -1 & -1 & -1 \\ -1 & 3 & -1 & -1 \\ -1 & -1 & 3 & -1 \\ -1 & -1 & -1 & 3 \end{bmatrix}$$

3.1.3. Consensus Algorithm

A consensus algorithm aims to reach a state consensus among the agents. When consensus is reached, the state difference between neighboring agents is zero. In the context of power sharing of multiple BESSs, the consensus is reached when all BESSs have the same utilization factor (i.e., the ratio between the injected or discharged power to a BESS' rated power). This means the power burden

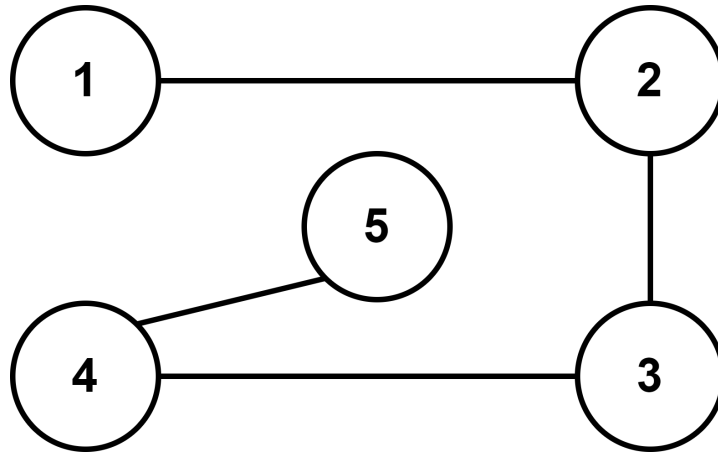


Figure 3.2: five-agent system with a line configuration. Agents 1 and 5 only have one neighbor each while the remaining have two.

will be shared proportionately among the BESSs according to their rated power. To reach a consensus, each agent applies Equation (3.2) [72]:

$$\dot{x}_i(t) = \sum_{j \in \mathcal{N}_i} a_{ij}(x_j(t) - x_i(t)) \quad (3.2)$$

Equation (3.2) guarantees convergence to a collective decision through the interaction of nearby agents. The equation implies that at $t \rightarrow \infty$, the value of $x_i(t) = x^* = c$ where x^* denotes a final value and c denotes a constant. Moreover, if the communication network is a balanced graph (the vertices have a similar number of edges), average consensus will be reached where the final value is the average of all initial states at time instance t as written in Equation (3.3).

$$x^* = \frac{\sum_i x_i}{n} \quad (3.3)$$

Since this work focuses on the calculation performed by each agent in every iteration, the discrete form of Equation (3.2) as written in Equation (3.4) is used.

$$x_i(k+1) = x_i(k) + \epsilon \sum_{j \in \mathcal{N}_i} a_{ij}[x_j(k) - x_i(k)] \quad (3.4)$$

In (3.4), k indicates the k^{th} iteration, the parameter ϵ indicates the consensus step size, and a_{ij} is the element of the adjacency matrix, which indicates the communication link between agent i and agent j . If there is a connection between agent i and agent j , then $a_{ij} = 1$. Otherwise, a_{ij} is zero.

By applying the consensus algorithm in (3.2) to a graph, a global dynamic as described by (3.5) can be observed.

$$\dot{x} = -Lx \quad (3.5)$$

Examples of global dynamics when using consensus algorithm explained in the form of Equation (3.5) have been discussed in prior works such as [14] and [12]; thus, it is omitted here.

To illustrate how the consensus algorithm works, an example graph of a MAS comprising five agents as illustrated in Figure 3.2 can be observed. The agents in the figure form a line configuration with agents 1 and 5 on the ends. In that configuration, the agents at the ends are only connected to one neighbor. Agents 2, 3, and 4, however, have each two neighbors connected to them. The configuration affects how the initial states converge in the sense that the agents follow the path that is the closest to them. For example, the state of agent 2 is directly affected by agent 3 and agent 1.

Table 3.1: Initial states of agents

Agents	X_1	X_2	X_3	X_4	X_5
Initial state value (t=0)	4	3	1	3	1

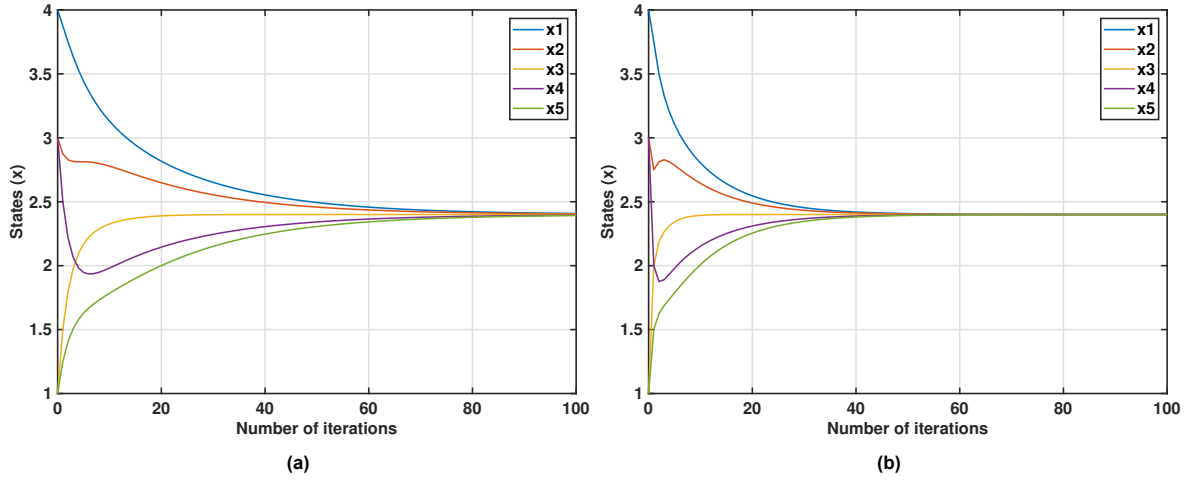


Figure 3.3: Convergence of a five-agent system: (a) $\epsilon = 0.125$ and (b) $\epsilon = 0.25$. The initial states converged to their average value with higher ϵ , yielding a faster convergence.

By referring to Equation (3.4), the estimated consensus states for agents 1 through 5 can be calculated. The first two calculation steps performed to reach a consensus for agents 1 and 2 are presented as follows:

1st step (t=1)

- Agent 1

$$x_1(1) = x_1(0) + \epsilon[x_2(0) - x_1(0)]$$

- Agent 2

$$x_2(1) = x_2(0) + \epsilon[(x_1(0) - x_2(0)) + (x_3(0) - x_2(0))]$$

2nd step (t=2)

- Agent 1

$$x_1(2) = x_1(1) + \epsilon[x_2(1) - x_1(1)]$$

- Agent 2

$$x_2(2) = x_2(1) + \epsilon[(x_1(1) - x_2(1)) + (x_3(1) - x_2(1))]$$

By assigning initial states $x_i(0)$ to the agents as presented in Table 3.1, the steps to consensus can be seen as illustrated in Figure 3.3. The figure shows the initial values converging to a consensus state $x^* = 2.4$. This state is also the average of all the initial values. On top of that, the convergence rate of the initial states under two different ϵ values can be observed. In Figure 3.3b, the initial states converged after 50 iterations, while in Figure 3.3a, the number of iterations needed is nearly twice. Hence, it can be implied that higher ϵ leads to faster convergence.

3.2. Control Algorithm for Voltage Support

In this section, a method for charge/discharge coordination of batteries is presented. The coordinated BESS control proposed in this work comprises a local voltage controller, a distributed consensus controller, and an SOC controller. By combining these three control in sequence, voltage control on the network can be performed.

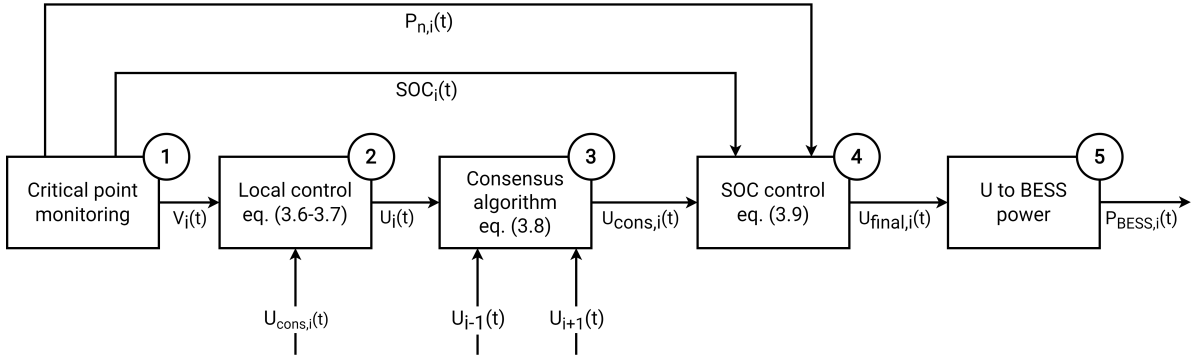


Figure 3.4: Proposed coordinated control strategy for the i^{th} bus. One control cycle starts with measuring voltage, net power, and battery SOC at the i^{th} bus and ends with feeding reference power value into the BESS.

A voltage control action starts at the local voltage controller and ends at the SOC controller. The local voltage controller determines the initial utilization factor needed to locally keep the voltage of the distribution network buses at a specified limit. A positive utilization factor indicates discharging, while a negative utilization factor indicates charging. After the initial utilization factor calculation, the portion of each BESS' participation in voltage control is then determined by the consensus controller. The consensus controller performs under limited communication links between neighboring BESSs and works based on the consensus algorithm. Lastly, the SOC controller serves to prevent the BESSs from saturating early and to balance out the SOC of all BESSs at the end of the day.

To summarize the sequences, a flow diagram showing the control strategy at the i^{th} bus is presented in Figure 3.4. There are five steps taken throughout one control cycle:

1. First, voltage regulation starts off with the measurement of voltage, BESS SOC, and net power of a bus. The measured voltage is used as an input to the local controller, while the net power and BESS SOC are used later in the SOC controller.
2. In the second step, the input voltage is compared to the predefined voltage limits. If the measured voltage falls outside the permitted range from V_{lower} to V_{upper} , then compensation by the BESS is required. The utilization factor required to locally tackle voltage violation at bus i is calculated using Equation (3.6) and (3.7). The calculated local utilization factor serves as an initial value for the consensus algorithm in the following step.
3. In the third step, the local utilization factor is shared equally among all BESSs by first calculating the consensus value using Equation (3.8). At consensus, all utilization factors have the same value, and therefore every BESS contribute proportionately according to their maximum capacity.
4. Following the consensus control, the consensus utilization factor is passed through a local SOC controller to ensure BESS has the right amount of SOC in the event of voltage violation. If the conditions described in Subsection 3.2.3 are met, the consensus utilization factor for that BESS is neglected, and the utilization factor based on the net power between PV and load is used instead. The output of this controller is the final utilization factor to be fed into the BESS.
5. In the final step, the final utilization factor $U_{\text{final},i}$ is multiplied by the BESS' rated power to obtain the reference power for the batteries. In this work, it is assumed that the BESSs always succeed in following the reference power. For that reason, the detailed control of the battery inverters is omitted.

3.2.1. Local Voltage Controller

The voltage controller aims to calculate the utilization factor required for each BESS to provide voltage support. It is triggered when the measured voltage in a bus (V_i) exceeds an upper voltage limit (V_{upper}) during overvoltage or falls below a lower voltage limit (V_{lower}). The general rule is that the difference between the two dictates how large the utilization factor is going to be.

Table 3.2: Notation description for Equations (3.6) and (3.7) .

Notation	Description
$U_i(t)$	Utilization utilization factor of node i at time instance t
$U_{add,i}(t)$	Additional utilization factor
m	Controller gain
$V_i(t)$	Measured voltage at node i
V_{upper} / V_{lower}	Upper voltage limit / Lower voltage limit
$V_{reset,upper} / V_{reset,lower}$	Upper reset limit / Lower reset limit

The local controller presented in this work has rules to increase or decrease the utilization factor and reset the utilization ratio. Suppose the voltage measured at a bus exceeds a predefined upper voltage limit. In that case, the utilization factor for the BESS in that location is increased from its previous value according to the difference between the voltage measurement value multiplied by a controller gain m . On the contrary, the utilization factor is decreased when the measured voltage is below the lower voltage limit. When the voltage is between the upper and lower voltage limits, the utilization factor does not change from its previous value; thus, the BESS maintains the amount of injected or absorbed power. Lastly, if the measured voltage is within a reset limit, the utilization factor is halved at every iteration to ultimately make its value virtually zero. The calculations based on these different conditions are formulated in Equation (3.6) and (3.7), while the description for each notation is presented in Table 3.2.

$$U_i(t) = \begin{cases} 0 & \text{at initial condition } (t = 0) \\ U_i(t-1) + U_{i,add}(t) & \\ U_i(t-1) * 0.5 & \text{if } V_{reset,low} < V_i(t) < V_{reset,high} \end{cases} \quad (3.6)$$

$$U_{add,i}(t) = \begin{cases} m \times (V_{upper} - V_i(t)) & \text{if } V_i(t) > V_{upper} \\ m \times (V_{lower} - V_i(t)) & \text{if } V_i(t) < V_{lower} \\ 0 & \text{if } V_{upper} < V_i(t) < V_{lower} \end{cases} \quad (3.7)$$

The local controller alone based on Equation (3.6) and (3.7), in principle, can solve voltage violations. However, it presents a problem in nodes with frequent violations as the BESSs there participate more in voltage regulation compared to the ones in places with fewer occasions. In most cases, buses at the end of a feeder network experience more violations, leading to a disproportionate burden among the BESSs in a network. Consequently, a controller to equally share the utilization factor is needed.

3.2.2. Consensus Controller

A consensus controller which works based on the consensus algorithm presented in Section 3.1 can drive the utilization factors of BESSs to an average value. By taking the local utilization factors as inputs, a consensus utilization factor can be obtained to then serve as a reference for the BESSs. The consensus utilization factor calculation in each bus at every iteration follows Equation (3.8).

$$U_{cons,i}(k) = U_i(k) + \epsilon \sum_{j \in N_i} a_{ij} [U_j(k) - U_i(k)] \quad (3.8)$$

According to Equation (3.8), the estimated consensus utilization factor at bus i is the local utilization factor added by the sum of the difference in utilization factor between that bus and the neighboring buses multiplied by a parameter ϵ . The output of this equation becomes the input to the SOC controller which performs several logical checks.

3.2.3. SOC Controller

Under voltage control mode only, a BESS may not have the right amount of charge to be able to absorb or release energy. On top of that BESSs in a network may have different initial SOC due to unpredictable weather and load conditions [14]; thus, creating a variation in terms of voltage support readiness among them. An SOC controller is therefore implemented to keep the BESSs within a set

Table 3.3: Notation description for Equation (3.9).

Notation	Description
$U_{\text{final},i}$	Final utilization factor of node i
$P_{\text{net},i}$	Net power at bus i
$P_{\text{bat},\text{rated}}$	Rated BESS power
$SOC_{\text{ESS},i}$	SOC at bus i
$SOC_{\text{lim},\text{charge}} / SOC_{\text{lim},\text{discharge}}$	SOC charging limit / SOC discharging limit
$P_{\text{lim},\text{pos}} / P_{\text{lim},\text{neg}}$	Positive net power limit / Negative net power limit

SOC limit. By doing so, the BESSs will always be ready to support the network and prevent undervoltage/overvoltage.

The SOC controller works locally and takes on the SOC of a BESS as well as the net power between PV and load at bus i ($P_{n,i}$) as its input. Conditional checks according to (3.9) are performed on those inputs with notations as described in Table 3.3.

$$U_{\text{final},i} = \begin{cases} -\frac{P_{n,i}}{P_{\text{bat},\text{rated}}}, & \text{if } SOC_{\text{ESS},i} < SOC_{\text{lim},\text{charge}} \text{ and } P_{n,i} \leq P_{\text{lim},\text{pos}} \\ -\frac{P_{n,i}}{P_{\text{bat},\text{rated}}}, & \text{if } SOC_{\text{ESS},i} > SOC_{\text{lim},\text{discharge}} \text{ and } P_{n,i} \geq P_{\text{lim},\text{neg}} \\ U_{i,\text{cons}}, & \text{otherwise} \end{cases} \quad (3.9)$$

During positive net power ($P_{\text{PV}} > P_{\text{Load}}$), if a BESS has an SOC that is less than a specified charging limit $SOC_{\text{lim},\text{charge}}$ and the net power does not exceed a certain positive limit $P_{\text{lim},\text{pos}}$, the BESS' utilization factor is the net power $P_{n,i}$ divided by the BESS' rated power $P_{\text{bat},\text{rated}}$. A similar condition is applied for a negative net power ($P_{\text{PV}} < P_{\text{Load}}$) not lower than the negative limit. When none of these conditions is met, the BESS will keep its consensus utilization factor from the consensus controller as its reference. As hinted previously, the output of the SOC controller will be the final utilization factor before it is multiplied by the BESS' rated power to become its reference power.

4

Simulation Setup of Low Voltage Distribution Network

This chapter describes the general process of evaluating the proposed control algorithm as well as the simulation setup. Section 4.1 opens the chapter with an overview of the evaluation method and the test cases simulated. Section 4.2 presents the CIGRE model where the algorithm is evaluated. Afterward, details of the power profile used in the simulation are laid out in Section 4.3. Furthermore, the implementation of the CIGRE LV network in MATLAB/Simulink and the communication network of the proposed algorithm are discussed in Section 4.4 and 4.5, respectively. The chapter closes with a description of the model used to evaluate battery lifetime when using the proposed control is discussed in Section 2.3.

4.1. Voltage Control Strategy Evaluation Method

The strategy proposed in Chapter 3 is evaluated regarding voltage behavior, control behavior, and effects on battery lifetime. To do so, a quasi-static load flow simulation is first performed. Afterward, the result is used for an offline battery lifetime calculation. Both simulations are performed in MATLAB/Simulink using the Specialized Power System toolbox. A general sequence of the simulations which shows the input and output data is illustrated in Figure 4.1.

In quasi-static load flow simulation, multiple load flow calculations are carried out with a user-defined time step to obtain time-dependent aspects of power flow, such as voltage variation within a day. This simulation is suitable for this work as electromagnetic transients and harmonics do not need to be considered. Time series voltage profiles and the BESSs' SOC and current profile based on the input mismatch are created from the simulation. These profiles are used to create a synthetic current profile as input to the battery model in which the battery capacity loss is calculated.

There are four case studies presented in this work to evaluate the proposed strategy. The first is a base case where the proposed strategy is tested in a week of summer. In this case study, the voltage profile when using the proposed strategy is compared to when no BESS is present in the network. In the second case study, the initial SOC of the batteries are varied to see the readiness of the control in an extended simulation period. In the third case study, the proposed strategy is tested against a week of winter. In the final case study, an additional generation capacity of the PV is added. Table 4.1 summarizes the case studies present in this work.

4.2. CIGRE LV Distribution Test Feeder Specification

The test cases presented in Section 4.1 are simulated on a modified CIGRE LV distribution test feeder [5]. This test feeder mainly represents an urban radial secondary distribution, which has small distances between the buses [73]. Modifications are made to the line parameters, as will be explained later in Subsection 4.2.2.

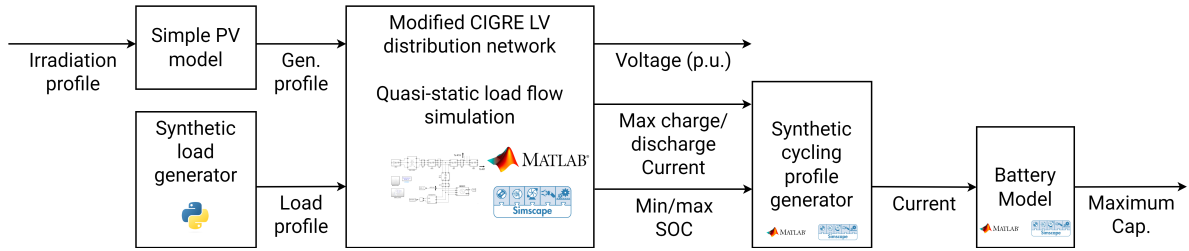


Figure 4.1: General overview of information flow and simulation sequence.

Table 4.1: Summary of case studies used to evaluate the proposed control strategy.

No.	Case Study	Variation
1	Base case	BESS + Proposed control
2	Different initial SOC	40%,40%,45%,50%,55%
3	Season change	Winter
4	Addition of PV generation	+10%

An overview of the modified CIGRE LV network illustrated as a single-line diagram is displayed in Figure 4.2. Based on the figure, the network has five loads, each representing a four-household small apartment building. The number of households mentioned here is related to the demand profile discussed later in Section 4.3. The loads are variable to represent daily changes. In addition, all units are assumed to have a unity power factor ($PF = 1$). Further, the network parameters will be explained below.

4.2.1. MV Grid and Transformer Specification

On the medium voltage (MV) side, there exists a 20 kV bus that supplies power to the residential feeder. The bus is modeled as a three-phase voltage source with a short circuit level of 100 MVA at its base voltage. Additionally, the short circuit ratio (X/R) is set to 1 to represent a weak grid as defined in [16].

The voltage from the MV side is stepped down using a 500 kVA, 20 kV/0.4 kV, Δ -Y distribution transformer, which supplies different residential loads. The transformer's rating is set to 500 kVA to prevent it from saturating under heavy load. Additionally, the windings have internal resistance and reactance of 0.01 and 0.04 p.u., respectively for both primary and secondary winding. Table B.1 in the appendix presents the full MV grid and transformer specifications used in the simulation.

4.2.2. Line Specification

The lines in Figure 4.2 is segmented with equal lengths of 80 m from R1–R18. Two types of lines are used, Z1 and Z2, each having different per unit km resistance and reactance value. The line distances and impedance per unit kilometers are modified from the original specifications stated in [5]. These modifications are made to exaggerate the effects on voltage due to the presence of a power mismatch between PV generation and load. A full specification of the lines used in this simulation can be seen under Table B.2.

4.2.3. Battery Energy Storage Units Specification

There are five BESS units integrated into the CIGRE LV network. Similar to the load, the capacity of each BESS unit represents the typical installed capacity in a four-household small apartment. The installed BESS capacity typically ranges from 5 to 10 kWh for one household. Thus this work aims at around 40 kWh. Besides, these units are located at the same AC bus with the load and PV panels. Each BESS consists of lithium iron phosphate (LiFePO_4) cells rated at 3.3 V, 2.3 Ah. This specification follows the cell specification of the ANR26650M1-B by A123 Systems. Furthermore, the cells have a 122s, 44p configuration, which means there are 122 cells in series forming a string and 44 strings in parallel. A system-level specification of the BESS is shown in Table 4.2. To see a detailed specification for each cell, readers can refer to Appendix C.

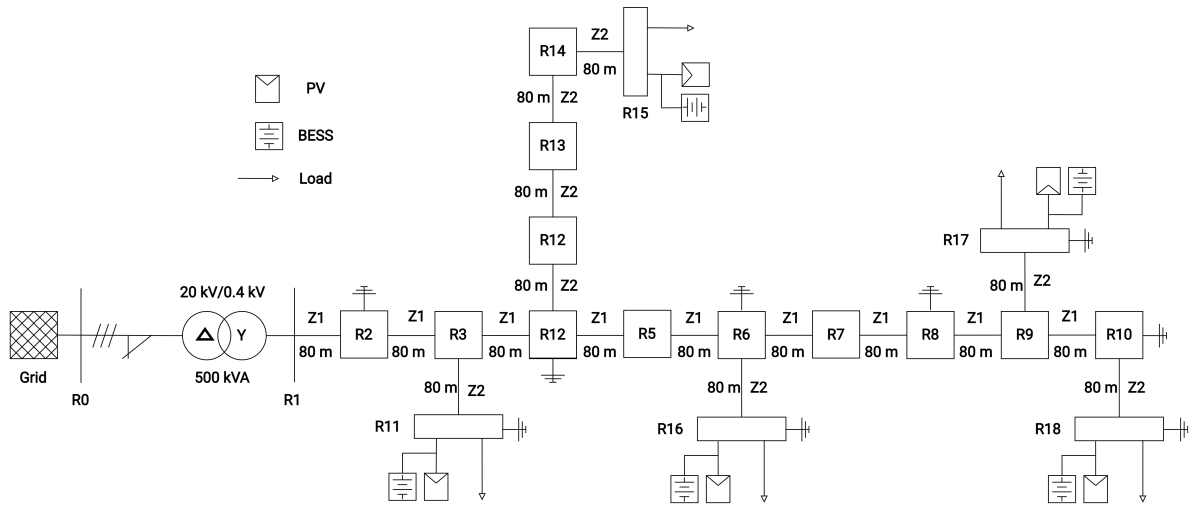


Figure 4.2: Single line diagram of the modified CIGRE LV distribution network. The Network has five load + PV combinations and five BESS. Source: adapted from [5].

Table 4.2: BESS specification: system level

Specification	Value
System nominal voltage	402.6 V
System nominal capacity	101.2 Ah
Cell configuration	122s, 42p
Total energy	40.6 kWh
BESS power (0.5 C)	20.3 kW

Table 4.3: Voltage controller parameters.

Control Parameter	Value
V_{upper}	1.05 p.u.
V_{lower}	0.95 p.u.
$V_{reset,upper}$	1.003 p.u.
$V_{reset,lower}$	0.997 p.u.
m	0.3
$SOC_{lim,charge}$	55%
$SOC_{lim,discharge}$	50%
$P_{lim,pos}$	2500 W
$P_{lim,neg}$	-2500 W

4.2.4. Controller Parameter

The control algorithm in Section 3.2 mentions several parameters to be set. In this work, the parameter for the simulated control is set according to the values displayed in Table 4.3. The parameters V_{upper} and V_{lower} in the table follow the voltage deviation limits in ANSI C84.1[18]. Meanwhile, the other parameters are the results of tuning during the base case simulation.

4.3. Power Profile

This section describes the demand and generation profiles in each of the buses. A synthetic profile that mimics the typical weekly load of an apartment building is generated for the demand profile while real irradiation measurement, converted to power, is used to represent power generated from PV.

4.3.1. Synthetic Demand Profile

The demand profile in this work is synthesized using the Probabilistic Load Profile Generator presented in [74]. How it works is that every appliance in each household of an apartment building has a predetermined probability of being turned on at a certain point during the day. For example, a kettle has a probability of being turned on of 0.5 at 8 A.M. A random number between 0 to 1 is then generated at every time step and if the generated number is smaller than the probability, then the device is added to the load profile. An important assumption made in [74] is that the households use gas-based air conditioning systems; therefore, eliminating electrical demand for space heating. By doing so, it can also be assumed that the scale of demand will be similar throughout the year as usually the energy demand difference during various seasons owes to heating.

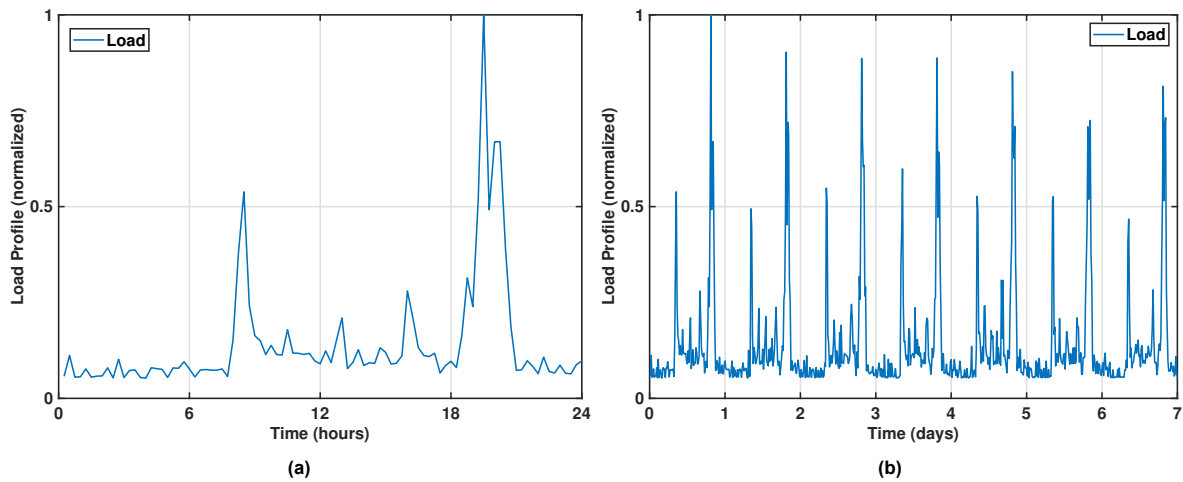


Figure 4.3: Demand profile for a small apartment building containing four households: (a) Day profile and (b) Week profile.

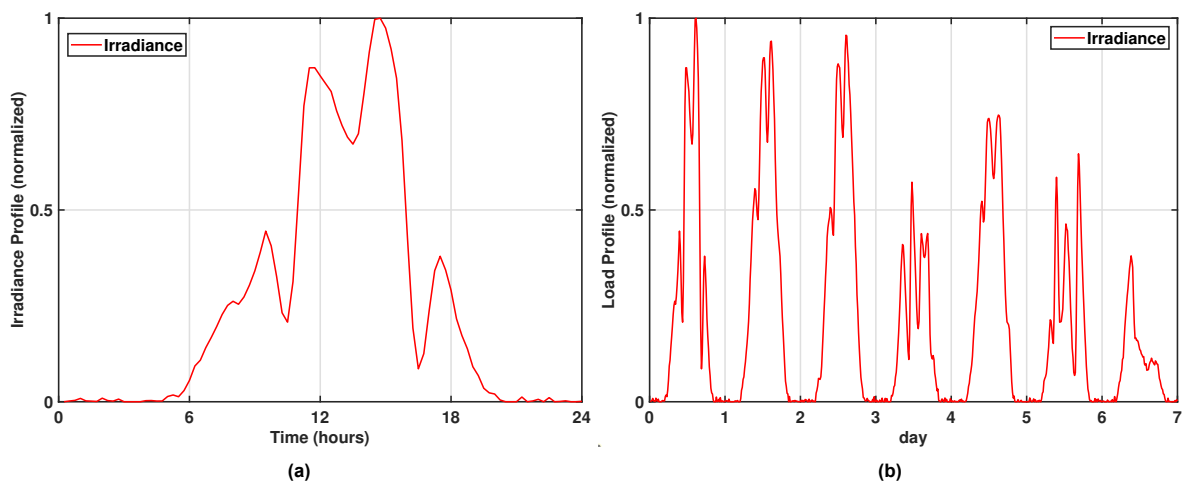


Figure 4.4: Irradiance profile in Delft during mid-July 2005: (a) Day profile and (b) Week profile.

The profile generated from the Probabilistic Load Generator to be used in this work is depicted in Figure 4.3. It represents the aggregated demand of four households in a small apartment building and is scaled to correspond to a maximum demand of 10 kW. The curve of the synthetic profile is visually similar to real measurement profiles in [75] and [76]; thus, it can be considered valid.

4.3.2. PV Power Profile

The PV power profile is estimated based on the irradiation profile at a certain location and time. For this work, a one-week irradiation profile in Delft from July 2005 obtained from the PV GIS online tool [77] is used to generate the PV power profile. The original data has a 1-hour measurement interval, while PV power simulations typically take 15-minute interval data. The Modified Akima Interpolation method [78] is therefore applied to fill in the missing points of the data and increase its resolution. Additionally, random numbers with normal distribution are applied to the data points to represent uncertainty. A final product of the modified irradiance profile is depicted in Figure 4.4.

The normalized irradiance profile presented in Figure 4.4 serves as a basis for scaling PV power. Depending on the scenario being tested, the normalized profile can simply be multiplied by a predetermined gain. In this particular work, the power generated from PV is scaled in a way that corresponds to a positive net power of 9 kW. More details regarding this subject are discussed in Subsection 4.3.3.

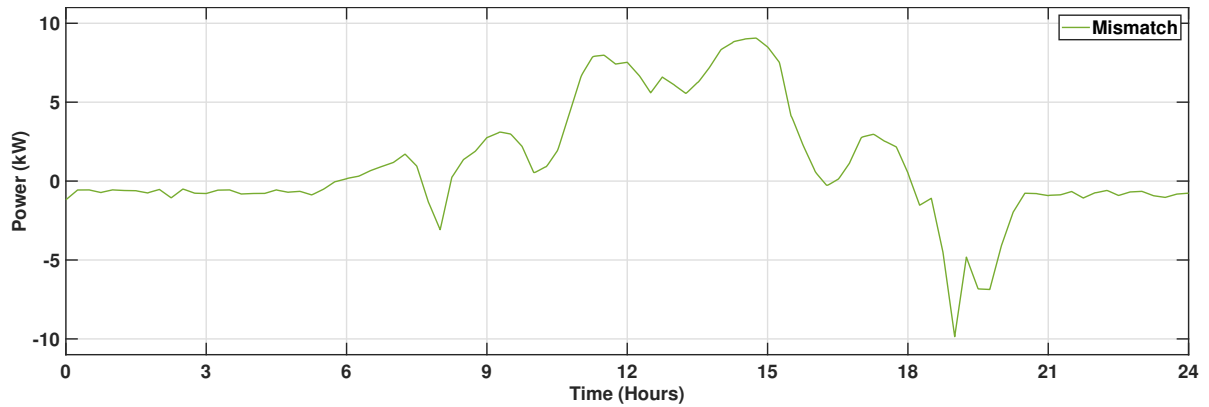


Figure 4.5: One-day mismatch profile taken from the 15th day of July 2005.

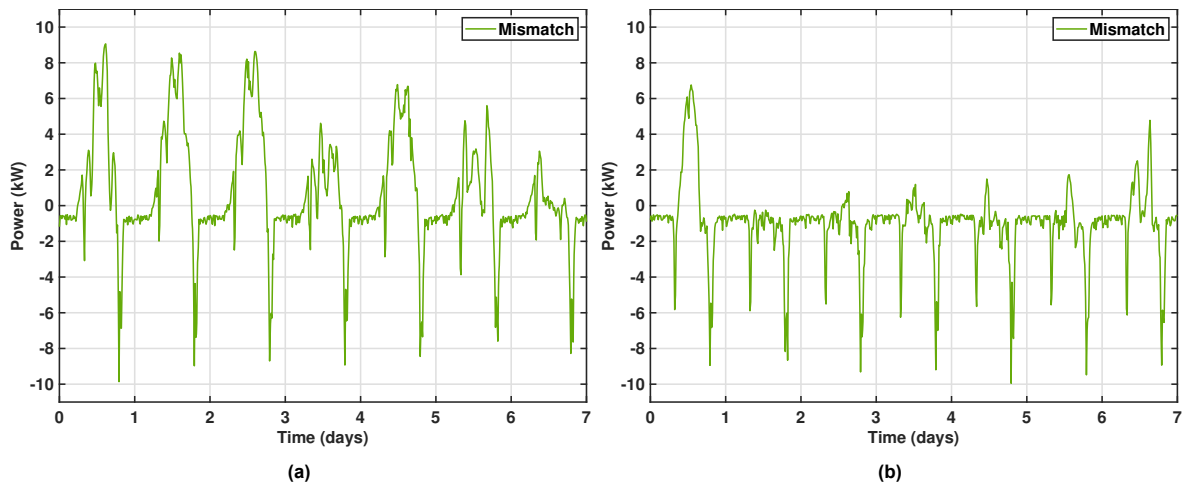


Figure 4.6: One-week mismatch profiles of two different seasons: (a) Summer (mid-July) and (b) Winter (mid-January).

4.3.3. Mismatch Profile

By combining both load and PV profiles, a one-day and seven-day mismatch profile can be obtained, as shown in Figures 4.5 and 4.6a, respectively. The profile's largest negative mismatch (PV shortage) is scaled to -10 kW. Meanwhile, the largest positive mismatch (PV surplus) corresponds to 9 kW. This value is used as the base profile for testing the proposed control algorithm on the CIGRE LV network. In addition to the base profile, a seven-day profile during winter is also synthesized to evaluate the effect of season change on the proposed control algorithm. This profile is based on the irradiance in January and is depicted in Figure 4.6b. The main difference between the winter and base profile is reflected at times of positive mismatch. This difference is due to less available sunlight during winter. Meanwhile, both profiles are similar during times of negative mismatch because it is assumed that increased energy demand during the winter is mainly due to space heating while no electrical heating equipment is used in the households.

4.4. LV Network Model MATLAB/Simulink

Using the network information provided in the 4.2, a simulation model is built on MATLAB/Simulink as shown in Figure 4.7. The PVs, loads, and BESSs are represented by phasor models from the example library of microgrid systems in [79]. Additionally, the lines are represented as R-L impedances while the line capacitances are omitted due to relatively short cable lengths compared to transmission lines [73]. The phasor-discrete mode is used for the simulation since it could capture low-frequency, time-varying voltage dynamics. In more detail, a sample time of 1 second is chosen to save simulation time while keeping a good controller performance.

Table 4.4: Notation summary of Equation (4.1) through (4.4). To understand the details and derivation of each variable, the reader can refer to [70].

Notation	Description
Q	Remaining battery capacity
ε	Battery aging factor
α	Aging exponent
Q_{BoL}, Q_{EoL}	Battery capacity at beginning of life (BoL) and end of life (EoL). EoL typically set at 80% BoL
N_{eq}	Equivalent number of cycles
N_c	Maximum number of cycle to EoL
N_{c_ref}	Maximum number of cycles at $DOD = DOD_{ref}$, $C\text{-rates} = (I_{dis_ref}, I_{ch_ref})$, and $T = T_{ref}$
DOD, DOD_{ref}	Depth of discharge and reference depth of discharge
I_{dis_ave}, I_{ch_ave}	Average discharge and charge current
I_{dis_ref}, I_{ch_ref}	Reference discharge and charge current
T_{ref}, T_a	Reference temperature and ambient temperature

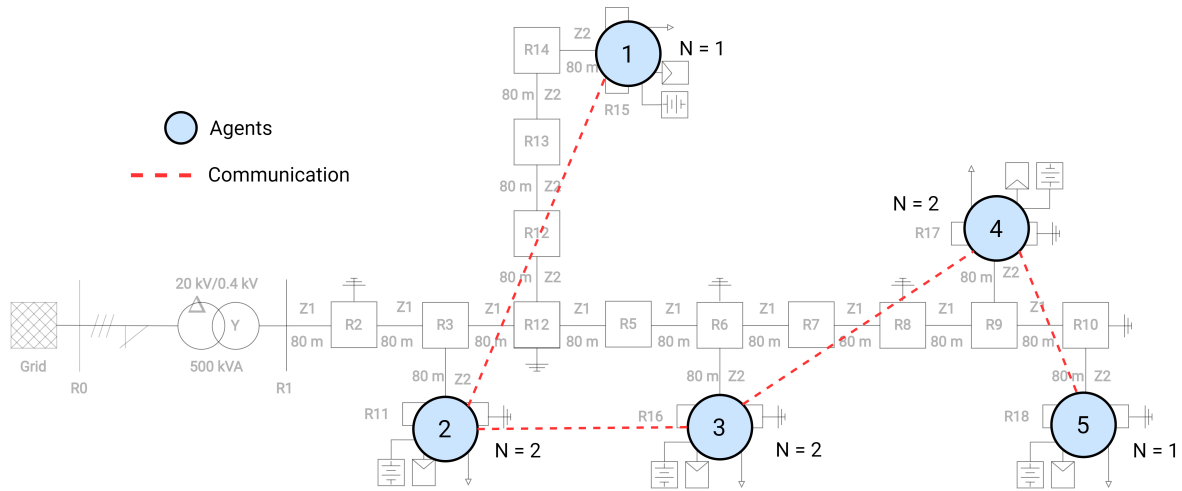


Figure 4.8: Communication network of the modified CIGRE LV distribution network. The agents form a line-shaped network. N indicates the number of neighbors each agent has.

SoC at the beginning and end of the cycle is 100% [70]. Furthermore, the model implies that the aging rate of batteries increases along with the increase in the magnitude of the stress factors, with an exception for ambient temperature. The aging effect becomes more apparent for ambient temperatures under very low and high magnitudes. Additionally, there are five parameters on top of the mentioned variables that need to be identified ($N_{c_ref}, \xi, \gamma_1, \gamma_2, \psi$). These parameters are determined using life cycle curves at different cycling conditions, usually given in battery datasheets [70]. To understand the derivation of these parameters, readers can refer to [70].

The aging model used in this work is embedded in the generic battery model block in Simulink, and it takes in current and ambient temperature as inputs. However, it cannot simply take the irregular cycling profile provided by the quasi-static load flow simulation due to the way how a cycle is calculated in the existing model. Considering this limitation, a synthetic cycling profile based on the worst operating condition of the battery when using the proposed control is made. Four parameters are considered for this cycling profile, namely maximum charging/discharging current, maximum SOC, and minimum SOC. The synthetic profile used for this work is shown in Figure 4.9, while a summary of the parameters of the synthetic cycling profile is presented in Table 4.5.

The synthetic cycling profile is a series of charging and discharging at a predefined SOC range and maximum charging/discharging current. It starts with a discharging process from a specified maximum SOC under a maximum discharging current. Once the minimum SOC limit is reached, the battery is charged under the maximum charging current until its maximum SOC is reached again.

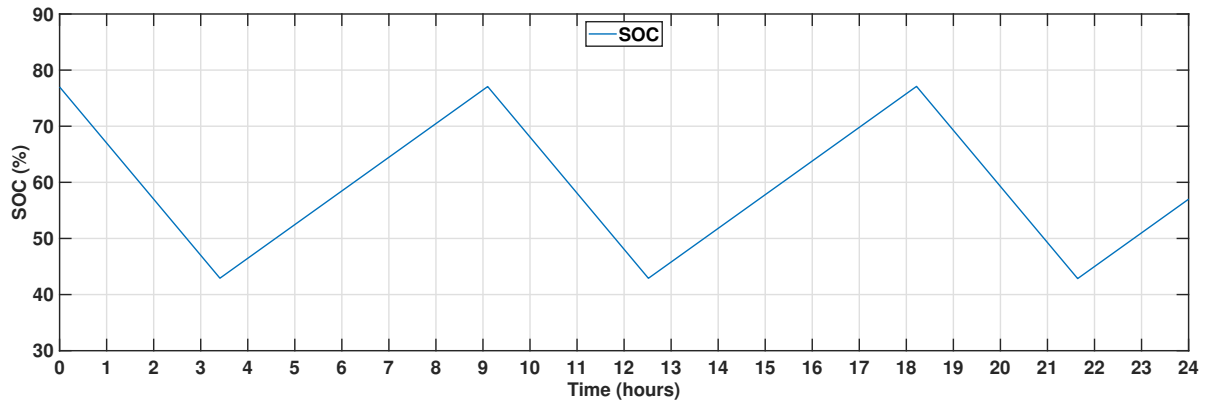


Figure 4.9: Synthetic regular cycling profile based on worst operating conditions of BESSs

Table 4.5: Synthetic cycling profile parameters for battery lifetime estimation

No.	Parameter	Value
1	Max. discharge current	0.1 C
2	Max. charge current	0.06 C
3	Max. SOC	77%
4	Min SOC	43%

There are several limitations and assumptions considered when evaluating battery lifetime for the proposed control. First, only the SOC profile from the BESS experiencing the worst voltage violation (i.e., BESS18) is taken because the BESS is predicted to contribute the hardest. Second, by taking the synthetic cycling profile, the result may not accurately depict the aging characteristic from using the proposed control. However, using maximum values as the cycling variables can give a safe estimation of the battery's lifetime. Third, the overall estimation model is decoupled from the quasi-static load flow simulation of the CIGRE LV network model to allow faster simulation time. Fourth, the temperature effect in Equation 4.4 is ignored due to the very low operating current later explained in Chapter 5. Lastly, It is assumed that the cells within the battery pack are perfectly balanced and have uniform characteristics. In practice, some cell-to-cell variation is common.

5

Simulation results and discussion

This chapter presents the simulation results of the proposed control strategy in a CIGRE LV network and its implication on battery lifetime. Section 5.1 discusses the voltage profiles and BESS participation behavior during voltage support under different test cases. In Section 5.2 the estimated lifetime of the BESS when using the proposed strategy is discussed.

5.1. Voltage behavior and BESS participation

This section aims to evaluate the proposed control's behavior with a focus on the voltage profiles of the buses of the CIGRE LV network and BESS participation. Four case studies presented in Chapter 4, with each having two variations, are tested against the proposed control.

5.1.1. Base Case

The base case includes a variation where no BESS is present and another variation that includes the proposed control. The no-BESS variation serves as a comparison basis for the proposed control strategy. The other variation demonstrates the voltage support action when using the proposed strategy.

CIGRE LV Network With No BESS

Voltage limits are violated when there is no voltage control implemented in the modified CIGRE LV Network. As depicted in Figure 5.1a, voltage limits of 1.05 p.u. and 0.95 p.u are being broken. In more detail, overvoltage is observed in buses R16 to R18 during the peak generation period (between Time = 11 hours and 15 hours), while undervoltage is observed in every bus except for R11 during peak demand (Time = 19 hours). The maximum voltage that corresponds to this violation is 1.068 p.u., whereas the minimum is 0.913 p.u.

Through observation of the resulting voltage profile, the similarity between the voltage and the mismatch profile previously shown in Figure 4.5 can be highlighted. The voltage rises in proportion to the increase in the positive mismatch. Conversely, voltage drops in the presence of a negative mismatch. This similarity reflects the relationship between bus voltage and net power depicted in Equation 2.9.

Another interesting point which is also a reflection of Equation 2.9 is the relation between violation severity and bus distance from the MV/LV transformer. Voltage violations are more severe in buses that are further away from the grid (i.e., bus R18 compared to R11). This owes to the higher grid-to-bus line impedance for those far buses.

CIGRE LV Network With BESS and Distributed Control

Using the distributed control strategy, the BESSs participate evenly while tackling voltage violations. Overvoltage and undervoltage are eliminated as depicted in Figure 5.1b. On top of that, the BESSs demonstrate even participation as represented by their uniform utilization factor in Figure 5.2.

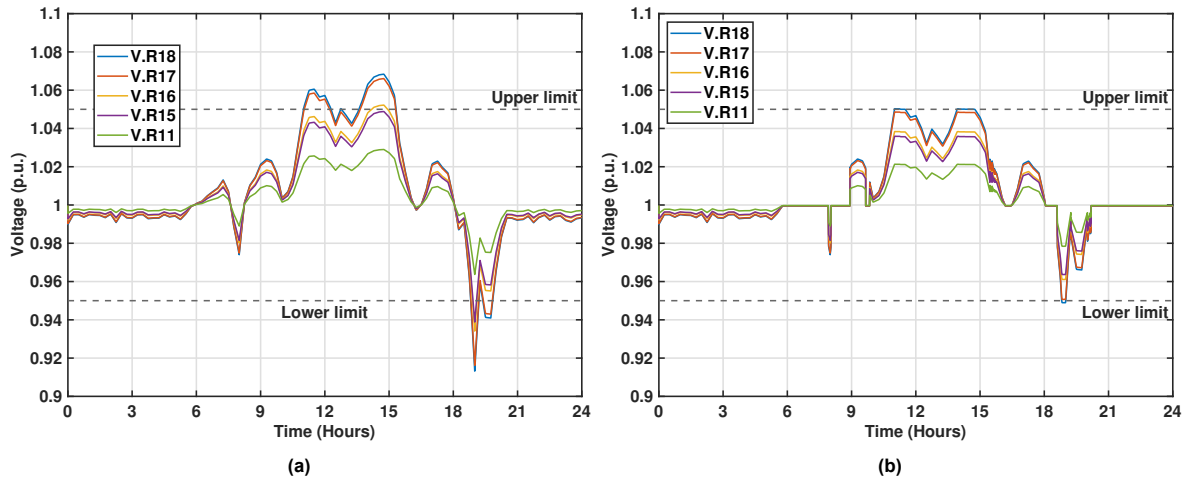


Figure 5.1: One-day voltage profiles of the buses in the modified CIGRE LV network: (a) Without BESS and (b) With BESS and proposed control. Voltage violation occurs in the absence of BESS.

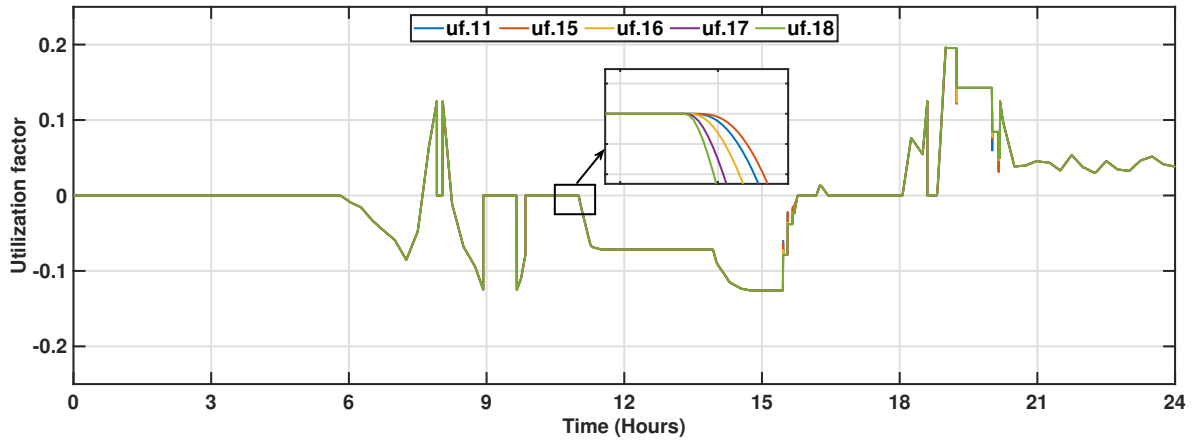


Figure 5.2: Utilization factor of the BESSs in the modified CIGRE LV network. The BESS under the worst voltage violation leads the change in the utilization factors.

Further observation from the BESSs' utilization factors shows the information-sharing behavior of the BESSs when using the consensus algorithm. Generally, the BESS under worst voltage violation leads the change of other BESSs' utilization factor followed by the BESSs closest to the information provider for a given communication graph. This premise is explained by the order of change in the utilization factors when voltage violation occurs, shown in Figure 5.2. In the detailed view of the figure, the utilization factor for BESS18 drops first, and subsequently for BESS17, 16, 11, and 15. Moreover, the change follows the order of the agents in the communication network according to Figure 4.5.

In addition to the voltage control feature, the proposed distributed control allows the BESS to charge and discharge when voltage support is not needed (during SOC control mode). The behavior of the SOC control mode is reflected in Figure 5.3a by instances when the voltage profile lays flat at 1 p.u. The net power in the buses during that time is fully compensated by the BESS and therefore the measured voltage does not deviate from its normalized value.

With regard to SOC, charging and discharging of the BESSs while not used for voltage support allows them to keep their SOC within a predefined limit. As shown in Figure 5.4a, the BESSs' SOC are brought back to between 50 and 55 % at the end of the day. By keeping this limit the BESSs are ensured to be ready to support network voltage on any occasion.

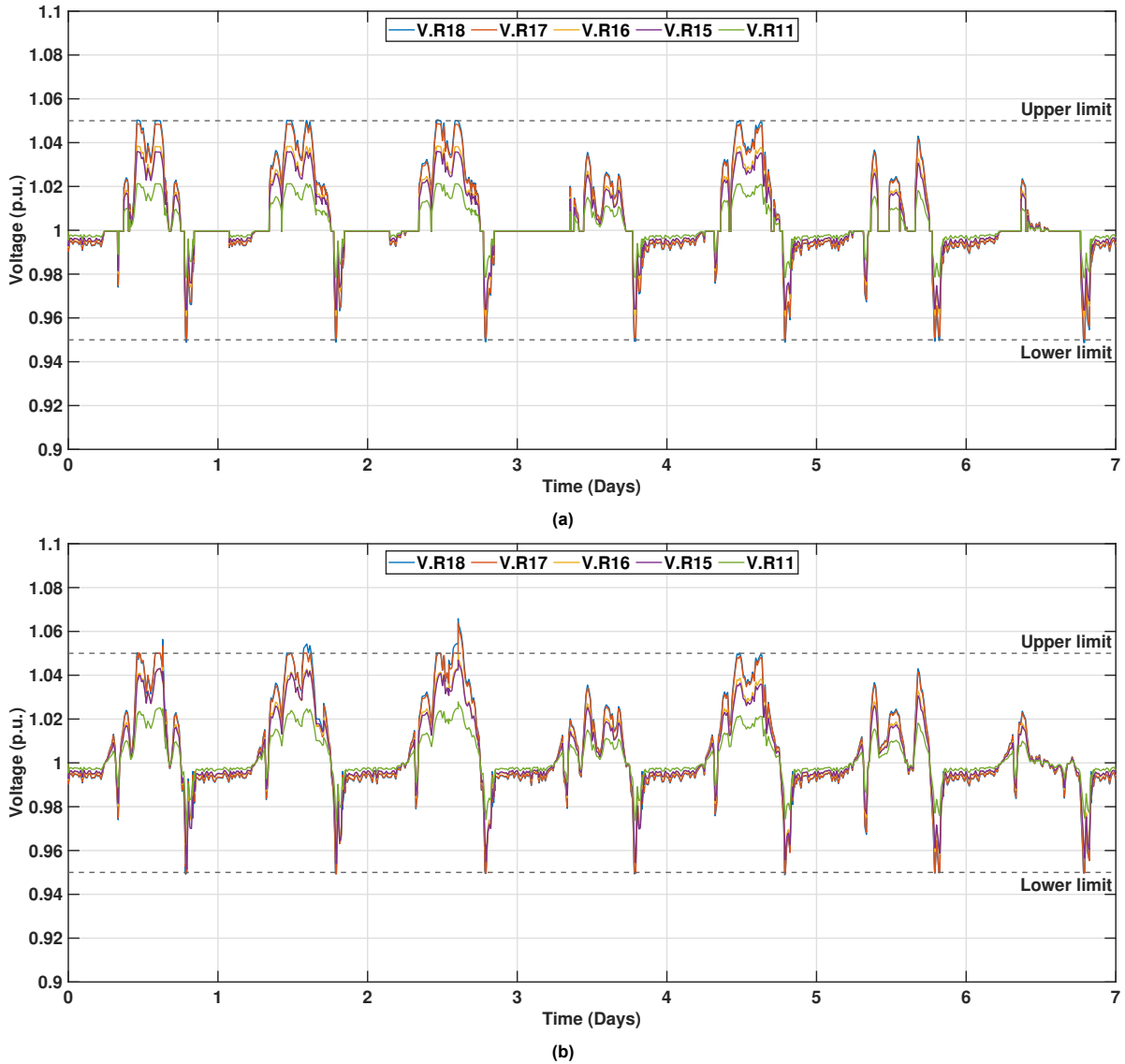


Figure 5.3: Seven-day bus voltage profiles in the modified CIGRE LV network: (a) Using proposed control and (b) Using decentralized control only.

To further highlight the advantage of the distributed control, the voltage behavior in the modified LV network is also compared to when only using a decentralized control strategy. As previously indicated decentralized control strategy is the simplest form of voltage control when using BESSs. Similar to the proposed control, this strategy aims to keep the bus voltages within a predefined range between 0.95 and 1.05 p.u. The main difference is the absence of a consensus algorithm in the decentralized strategy.

By using decentralized control, the voltage violations in buses R15 to R18 that are present in Figure 5.1a are eliminated, but not fully as shown in Figure 5.3b. However, voltage support is only performed by BESSs in locations with voltage violations but not where the voltages are normal. This means there is a disproportionate level of participation from the BESSs as some of the buses do not experience any violation at all. Consequently, some of the BESSs become saturated early as depicted by the SOC of BESS18 in Figure 5.4b. With such SOC behavior, the BESS experiencing the worst voltage violation may not be ready to absorb or inject power because they have been charged or discharged to their SOC limit. This may lead to the compromise of the voltage support capability.

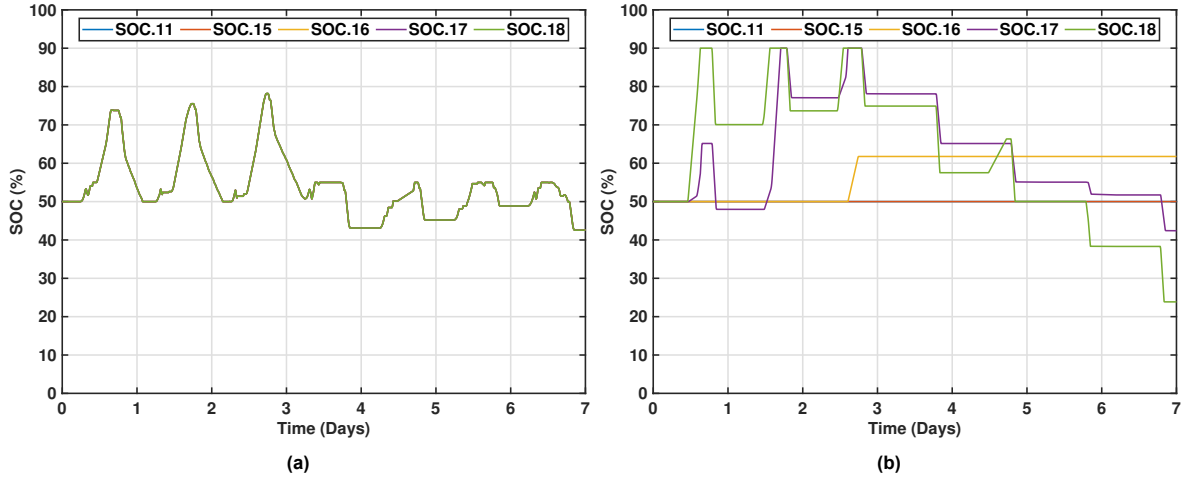


Figure 5.4: Seven-day SOC profiles in the modified CIGRE LV network: (a) Using proposed control and (b) Using decentralized control only.

Table 5.1: Initial SOC of the BESSs

		BESS11	BESS15	BESS16	BESS17	BESS18
SOC Variation	A	40%	40%	45%	50%	55%
	B	30%	40%	50%	70%	90%

Aside from compromise in voltage support capability, disproportionate participation from decentralized control leads to different aging characteristics between the BESSs. For example, the maximum charging capacity of BESS18 is shown to be repeatedly reached during seven days of simulation in Figure 5.4b, while BESS11 and BESS15 have zero participation. Following this SOC behavior, BESS18 will age faster compared to the other BESSs due to being cycled more. Details on the impacts of a battery's number of cycles toward its aging characteristic will be described in Section 5.2.

5.1.2. BESS Under Varying initial SOC

This subsection demonstrates the BESS operation under two variations of different initial SOC. The first tries to demonstrate the convergence behavior of the SOC to uniformize voltage support readiness by the end of each day (Figure 5.5). The second presents a situation where one of the BESSs has reached its maximum capacity (Figure 5.6). The initial SOC values assigned to each BESS for both variations are presented in Table 5.1.

Small SOC Difference

Under a small SOC difference, voltage regulation is achieved with the BESSs' SOC converging by the end of the first simulation day. This convergence is mainly due to the SOC controller defined in Subsection 3.2.3 where the battery is charged under positive mismatch or discharged under negative mismatch up to a specified SOC limit. The way how the SOC controller works can be explained by thoroughly following the SOC and power profile of BESS18.

Figure 5.5b shows the SOC profile of BESS18. In the figure, BESS18 is discharged from a 55% charge to a limit of 50% due to a negative mismatch at the start of the day. The mismatch in this period is small, and thus will not cause any voltage violation. After the discharged limit is reached, BESS18 stays idle as indicated by Box 1 in Figure 5.5b, where there is zero power because there is no voltage violation. The other BESSs also stay idle because they are either at 50% SOC or below. In Box 2, a positive mismatch is present; therefore all the BESSs are charged to reach 55%. In this regime, the 55% SOC limit is reached the fastest by BESS18 and so it goes to idle mode before the other BESSs. Box 3 shows the BESSs being discharged at negative mismatch and finally converging at 50% SOC. From that point onwards, the BESSs work normally, similar to when they have the same initial SOC.

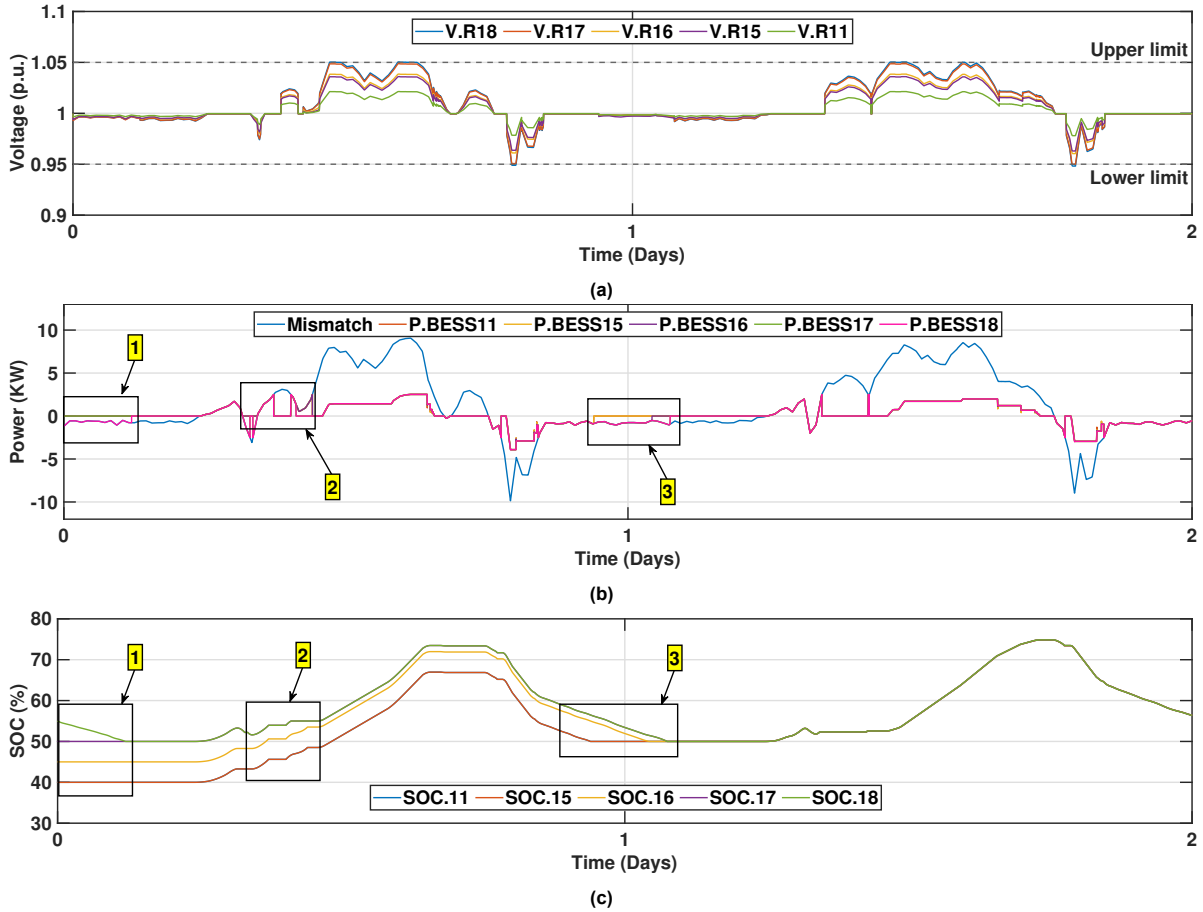


Figure 5.5: Proposed control under slight initial SOC difference - Variation A: (a) Voltage, (b) Power, and (c) SOC profiles. Positive power values indicate charging.

Extreme SOC Difference

BESSs with the proposed control strategy are also able to provide voltage support under extreme initial SOC differences. Throughout the three-day simulation, only a small overvoltage is present during the first day as shown by a detailed view in Figure 5.6a when BESS18 is charged to its maximum limit and cannot provide further voltage support. The overvoltage, however, happens for a very short period when BESS18 transitions to stop charging.

As a result of one BESS being unavailable, other BESSs that have the capacity will work harder to compensate for any missing contribution. A detailed view in Figure 5.6b shows the charging power of BESS11 through 17 increase to a little under 5 kW when the power of BESS18 transitions from 2.5 kW to zero. Furthermore, BESS11 through 17 maintain their power for as long as the peak generation period and then stand by for the next voltage support.

With regard to SOC convergence, the SOC controller under extreme SOC difference works similarly to the previous case and convergence can also be reached. As seen in Figure 5.6c, the SOC of all BESSs aim toward a uniform value in the range of 50 to 55% according to the controller parameters. Compared to the case where the SOC difference is small, the BESSs' SOC takes longer to converge. Despite the lengthier convergence, the voltage support capability of the proposed strategy is not hampered. To achieve faster convergence, the charging/discharging power limit can be set to a larger magnitude; hence, allowing the BESSs to reach the 50 to 55% range quicker. However, a careful tuning process must be performed to prevent control failure due to a very fast transition from SOC control to voltage control.

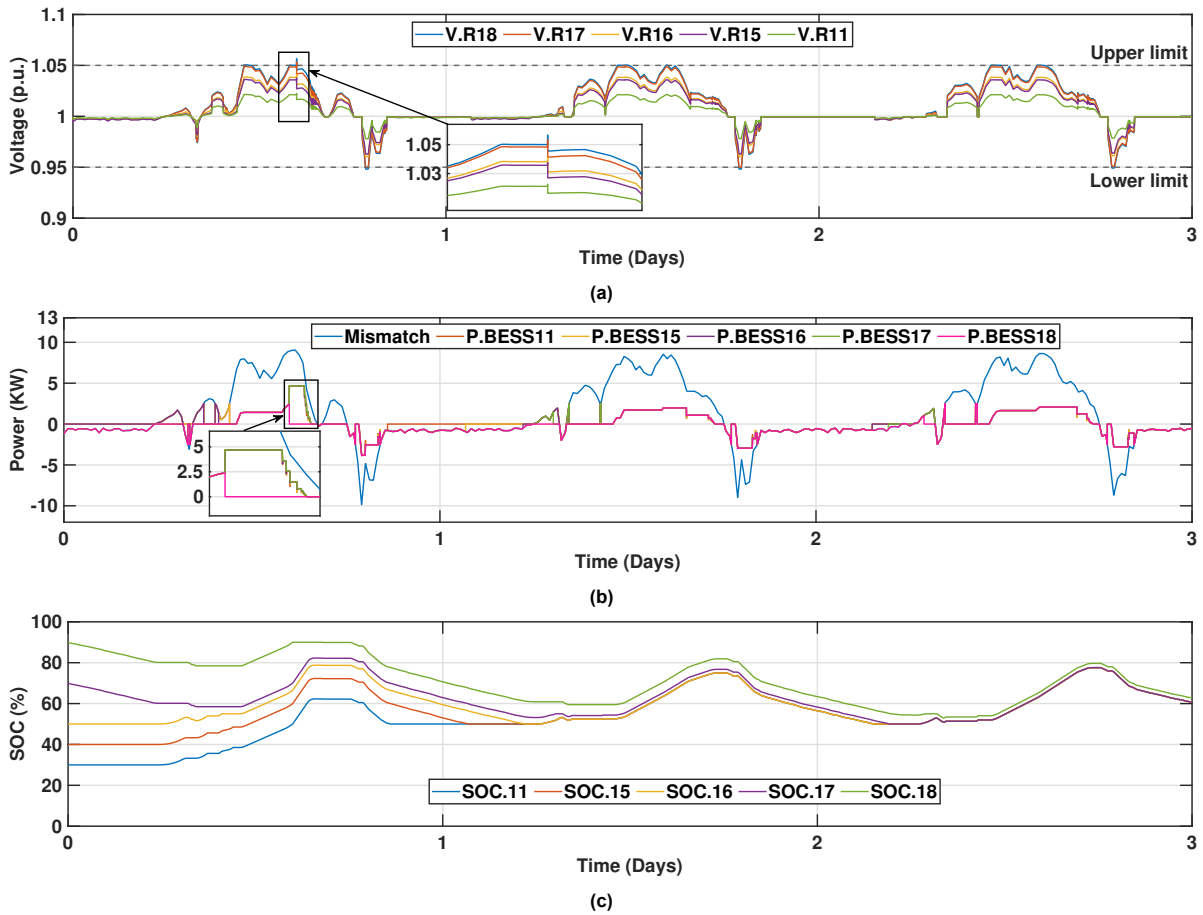


Figure 5.6: Proposed control under extreme initial SOC difference (variation B): (a) Voltage, (b) Power, and (c) SOC profiles. Positive power values indicate charging.

5.1.3. BESS Under Seasonal Change

The proposed control and BESSs are also tested against a week of winter and a week of autumn. The specific days of winter week correspond to 15 to 21 January, which represents days where there is little to no sunlight available during the day. Meanwhile, 15 to 22 October is taken for the autumn week to represent a transitory period between summer and winter. It is assumed that a week in spring is similar to a week in autumn in terms of sun hours; therefore, only the latter is taken for the simulation of the transitory period.

Winter

During winter months, the proposed control and BESSs are not able to continuously prevent undervoltage but can normally mitigate overvoltage. This is displayed in Figure 5.7a, where the bus voltages fall below the predefined limit of 0.95 p.u. toward the end of the fourth day of the simulation. The inability of the BESSs in preventing undervoltage is a consequence of the few to no positive mismatch occurrence as illustrated in Figure 5.7b. As a result, the BESSs SOC is declining when compared to each simulation day, and finally, the BESSs' minimum SOC limit of 10% are reached (Figure 5.7c). When this limit is reached, the BESSs cannot provide any more power.

To overcome the lack of energy when supporting network voltage in the winter period, the BESSs need to be charged more before peak demand hours. One way to achieve this is by scheduling the BESS charging outside of the peak demand period on top of the defined charging rules. For example, an intuitive approach is to set charging outside of voltage support during the day at around 11:00 to 17:00, when there is low demand according to the demand profile in Figure 4.3b. Alternatively, the optimal time of charge can be determined by first predicting the time of low demand using a data-driven approach. A combination of historical data and a machine learning algorithm can be used to map out the

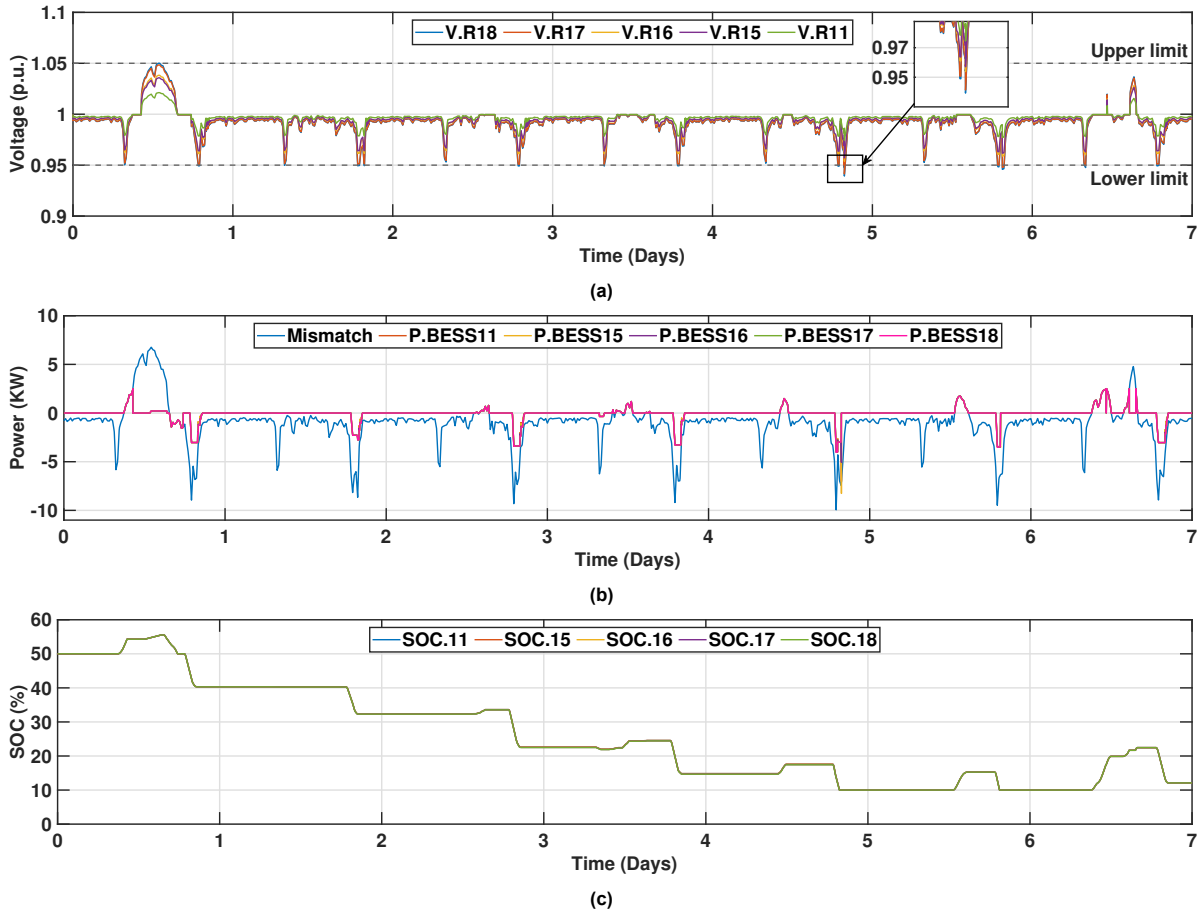


Figure 5.7: Proposed control in winter period: (a) Voltage, (b) Power, and (c) SOC profiles. The SOC of each BESS is generally declining from the first to the last day of simulation.

typical consumer load profile during winter. However, since this charging strategy involves machine learning, the challenge would be finding a good data set.

Besides scheduled charging, a straightforward but less effective approach is to add PV generation. Adding more PV will boost positive net power generation during the day and therefore allow the BESSs to store energy to be used during peak demand periods. This approach, however, has limitations especially when considering the summer case. Due to more PV being introduced, there will be a rise in the positive mismatch peaks and therefore leading to overvoltage in the network. The effect of added PV generation on the voltage support capability is discussed in detail in Subsection 5.1.4.

Autumn

During the autumn period, the proposed control strategy can provide voltage support in a similar fashion to the base case. Bus voltages are kept between 0.95 and 1.05 p.u. while SOC profiles are maintained between their maximum and minimum limits as shown in Figure 5.8a and 5.8c, respectively. This similar performance between the two cases is because of their comparable mismatch profile. Their only difference is that in the week taken for autumn, there are days where the positive mismatch is close to zero. Nonetheless, their magnitude of peak generation in the rest of the week is similar at around 9 kW.

One important note from the simulation provided in this work is that the mismatch profile of the autumn period is taken while assuming the middle of autumn as an average representative. In reality, the mismatch profile will vary depending on the day and month of the season as well as the data source. For example, if the mismatch profile is taken from the early period of autumn such as September, the results will resemble the base case more. Conversely, if the later month of autumn is used, the results will be closer to that of the winter period.

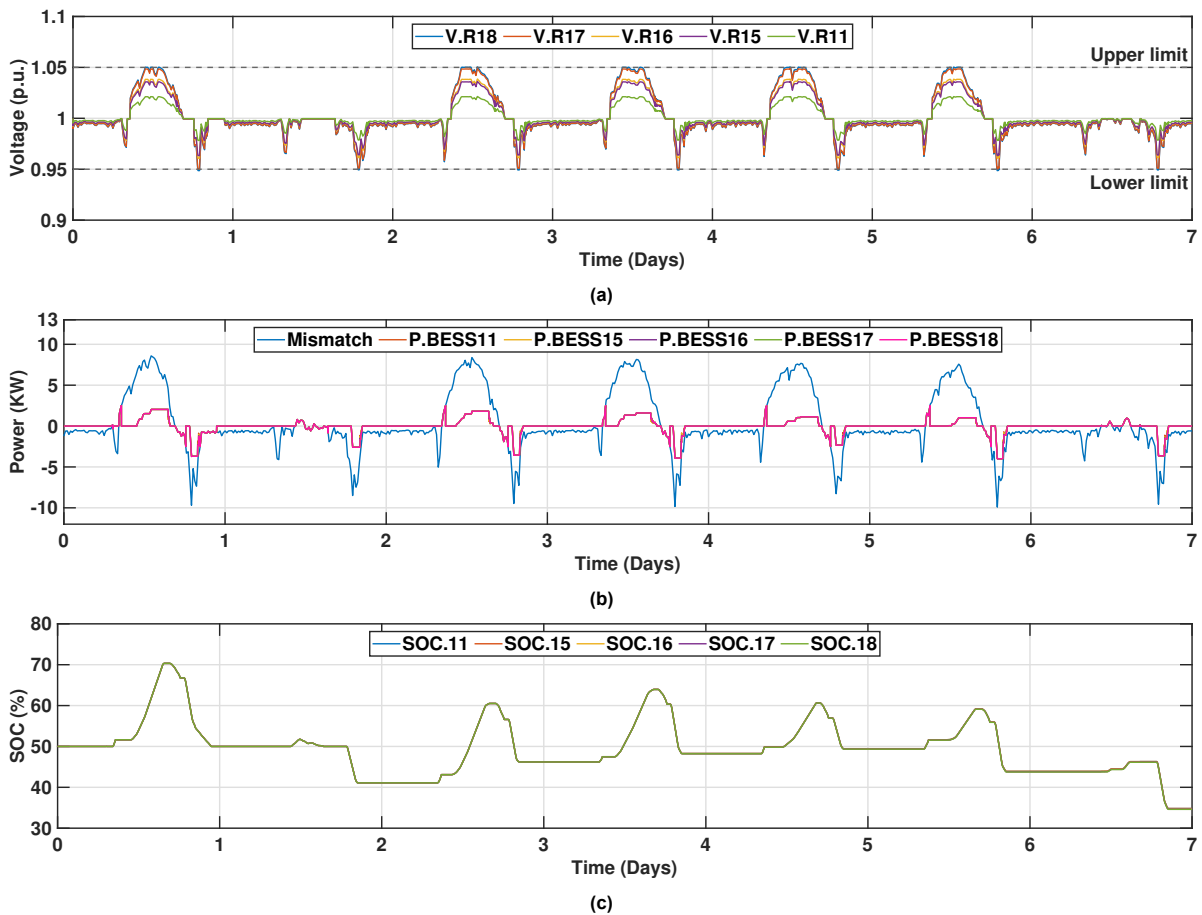


Figure 5.8: Proposed control in autumn period: (a) Voltage, (b) Power, and (c) SOC profiles. The general behavior of the BESSs is similar to the base case.

5.1.4. BESS Under Varying PV Penetration

The last test for the proposed control involves two variations of PV generation in the network. The first variation involves adding 10% more PV to the base case, while the second adds 25% more. Figure 5.9 depicts the voltage, power, and utilization factor profiles from a one-week simulation when 10% PV is added, while Figure 5.10 shows the profiles under 25% addition with respect to the base case.

Generally, adding more PV generation speeds up the charging of BESSs due to higher generation peak values and longer periods of positive mismatch. Higher peaks lead to more power required to be absorbed by the BESSs, which consequently increases the possibility of overvoltage. Meanwhile, the likelihood of undervoltage decrease due to the large reserve of energy that the BESSs store during the day. Details of this behavior can be observed from the following case-by-case description.

+10% Addition

Although small changes can be observed compared to the base case, adding 10% PV generation with respect to the base case poses a small risk of compromising the proposed control and BESSs voltage support capability during peak generation periods. This risk owes to the limited capacity of the BESS to absorb power if overvoltage were to happen. As seen in Figure 5.9c the BESSs are charged to their maximum SOC limit of 90% on the third day of simulation. Supposedly, any higher positive mismatch would cause voltage violation. However, the maximum SOC limit is only reached after the peaks that would otherwise cause an overvoltage have settled down.

Contrary to operation during peak generation periods, operation of BESSs in supporting voltage during peak demand presents no problem. For example, as seen inside the detailed view in Figure 5.9c the BESSs are only depleted by a little more than 10% to provide voltage support during the peak demand

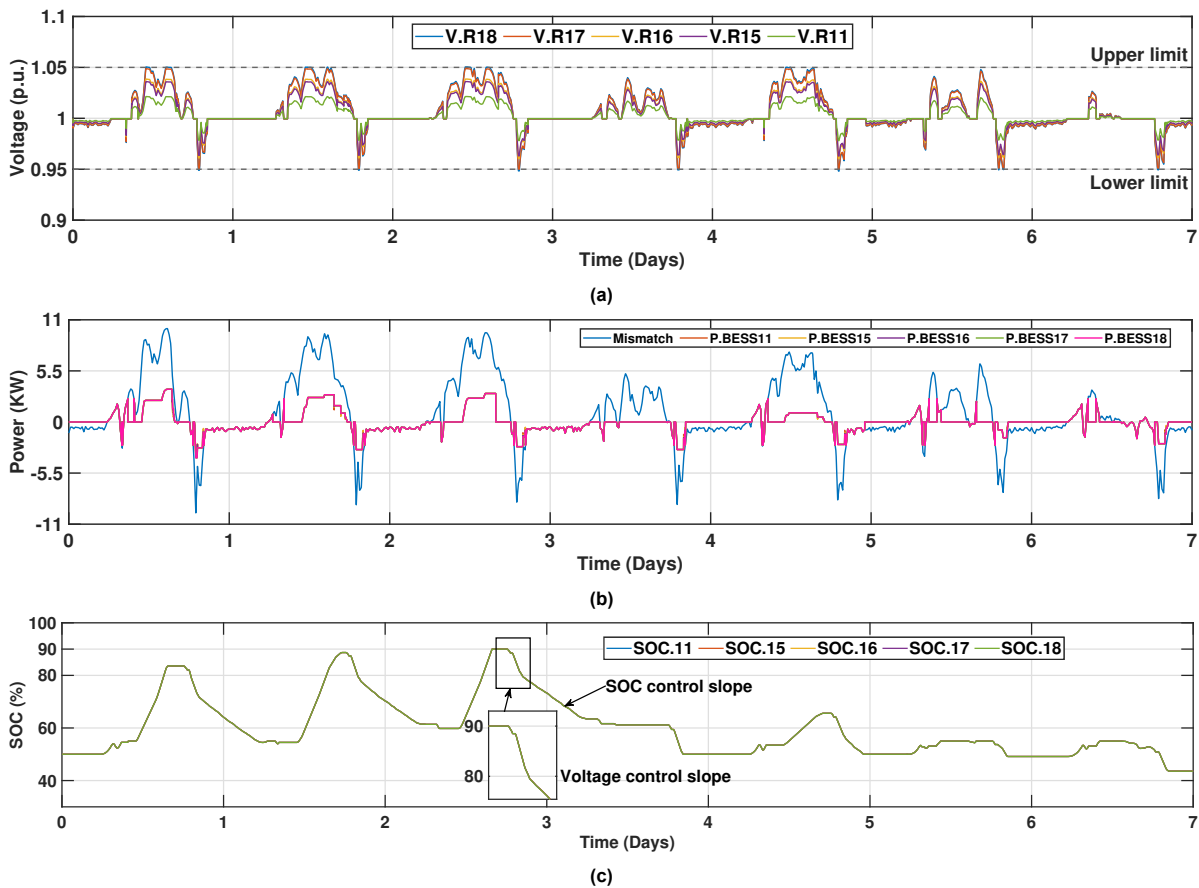


Figure 5.9: Proposed control with +10% PV w.r.t base case: (a) Voltage, (b) Power, and (c) SOC profiles. The BESSs hit their charging limit at the end of the second day. Moreover, The SOC controller works to maintain the BESSs' charge as

period. Moreover, the remaining SOC after providing voltage support are far from their minimum limit of 10%. Consequently, the BESSs have large reserves of energy to prevent undervoltage. Following voltage support, SOC control takes place to maintain the BESSs' charge at 50 to 55% by discharging the abundant stored energy as shown by the voltage control slope.

+25% Addition

When power generated from PV is further added to +25% with respect to the base case, BESSs are only able to provide partial voltage support during peak generation periods. In more detail, voltage jumps can be observed in the first three days of the simulation as depicted in Figure 5.10a. During the peak period of the first day, the voltage in bus 18 is measured at a little over 1.08 p.u. Meanwhile, the measurement on the second and third day has similar values to the first day.

The jump is mainly caused by the inability of BESSs to absorb excess generation. Figure 5.10c shows this inability as the BESSs reach their maximum capacity of 90% SOC around the same time as the peak generation. Due to the inherent characteristic of the BESSs, the charging power is immediately cut off resulting in the jumps.

Despite experiencing voltage jumps during the peak generation period, the voltage support capability of the BESSs during peak demand periods remains unchanged compared to the base case. Moreover, the capability matches that of the +10% PV case because both cases have excess PV. Besides, the BESSs' charges are far from its minimum SOC limit of 10% throughout the simulation.

From these two cases, it can be implied that the inability of BESSs to support voltage at a high PV penetration boils down to its lack of capacity. A simple solution to prevent it is for the BESSs to be sized larger; thus, allowing more energy to be absorbed in peak generation periods. Alternatively,

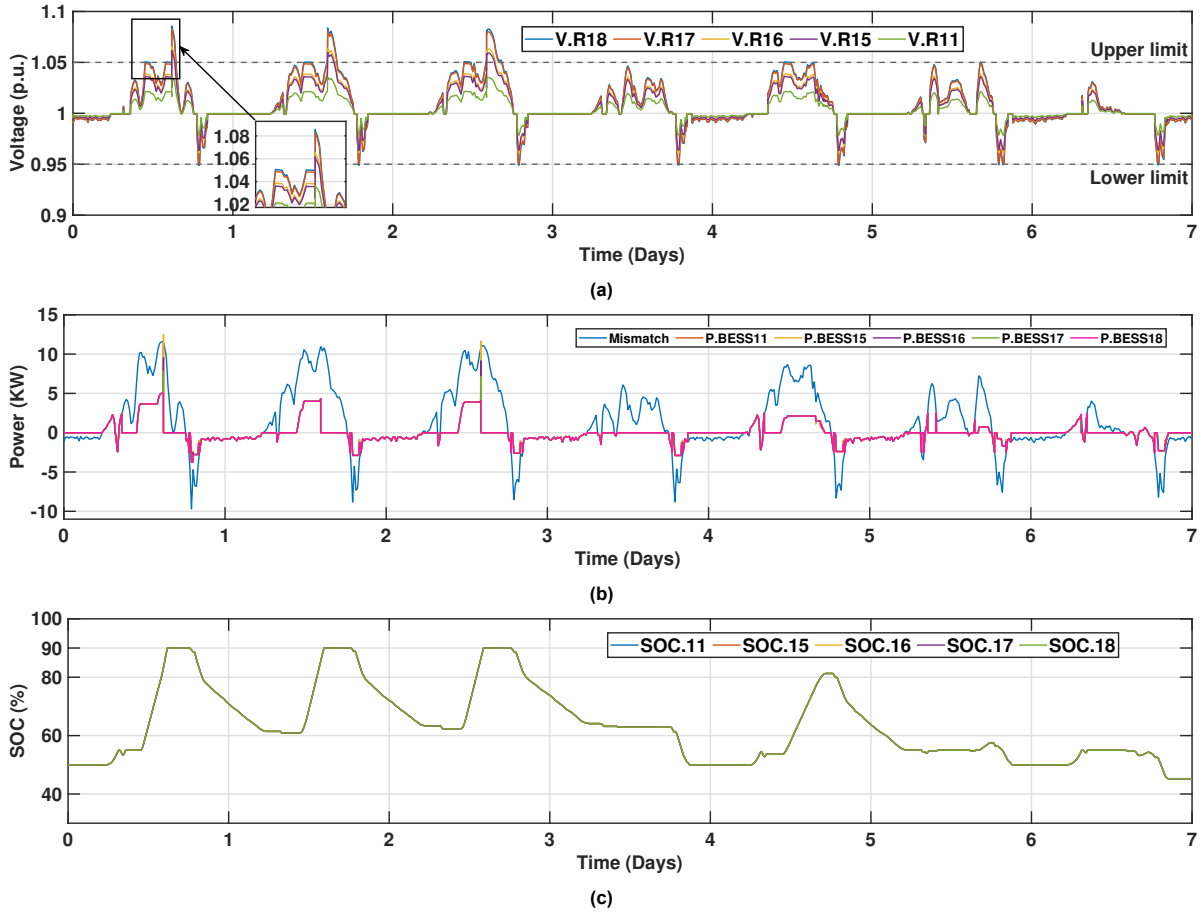


Figure 5.10: Proposed control with +25% PV w.r.t base case: (a) Voltage, (b) Power, and (c) SOC profiles. The BESSs hit their charging limit at the end of the second day.

reactive power control and PV curtailment can be used in combination with the BESSs to cater to large peaks. The idea of curtailment is that the power production is cut down from the PV; therefore, less power is being injected into the grid. Lastly, although not considered in this work, a combination of the proposed voltage control method with EV smart charging can be implemented. EVs are essentially distributed batteries with similar capacity range to residential-scale BESSs, but with the possibility to be moved around. Coordinating the charging time and power of these EVs can also help alleviate overvoltage in LV distribution network.

5.2. Battery Lifetime Estimation

Besides behavior evaluations of the proposed control strategy, its effect on battery lifetime is also investigated. BESS18, being the battery located in the bus under the most severe voltage violation, is used as a representative for the worst-case scenario. Using the methods presented in Chapter 4 the battery lifetime of BESS18 based on four stress factors is estimated.

Generally, there is no significant effect on the battery's maximum capacity when using the proposed control strategy. This can be observed in Figure 5.11 where only a small and linear decline is present in the battery's maximum capacity over one simulation year from 104.23 Ah to 103.23 Ah. In percentage terms, this corresponds to a 0.95% loss with respect to its initial maximum capacity. To illustrate the significance of the capacity loss, end of life capacity for a battery is usually defined as 80% of its beginning-of-life capacity. If the capacity calculation were to be extrapolated, the battery would still be available for approximately 20 years. On a side note, there is a small difference in the battery's maximum capacity presented here and in Chapter 4 due to the parametrization process before the simulation.

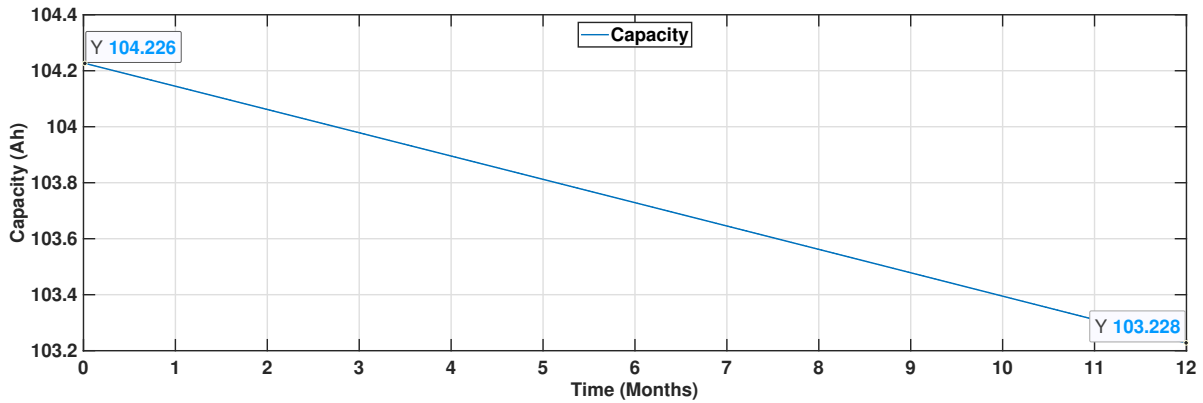


Figure 5.11: Maximum battery capacity in Ah (one-year simulation).

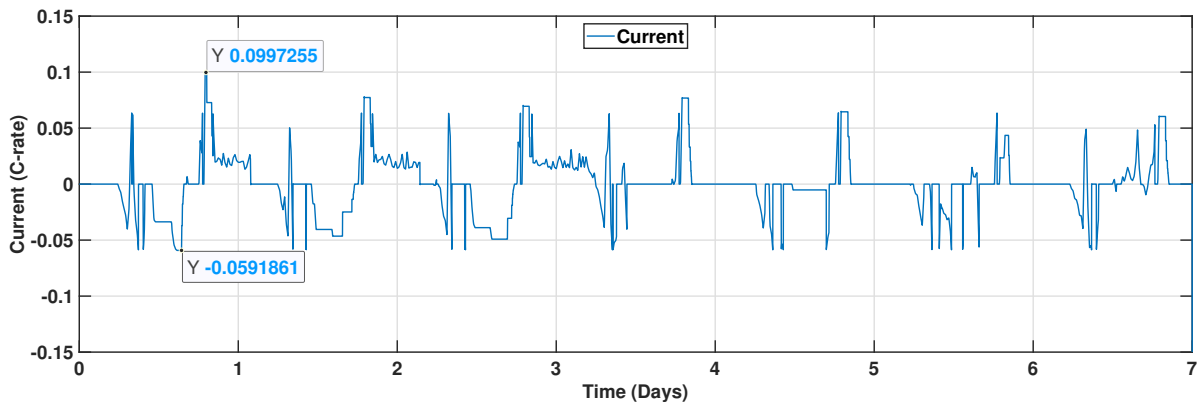


Figure 5.12: Battery current in C-rate (one-week simulation). A positive value indicates discharging while a negative value indicates charging.

It is important to note that the lifetime estimation is a result of a synthetic cycling profile. That cycling profile takes the worst operating condition of a real profile as its parameters. Moreover, there are more cycles in a day when using the synthetic profile. With that in mind, the real cycling profile would theoretically result in longer life because it imposes less stress on the battery.

One main factor that causes the maximum capacity loss to be small is the small current drawn or injected into the battery. This is depicted in Figure 5.12, where the maximum discharging current and maximum charging current is approximately 0.1 C and 0.06 C (corresponding to a maximum capacity of 100.8 Ah). As already explained in Section 4.6, a large current magnitude results in a great capacity fade, and conversely, small current yields a small capacity fade [70]. Compared to the battery manufacturer's testing current of 3 A (1.25 C) in charge mode and 20 A (8.3 C) in discharge mode at a cell level, the simulated charge and discharge current is only a fraction.

Besides small current magnitude, small capacity fade is also a result of a small depth of discharge. Looking back at the weekly SOC profile in Figure 5.4a, the battery is only operated on a narrow SOC range of 43 to 77%; thus corresponding to a depth of discharge of 34%. To complement the DOD observation, the number of equivalent cycles should also be into account, which in the simulation is shown to be 111 after one year as seen in Figure 5.13. For comparison, the ANR26650M1-B cell used in this work is expected to be able to carry out more than 1400 cycles before its end-of-life capacity when operated under 100% depth of discharge. The depth of discharge and the number of equivalent cycles from the simulation are only a fraction compared to the manufacturer's specification and hence the small capacity fade result.

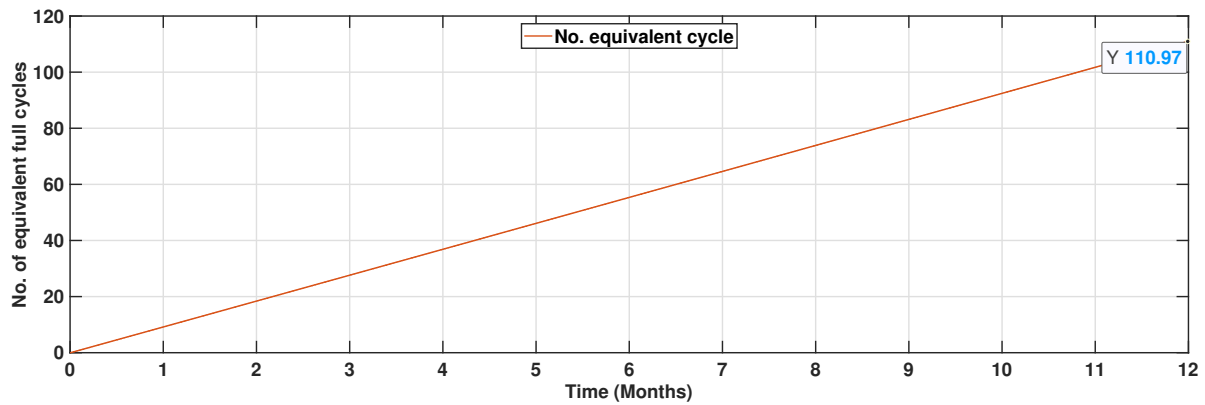


Figure 5.13: Number of equivalent cycles (one-year simulation).

Despite the cycling effects from the proposed control strategy being known to be small, the effect of calendar aging is not investigated in this work. As indicated in Chapter 1 this work focuses on the effect of cycling on battery lifetime; thus, calendar aging is omitted. However, the battery's operating current is found to be low, so it is important to consider the aging of batteries when in idle condition. For context, LFP-type batteries generally exhibit 3-5% fade relative to their initial maximum capacity after a year of idleness at 25°C [80], [81], [82]. This implies the calendar effect might be more substantial than the cycling effect in the types of operations presented in this work.

5.3. Results Summary

To close this chapter, the important takeaways from simulating the proposed control strategy and its effect on battery lifetime are presented in Table 5.2.

Table 5.2: Key points of simulation results.

Voltage support behavior		
Case study	Battery SOC (%)	Voltage support
Base	Uniform SOC throughout simulation	0.95 - 1.05 p.u. limits obeyed
SOC variation	Battery SOC converge to a uniform value	-
Season variation	Generally declining in winter	Limited support in winter
PV variation	Maximum SOC limit reached on +25% PV	Overvoltage on +25% PV
Lifetime estimation		
Maximum capacity	Small decline (0.95%/year)	
Battery current	Small with respect to manufacturer specification (0.15 C and -0.06 C)	
Depth of discharge	34% compared to manufacturer testing at 100%	
Equivalent cycle	A fraction compared to manufacturer specification (110 cycles/year)	

6

Conclusion

In this work, a distributed control strategy for residential BESS which aims to provide voltage support has been formulated. The proposed strategy has been tested in a MATLAB/Simulink simulation of an LV distribution network under variations of case studies. Furthermore, insights into the battery lifetime when using the proposed strategy have been made.

Conclusive remarks of this work answer four research sub-questions presented in the introduction:

1. **How is the voltage behavior of an LV network under high PV penetration?**
2. **How does the proposed distributed BESS control strategy affect the voltage performance of an LV network?**
3. **How is the control behavior of the proposed strategy when performing voltage support?**
4. **How does the proposed control strategy affect battery lifetime?**

In an LV network with high PV penetration, the voltage rises or drops proportionally to the power mismatch and can violate limits during peak periods. Overvoltage can occur during peak generation periods and conversely, undervoltage occurs in peak demand periods. Moreover, voltage violation is more severe in buses that are further from the MV/LV transformer. This is a result of the impedance of a line leading to a bus becoming larger as they span further away from the transformer. As the impedance becomes larger, so does the voltage difference measured between the transformer and the bus according to Equation 2.9.

The proposed control strategy can provide voltage support in an LV network. In more detail, the control strategy commands the BESSs in the LV network to absorb or inject power in the case of a large mismatch. Furthermore, the voltage support burden is shared among the BESSs to prevent disproportionate contributions using the consensus controller. Additionally, the proposed control strategy works over an extended period of time owing to the help of an SOC controller to maintain the BESSs at a certain SOC level.

The proposed strategy has also been tested against various operating conditions. Under extreme initial SOC variation, the proposed strategy allows the BESSs to share their voltage support burden in the case of one BESS being unavailable. Additionally, it also allows the different BESS SOC to converge with the help of an SOC controller. Regarding PV variations, the addition of PV generation speeds up the charging of BESS due to more power, and thus larger battery capacity might be required to prevent early saturation. As for season change, the proposed strategy can work during the transitory season but can only partially support voltage in winter as very few charging windows from positive mismatch are present. A scheduled charging might be added to the proposed strategy to overcome this shortcoming.

Concerning battery lifetime, there is a small effect from the proposed strategy's cycling profile. Only a slight capacity fade of 0.95% over one year is observed when using the proposed strategy under the base case. This stems from the small operating current of the BESS when performing voltage support

under the proposed strategy. In addition to the small operating current, the small DOD from using the strategy also plays a role. Besides, calendar aging must also be taken into account due to the small operating current.

Answers to the research sub-questions help answer the main research question:

How can residential-scale BESSs be controlled in a distributed manner to regulate voltage in a low-voltage distribution network under high PV penetration while evaluating their battery lifetime characteristic?

All in all, a distributed control strategy that can regulate voltage in an LV network with high PV penetration has been made and tested. The strategy works in most of the test cases of varying initial SOC, PV penetration, and season change and is able to support voltage under an extended period of time. The resulting battery degradation from the proposed strategy is small as the BESSs are only exposed to small currents and small DOD.

6.1. Future Works

There are research gaps in the area of distributed control of BESSs, which have not been investigated due to the scope or time constraints of this work. To make further improvements from this work, several areas can be explored as follows:

- 1. Method to optimize communication network topology considering line losses:**
In the presented study, a communication network with a line topology connects all the BESSs to allow burden sharing. The contribution of each BESS is equally shared without considering the line loadings and losses. A method can be formulated to optimize the communication network topology and grouping of BESSs to minimize losses and congestion.
- 2. Combination of distributed control with a scheduled charging/discharging strategy:**
During the winter period, the proposed control was shown to be less effective due to less available sunlight. To combat this shortcoming, a scheduled charging/discharging strategy based on predictive methods on top of the proposed strategy is worth exploring.
- 3. Effect of calendar aging on BESSs:**
The lifetime evaluation in this work focuses on cyclic aging. However, the resulting cycling profiles from using the proposed strategy were found to be small, even with a synthetic, regular cycling profile due to its low operating current and narrow depth of discharge. To gain more insight into the degradation of batteries used in voltage support, an investigation into the calendar aging effects of the batteries is a possible direction.
- 4. Techno-economic analysis with respect to the estimated lifetime of the batteries and incentive mechanism:**
With insights into battery lifetime, a techno-economic analysis can be performed to investigate the feasibility of using BESSs in the presented manner and compare it to other use cases. Furthermore, the optimization of line losses mentioned in the first recommendation can also be translated into monetary terms.
- 5. Applications on electric vehicles and battery swapping stations:**
In some ways, electric vehicles and battery swapping stations are similar to residential BESSs as they are generally connected to LV networks and have the same range of capacity and power. The difference is that there are uncertainties associated with their available capacities as they are moved around and the charging behavior of consumers is challenging to predict. The technical feasibility of coordinating these storage assets for voltage support is worth investigating as their numbers are expected to increase in the future.

References

- [1] International Energy Agency (IEA), *Renewable Energy Market Update - June 2023*, <https://www.iea.org/reports/renewable-energy-market-update-june-2023>, License: CC BY 4.0, IEA, Paris, 2023.
- [2] A. Cortés, J. Mazón, and J. Merino, "Strategy of management of storage systems integrated with photovoltaic systems for mitigating the impact on lv distribution network," *International Journal of Electrical Power & Energy Systems*, vol. 103, pp. 470–482, 2018, ISSN: 0142-0615. DOI: <https://doi.org/10.1016/j.ijepes.2018.06.012>. [Online]. Available: <https://www.sciencedirect.com/science/article/pii/S0142061518306690>.
- [3] M. Z. Daud, A. Mohamed, M. C. Wanik, and M. A. Hannan, "Performance evaluation of grid-connected photovoltaic system with battery energy storage," in *2012 IEEE International conference on Power and Energy (PECON)*, IEEE, pp. 337–342, ISBN: 1467350192.
- [4] V. Kalkhambkar, R. Kumar, and R. Bhakar, "Optimal sizing of pv-battery for loss reduction and intermittency mitigation," in *International Conference on Recent Advances and Innovations in Engineering (ICRAIE-2014)*, IEEE, pp. 1–6, ISBN: 1479940402.
- [5] CIGRE, "Benchmark systems for network integration of renewable and distributed energy resources," CIGRE, Report, 2014.
- [6] T. J. T. Hashim, A. Mahomed, and H. Shareef, "A review on voltage control methods for active distribution networks," *Przeгляд Elektrotechniczny*, pp. 304–312, 2012.
- [7] P. Chaudhary and M. Rizwan, "Voltage regulation mitigation techniques in distribution system with high pv penetration: A review," *Renewable and Sustainable Energy Reviews*, vol. 82, pp. 3279–3287, 2018, ISSN: 1364-0321. DOI: <https://doi.org/10.1016/j.rser.2017.10.017>. [Online]. Available: <https://www.sciencedirect.com/science/article/pii/S1364032117313989>.
- [8] S. Alyami, Y. Wang, C. Wang, J. Zhao, and B. Zhao, "Adaptive real power capping method for fair overvoltage regulation of distribution networks with high penetration of pv systems," *IEEE Transactions on Smart Grid*, vol. 5, no. 6, pp. 2729–2738, 2014, ISSN: 1949-3061. DOI: 10.1109/TSG.2014.2330345.
- [9] H. Sun, Q. Guo, J. Qi, *et al.*, "Review of challenges and research opportunities for voltage control in smart grids," *IEEE Transactions on Power Systems*, vol. 34, no. 4, pp. 2790–2801, 2019, ISSN: 1558-0679. DOI: 10.1109/TPWRS.2019.2897948.
- [10] K. Prakash, M. Ali, M. N. I. Siddique, *et al.*, "A review of battery energy storage systems for ancillary services in distribution grids: Current status, challenges and future directions," *Frontiers in Energy Research*, vol. 10, 2022. DOI: 10.3389/fenrg.2022.971704.
- [11] M. Al-Saffar and P. Musilek, "Reinforcement learning-based distributed bess management for mitigating overvoltage issues in systems with high pv penetration," *IEEE Transactions on Smart Grid*, vol. 11, no. 4, pp. 2980–2994, 2020. DOI: 10.1109/TSG.2020.2972208.
- [12] Y. Wang, K. T. Tan, X. Y. Peng, and P. L. So, "Coordinated control of distributed energy-storage systems for voltage regulation in distribution networks," *IEEE Transactions on Power Delivery*, vol. 31, no. 3, pp. 1132–1141, 2016, ISSN: 1937-4208. DOI: 10.1109/TPWRD.2015.2462723.
- [13] K. E. Antoniadou-Plytaria, I. N. Kouveliotis-Lysikatos, P. S. Georgilakis, and N. D. Hatziaargyriou, "Distributed and decentralized voltage control of smart distribution networks: Models, methods, and future research," *IEEE Transactions on Smart Grid*, vol. 8, no. 6, pp. 2999–3008, Nov. 2017, ISSN: 1949-3061. DOI: 10.1109/TSG.2017.2679238.
- [14] M. Zeraati, M. E. Hamedani Golshan, and J. M. Guerrero, "Distributed control of battery energy storage systems for voltage regulation in distribution networks with high pv penetration," *IEEE Transactions on Smart Grid*, vol. 9, no. 4, pp. 3582–3593, 2018. DOI: 10.1109/TSG.2016.2636217.

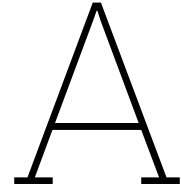
- [15] W. Kang, M. Chen, Y. Guan, B. Wei, J. C. Vasquez Q., and J. M. Guerrero, "Event-triggered distributed voltage regulation by heterogeneous bess in low-voltage distribution networks," *Applied Energy*, vol. 312, p. 118597, 2022, ISSN: 0306-2619. DOI: <https://doi.org/10.1016/j.apenergy.2022.118597>. [Online]. Available: <https://www.sciencedirect.com/science/article/pii/S0306261922000757>.
- [16] Y. Zhang, S. H. F. Huang, J. Schmall, J. Conto, J. Billo, and E. Rehman, "Evaluating system strength for large-scale wind plant integration," in *2014 IEEE PES General Meeting | Conference & Exposition*, pp. 1–5, ISBN: 1-4244-1298-6. DOI: 10.1109/PESGM.2014.6939043.
- [17] *NEN-EN 50160:2022 en, en*, Current standard. [Online]. Available: <https://www.nen.nl/en/nen-en-50160-2022-en-305139> (visited on 07/06/2023).
- [18] ANSI, *American national standard for electric power systems and equipment— voltage ratings (60 hertz)*, Standard, 2020.
- [19] K. Suresh and P. Kanakasabapathy, "A review of voltage stability issues in distribution system influenced by high pv penetration and its mitigation techniques," *International Journal of Renewable Energy Research*, vol. 13, no. 1, pp. 236–244, 2023, Export Date: 23 June 2023; Cited By: 0. DOI: 10.20508/ijrer.v13i1.13388.g8678. [Online]. Available: <https://www.scopus.com/inward/record.uri?eid=2-s2.0-85151525762&doi=10.20508%2fijrer.v13i1.13388.g8678&partnerID=40&md5=7e5c15b433ee60fae339b869ffa92079>.
- [20] H. A. Khan and M. Rihan, "Voltage regulation challenges in highly solar pv penetrated distribution networks," in *2022 1st International Conference on Sustainable Technology for Power and Energy Systems, STPES 2022*, Export Date: 23 June 2023; Cited By: 0. DOI: 10.1109/STPES54845.2022.10006622. [Online]. Available: <https://www.scopus.com/inward/record.uri?eid=2-s2.0-85147258579&doi=10.1109%2fSTPES54845.2022.10006622&partnerID=40&md5=e8b90916e65221b104cff93d2301ea66>.
- [21] W. Commons, *File:tap changing switch.gif — wikimedia commons, the free media repository*, [Online; accessed 24-June-2023], 2021. [Online]. Available: [%5Curl%7Bhttps://commons.wikimedia.org/w/index.php?title=File:Tap_changing_switch.gif&oldid=567143969%7D](https://commons.wikimedia.org/w/index.php?title=File:Tap_changing_switch.gif&oldid=567143969%7D).
- [22] L. F. Costa, G. D. Carne, G. Buticchi, and M. Liserre, "The smart transformer: A solid-state transformer tailored to provide ancillary services to the distribution grid," *IEEE Power Electronics Magazine*, vol. 4, no. 2, pp. 56–67, 2017, ISSN: 2329-9215. DOI: 10.1109/MPPEL.2017.2692381.
- [23] J. E. Huber and J. W. Kolar, "Solid-state transformers: On the origins and evolution of key concepts," *IEEE Industrial Electronics Magazine*, vol. 10, no. 3, pp. 19–28, 2016, ISSN: 1941-0115. DOI: 10.1109/MIE.2016.2588878.
- [24] C. Battistelli and A. Monti, "Chapter 5 - dynamics of modern power systems," in *Converter-Based Dynamics and Control of Modern Power Systems*, A. Monti, F. Milano, E. Bompard, and X. Guillaud, Eds. Academic Press, 2021, pp. 91–124, ISBN: 978-0-12-818491-2. DOI: <https://doi.org/10.1016/B978-0-12-818491-2.00005-5>. [Online]. Available: <https://www.sciencedirect.com/science/article/pii/B9780128184912000055>.
- [25] H. Shadfar, M. Ghorbani Pashakolaei, and A. Akbari Foroud, "Solid-state transformers: An overview of the concept, topology, and its applications in the smart grid," *International Transactions on Electrical Energy Systems*, vol. 31, no. 9, e12996, 2021, ISSN: 2050-7038. DOI: <https://doi.org/10.1002/2050-7038.12996>. [Online]. Available: <https://onlinelibrary.wiley.com/doi/abs/10.1002/2050-7038.12996>.
- [26] K. Gholami, M. R. Islam, M. M. Rahman, A. Azizivahed, and A. Fekih, "State-of-the-art technologies for volt-var control to support the penetration of renewable energy into the smart distribution grids," *Energy Reports*, vol. 8, pp. 8630–8651, 2022, ISSN: 2352-4847. DOI: <https://doi.org/10.1016/j.egy.2022.06.080>. [Online]. Available: <https://www.sciencedirect.com/science/article/pii/S2352484722012161>.
- [27] S. S. Alkaabi, H. H. Zeineldin, and V. Khadkikar, "Short-term reactive power planning to minimize cost of energy losses considering pv systems," *IEEE Transactions on Smart Grid*, vol. 10, no. 3, pp. 2923–2935, 2019, ISSN: 1949-3061. DOI: 10.1109/TSG.2018.2815434.

- [28] R. Luthander, D. Lingfors, and J. Widén, “Large-scale integration of photovoltaic power in a distribution grid using power curtailment and energy storage,” *Solar Energy*, vol. 155, pp. 1319–1325, 2017, ISSN: 0038-092X. DOI: <https://doi.org/10.1016/j.solener.2017.07.083>. [Online]. Available: <https://www.sciencedirect.com/science/article/pii/S0038092X17306680>.
- [29] S. Ghosh, S. Rahman, and M. Pipattanasomporn, “Distribution voltage regulation through active power curtailment with pv inverters and solar generation forecasts,” *IEEE Transactions on Sustainable Energy*, vol. 8, no. 1, pp. 13–22, 2017, ISSN: 1949-3037. DOI: 10.1109/TSTE.2016.2577559.
- [30] R. Tonkoski and L. A. C. Lopes, “Voltage regulation in radial distribution feeders with high penetration of photovoltaic,” in *2008 IEEE Energy 2030 Conference*, pp. 1–7. DOI: 10.1109/ENERGY.2008.4781021.
- [31] *A behind the scenes take on lithium-ion battery prices*, Blog, Mar. 2019. [Online]. Available: <https://about.bnef.com/blog/behind-scenes-take-lithium-ion-battery-prices/>.
- [32] M.-A. Hamidan and F. Borousan, “Optimal planning of distributed generation and battery energy storage systems simultaneously in distribution networks for loss reduction and reliability improvement,” *Journal of Energy Storage*, vol. 46, p. 103844, 2022, ISSN: 2352-152X. DOI: <https://doi.org/10.1016/j.est.2021.103844>. [Online]. Available: <https://www.sciencedirect.com/science/article/pii/S2352152X21015139>.
- [33] M. Stecca, L. R. Elizondo, T. B. Soeiro, P. Bauer, and P. Palensky, “A comprehensive review of the integration of battery energy storage systems into distribution networks,” *IEEE Open Journal of the Industrial Electronics Society*, vol. 1, pp. 46–65, 2020, ISSN: 2644-1284. DOI: 10.1109/OJIES.2020.2981832.
- [34] A. Alzahrani, H. Alharthi, and M. Khalid, “Minimization of power losses through optimal battery placement in a distributed network with high penetration of photovoltaics,” *Energies*, vol. 13, no. 1, p. 140, 2020, ISSN: 1996-1073. [Online]. Available: <https://www.mdpi.com/1996-1073/13/1/140>.
- [35] O. B. Adewumi, G. Fotis, V. Vita, D. Nankoo, and L. Ekonomou, “The impact of distributed energy storage on distribution and transmission networks’ power quality,” *Applied Sciences*, vol. 12, no. 13, p. 6466, 2022, ISSN: 2076-3417. [Online]. Available: <https://www.mdpi.com/2076-3417/12/13/6466>.
- [36] S. Hashemi and J. Østergaard, “Efficient control of energy storage for increasing the pv hosting capacity of lv grids,” *IEEE Transactions on Smart Grid*, vol. 9, no. 3, pp. 2295–2303, 2018, ISSN: 1949-3061. DOI: 10.1109/TSG.2016.2609892.
- [37] S. Barcellona, D. De Simone, and L. Piegari, “Simple control strategy for a pv-battery system,” *The Journal of Engineering*, vol. 2019, no. 18, pp. 4809–4812, 2019, ISSN: 2051-3305. DOI: <https://doi.org/10.1049/joe.2018.9269>. [Online]. Available: <https://ietresearch.onlinelibrary.wiley.com/doi/abs/10.1049/joe.2018.9269>.
- [38] F. Marra, G. Yang, C. Træholt, J. Østergaard, and E. Larsen, “A decentralized storage strategy for residential feeders with photovoltaics,” *IEEE Transactions on Smart Grid*, vol. 5, no. 2, pp. 974–981, 2014, ISSN: 1949-3061. DOI: 10.1109/TSG.2013.2281175.
- [39] A. T. Procopiou, K. Petrou, L. F. Ochoa, T. Langstaff, and J. Theunissen, “Adaptive decentralized control of residential storage in pv-rich mv–lv networks,” *IEEE Transactions on Power Systems*, vol. 34, no. 3, pp. 2378–2389, 2019. DOI: 10.1109/TPWRS.2018.2889843.
- [40] L. Wang, D. H. Liang, A. F. Crossland, P. C. Taylor, D. Jones, and N. S. Wade, “Coordination of multiple energy storage units in a low-voltage distribution network,” *IEEE Transactions on Smart Grid*, vol. 6, no. 6, pp. 2906–2918, 2015, ISSN: 1949-3061. DOI: 10.1109/TSG.2015.2452579.
- [41] T. Tewari, A. Mohapatra, and S. Anand, “Coordinated control of oltc and energy storage for voltage regulation in distribution network with high pv penetration,” *IEEE Transactions on Sustainable Energy*, vol. 12, no. 1, pp. 262–272, 2021, ISSN: 1949-3037. DOI: 10.1109/TSTE.2020.2991017.
- [42] Z. Zhang, C. Dou, D. Yue, Y. Zhang, B. Zhang, and Z. Zhang, “Event-triggered hybrid voltage regulation with required bess sizing in high-pv-penetration networks,” *IEEE Transactions on Smart Grid*, vol. 13, no. 4, pp. 2614–2626, 2022, ISSN: 1949-3061. DOI: 10.1109/TSG.2022.3168440.

- [43] L. Xing, Y. Mishra, Y. C. Tian, *et al.*, “Distributed voltage regulation for low-voltage and high-pv-penetration networks with battery energy storage systems subject to communication delay,” *IEEE Transactions on Control Systems Technology*, vol. 30, no. 1, pp. 426–433, 2022, ISSN: 1558-0865. DOI: 10.1109/TCST.2021.3061651.
- [44] M. M. Kabir and D. E. Demirocak, “Degradation mechanisms in li-ion batteries: A state-of-the-art review: Degradation mechanisms in li-ion batteries: A state-of-the-art review,” en, *International Journal of Energy Research*, vol. 41, no. 14, pp. 1963–1986, Nov. 2017, ISSN: 0363907X. DOI: 10.1002/er.3762. [Online]. Available: <https://onlinelibrary.wiley.com/doi/10.1002/er.3762>.
- [45] D. Chen, “Microscopic investigations of degradation in lithium-ion batteries,” Thesis, 2012.
- [46] C. Zhong, Y. Deng, W. Hu, *et al.*, *Electrolytes for electrochemical supercapacitors*. CRC press, 2016.
- [47] P. Arora and Z. J. Zhang, “Battery separators,” *Chem Rev*, vol. 104, no. 10, pp. 4419–62, 2004, Arora, Pankaj Zhang, Zhengming John Journal Article United States 2005/01/27 Chem Rev. 2004 Oct;104(10):4419-62. doi: 10.1021/cr020738u., ISSN: 0009-2665 (Print) 0009-2665. DOI: 10.1021/cr020738u.
- [48] W. Vermeer, G. R. C. Mouli, and P. Bauer, “A comprehensive review on the characteristics and modeling of lithium-ion battery aging,” *IEEE Transactions on Transportation Electrification*, vol. 8, no. 2, pp. 2205–2232, 2022, ISSN: 2332-7782. DOI: 10.1109/TTE.2021.3138357.
- [49] P. M. Attia, S. Das, S. J. Harris, M. Z. Bazant, and W. C. Chueh, “Electrochemical kinetics of sei growth on carbon black: Part i. experiments,” *Journal of The Electrochemical Society*, vol. 166, no. 4, E97, 2019, ISSN: 1945-7111. DOI: 10.1149/2.0231904jes. [Online]. Available: <https://dx.doi.org/10.1149/2.0231904jes>.
- [50] S. E. J. O’Kane, W. Ai, G. Madabattula, *et al.*, “Lithium-ion battery degradation: How to model it,” *Physical Chemistry Chemical Physics*, vol. 24, no. 13, pp. 7909–7922, 2022, ISSN: 1463-9076. DOI: 10.1039/D2CP00417H. [Online]. Available: <http://dx.doi.org/10.1039/D2CP00417H>.
- [51] T. Waldmann, B.-I. Hogg, and M. Wohlfahrt-Mehrens, “Li plating as unwanted side reaction in commercial li-ion cells – a review,” *Journal of Power Sources*, vol. 384, pp. 107–124, 2018, ISSN: 0378-7753. DOI: <https://doi.org/10.1016/j.jpowsour.2018.02.063>. [Online]. Available: <https://www.sciencedirect.com/science/article/pii/S0378775318301848>.
- [52] J. Christensen and J. Newman, “Cyclable lithium and capacity loss in li-ion cells,” *Journal of The Electrochemical Society*, vol. 152, no. 4, A818, 2005, ISSN: 1945-7111 0013-4651. DOI: 10.1149/1.1870752. [Online]. Available: <https://dx.doi.org/10.1149/1.1870752>.
- [53] U. Janakiraman, T. R. Garrick, and M. E. Fortier, “Review—lithium plating detection methods in li-ion batteries,” *Journal of The Electrochemical Society*, vol. 167, no. 16, p. 160552, 2020, ISSN: 1945-7111 0013-4651. DOI: 10.1149/1945-7111/abd3b8. [Online]. Available: <https://dx.doi.org/10.1149/1945-7111/abd3b8>.
- [54] Q. Liu, C. Du, B. Shen, *et al.*, “Understanding undesirable anode lithium plating issues in lithium-ion batteries,” *RSC Advances*, vol. 6, no. 91, pp. 88683–88700, 2016. DOI: 10.1039/C6RA19482F. [Online]. Available: <http://dx.doi.org/10.1039/C6RA19482F>.
- [55] J. Li, K. Adewuyi, N. Lotfi, R. G. Landers, and J. Park, “A single particle model with chemical/mechanical degradation physics for lithium ion battery state of health (soh) estimation,” *Applied Energy*, vol. 212, pp. 1178–1190, 2018, ISSN: 0306-2619. DOI: <https://doi.org/10.1016/j.apenergy.2018.01.011>. [Online]. Available: <https://www.sciencedirect.com/science/article/pii/S0306261918300114>.
- [56] R. Xu, Y. Yang, F. Yin, *et al.*, “Heterogeneous damage in li-ion batteries: Experimental analysis and theoretical modeling,” *Journal of the Mechanics and Physics of Solids*, vol. 129, pp. 160–183, 2019, ISSN: 0022-5096. DOI: <https://doi.org/10.1016/j.jmps.2019.05.003>. [Online]. Available: <https://www.sciencedirect.com/science/article/pii/S0022509619303126>.
- [57] C. Delacourt and M. Safari, “Life simulation of a graphite/lifepo4 cell under cycling and storage,” *Journal of The Electrochemical Society*, vol. 159, no. 8, A1283, 2012, ISSN: 1945-7111 0013-4651. DOI: 10.1149/2.049208jes. [Online]. Available: <https://dx.doi.org/10.1149/2.049208jes>.

- [58] I. Laresgoiti, S. Käbitz, M. Ecker, and D. U. Sauer, "Modeling mechanical degradation in lithium ion batteries during cycling: Solid electrolyte interphase fracture," *Journal of Power Sources*, vol. 300, pp. 112–122, 2015, ISSN: 0378-7753. DOI: <https://doi.org/10.1016/j.jpowsour.2015.09.033>. [Online]. Available: <https://www.sciencedirect.com/science/article/pii/S0378775315302949>.
- [59] J. Christensen and J. Newman, "Stress generation and fracture in lithium insertion materials," *Journal of Solid State Electrochemistry*, vol. 10, no. 5, pp. 293–319, 2006, ISSN: 1433-0768. DOI: 10.1007/s10008-006-0095-1. [Online]. Available: <https://doi.org/10.1007/s10008-006-0095-1>.
- [60] J. S. Edge, S. O'Kane, R. Prosser, *et al.*, "Lithium ion battery degradation: What you need to know," *en, Physical Chemistry Chemical Physics*, vol. 23, no. 14, pp. 8200–8221, 2021, ISSN: 1463-9076, 1463-9084. DOI: 10.1039/D1CP00359C. [Online]. Available: <http://xlink.rsc.org/?DOI=D1CP00359C>.
- [61] K. Liu, T. R. Ashwin, X. Hu, M. Lucu, and W. D. Widanage, "An evaluation study of different modelling techniques for calendar ageing prediction of lithium-ion batteries," *Renewable and Sustainable Energy Reviews*, vol. 131, p. 110017, 2020, ISSN: 1364-0321. DOI: <https://doi.org/10.1016/j.rser.2020.110017>. [Online]. Available: <https://www.sciencedirect.com/science/article/pii/S1364032120303087>.
- [62] Y. Wang, J. Tian, Z. Sun, *et al.*, "A comprehensive review of battery modeling and state estimation approaches for advanced battery management systems," *Renewable and Sustainable Energy Reviews*, vol. 131, p. 110015, 2020, ISSN: 1364-0321. DOI: <https://doi.org/10.1016/j.rser.2020.110015>. [Online]. Available: <https://www.sciencedirect.com/science/article/pii/S1364032120303063>.
- [63] S. Nejad, D. T. Gladwin, and D. A. Stone, "A systematic review of lumped-parameter equivalent circuit models for real-time estimation of lithium-ion battery states," *Journal of Power Sources*, vol. 316, pp. 183–196, 2016, ISSN: 0378-7753. DOI: <https://doi.org/10.1016/j.jpowsour.2016.03.042>. [Online]. Available: <https://www.sciencedirect.com/science/article/pii/S0378775316302427>.
- [64] M.-K. Tran, M. Mathew, S. Janhunen, *et al.*, "A comprehensive equivalent circuit model for lithium-ion batteries, incorporating the effects of state of health, state of charge, and temperature on model parameters," *Journal of Energy Storage*, vol. 43, p. 103252, 2021, ISSN: 2352-152X. DOI: <https://doi.org/10.1016/j.est.2021.103252>. [Online]. Available: <https://www.sciencedirect.com/science/article/pii/S2352152X2100949X>.
- [65] Z. Wang, J. Ma, and L. Zhang, "State-of-health estimation for lithium-ion batteries based on the multi-island genetic algorithm and the gaussian process regression," *IEEE Access*, vol. 5, pp. 21286–21295, 2017, ISSN: 2169-3536. DOI: 10.1109/ACCESS.2017.2759094.
- [66] M. Bercibar, F. Devriendt, M. Dubarry, *et al.*, "Online state of health estimation on nmc cells based on predictive analytics," *Journal of Power Sources*, vol. 320, pp. 239–250, 2016, ISSN: 0378-7753. DOI: <https://doi.org/10.1016/j.jpowsour.2016.04.109>. [Online]. Available: <https://www.sciencedirect.com/science/article/pii/S0378775316304827>.
- [67] A. Barré, B. Deguilhem, S. Grolleau, M. Gérard, F. Suard, and D. Riu, "A review on lithium-ion battery ageing mechanisms and estimations for automotive applications," *Journal of Power Sources*, vol. 241, pp. 680–689, 2013, ISSN: 0378-7753. DOI: <https://doi.org/10.1016/j.jpowsour.2013.05.040>. [Online]. Available: <https://www.sciencedirect.com/science/article/pii/S0378775313008185>.
- [68] Y. Li, K. Liu, A. M. Foley, *et al.*, "Data-driven health estimation and lifetime prediction of lithium-ion batteries: A review," *Renewable and Sustainable Energy Reviews*, vol. 113, p. 109254, 2019, ISSN: 1364-0321. DOI: <https://doi.org/10.1016/j.rser.2019.109254>. [Online]. Available: <https://www.sciencedirect.com/science/article/pii/S136403211930454X>.
- [69] J. Xing, A. P. Vora, V. Hoshing, *et al.*, "Comparison of li-ion battery degradation models for system design and control algorithm development," in *2017 American Control Conference (ACC)*, pp. 74–79, ISBN: 978-1-5090-5992-8. DOI: 10.23919/ACC.2017.7962933.

- [70] S. N. Motapon, E. Lachance, L. A. Dessaint, and K. Al-Haddad, "A generic cycle life model for lithium-ion batteries based on fatigue theory and equivalent cycle counting," *IEEE Open Journal of the Industrial Electronics Society*, vol. 1, pp. 207–217, 2020, ISSN: 2644-1284. DOI: 10.1109/OJIES.2020.3015396.
- [71] A. Amirkhani and A. H. Barshooi, "Consensus in multi-agent systems: A review," *Artificial Intelligence Review*, vol. 55, no. 5, pp. 3897–3935, 2022, ISSN: 1573-7462. DOI: 10.1007/s10462-021-10097-x. [Online]. Available: <https://doi.org/10.1007/s10462-021-10097-x>.
- [72] R. Olfati-Saber, J. A. Fax, and R. M. Murray, "Consensus and cooperation in networked multi-agent systems," *Proceedings of the IEEE*, vol. 95, no. 1, pp. 215–233, 2007, ISSN: 1558-2256. DOI: 10.1109/JPROC.2006.887293.
- [73] M. Wajahat, H. A. Khalid, G. M. Bhutto, and C. Leth Bak, "A comparative study into enhancing the pv penetration limit of a lv cigre residential network with distributed grid-tied single-phase pv systems," *Energies*, vol. 12, no. 15, p. 2964, 2019, ISSN: 1996-1073. [Online]. Available: <https://www.mdpi.com/1996-1073/12/15/2964>.
- [74] J. Alpízar-Castillo, *Probabilistic load profile generator*, https://github.com/jjac13/Probabilistic_Load_Profile_Generator, Accessed on 2023-06-26, 2022.
- [75] F. Angizeh, *Dataset on hourly load profiles for a set of 24 facilities from industrial, commercial, and residential end-use sectors*, Dataset, 2020. DOI: 10.17632/RFNP2D3KJP.1. [Online]. Available: <http://dx.doi.org/10.17632/RFNP2D3KJP.1>.
- [76] M. Schlemminger, T. Ohrdes, E. Schneider, and M. Knoop, "Dataset on electrical single-family house and heat pump load profiles in germany," *Scientific Data*, vol. 9, no. 1, p. 56, 2022, ISSN: 2052-4463. DOI: 10.1038/s41597-022-01156-1. [Online]. Available: <https://doi.org/10.1038/s41597-022-01156-1>.
- [77] Joint Research Centre (JRC) of the European Commission, *EU PVGIS - Photovoltaic Geographical Information System*, <https://ec.europa.eu/jrc/en/pvgis>, Accessed on November 2022.
- [78] MathWorks. "MATLAB Documentation: makima," MathWorks. (Sep. 2021), [Online]. Available: <https://nl.mathworks.com/help/matlab/ref/makima.html> (visited on 07/14/2023).
- [79] J. LeSage. "Systems-level microgrid simulation from simple one-line diagram," MATLAB Central File Exchange. (2023), [Online]. Available: <https://www.mathworks.com/matlabcentral/fileexchange/67060-systems-level-microgrid-simulation-from-simple-one-line-diagram> (visited on 07/14/2023).
- [80] P. Keil, S. F. Schuster, J. Wilhelm, *et al.*, "Calendar aging of lithium-ion batteries," *Journal of The Electrochemical Society*, vol. 163, no. 9, A1872, 2016, ISSN: 1945-7111. DOI: 10.1149/2.0411609jes. [Online]. Available: <https://dx.doi.org/10.1149/2.0411609jes>.
- [81] H. Ali, H. Beltran, N. J. Lindsey, and M. Pecht, "Assessment of the calendar aging of lithium-ion batteries for a long-term—space missions," *Frontiers in Energy Research*, vol. 11, 2023, ISSN: 2296-598X. DOI: 10.3389/fenrg.2023.1108269. [Online]. Available: <https://www.frontiersin.org/articles/10.3389/fenrg.2023.1108269>.
- [82] M. Naumann, M. Schimpe, P. Keil, H. C. Hesse, and A. Jossen, "Analysis and modeling of calendar aging of a commercial lifepo4/graphite cell," *Journal of Energy Storage*, vol. 17, pp. 153–169, 2018, ISSN: 2352-152X. DOI: <https://doi.org/10.1016/j.est.2018.01.019>. [Online]. Available: <https://www.sciencedirect.com/science/article/pii/S2352152X18300665>.



Utilization Factor Calculation

In this appendix, the Simulink representations of the proposed control strategy are illustrated. As indicated in Chapter 3, the control is divided into local control, consensus control, and SOC control. An overview of the proposed control is depicted in Figure A.1 while detailed views of each control part are presented in Figure A.2 and A.3. In addition to the block diagrams, the source code to represent the consensus algorithm is listed in Listing A.1

Listing A.1: Consensus Algorithm Source code

```
1 % Consensus Algorithm
2 % This code takes in the local utilization factors u15,u11,u16,u17,u18
3 % and calculates the average of the factors.
4 % The parameter maxiter indicates the number of iterations allowed before proceeding into the
   next simulation step in the quasi-static load flow simulation.
5 % Epsilon indicates the step size when calculating the consensus value
6
7 function [ucon15, ucon11, ucon16, ucon17, ucon18] = fcn(u15,u11,u16,u17,u18,maxiter,epsilon)
8
9 for iter = 1:maxiter %maxiter indicates the number of iterations allowed in a sample
10
11 temp15 = u15 + epsilon*((u11-u15)); %u15 is neighbor u11
12 temp11 = u11 + epsilon*((u15-u11)+(u16-u11)); %u11 is neighbor to u15 and u16
13 temp16 = u16 + epsilon*((u11-u16)+(u17-u16)); %u16 is neighbor to u11 and u17
14 temp17 = u17 + epsilon*((u16-u17)+(u18-u17)); %u17 is neighbor to u16 and u18
15 temp18 = u18 + epsilon*((u17-u18)); %u18 is only neighbor to u17
16
17
18 u15 = temp15;
19 u11 = temp11;
20 u16 = temp16;
21 u17 = temp17;
22 u18 = temp18;
23
24 end
25 ucon15 = u15;
26 ucon11 = u11;
27 ucon16 = u16;
28 ucon17 = u17;
29 ucon18 = u18;
```

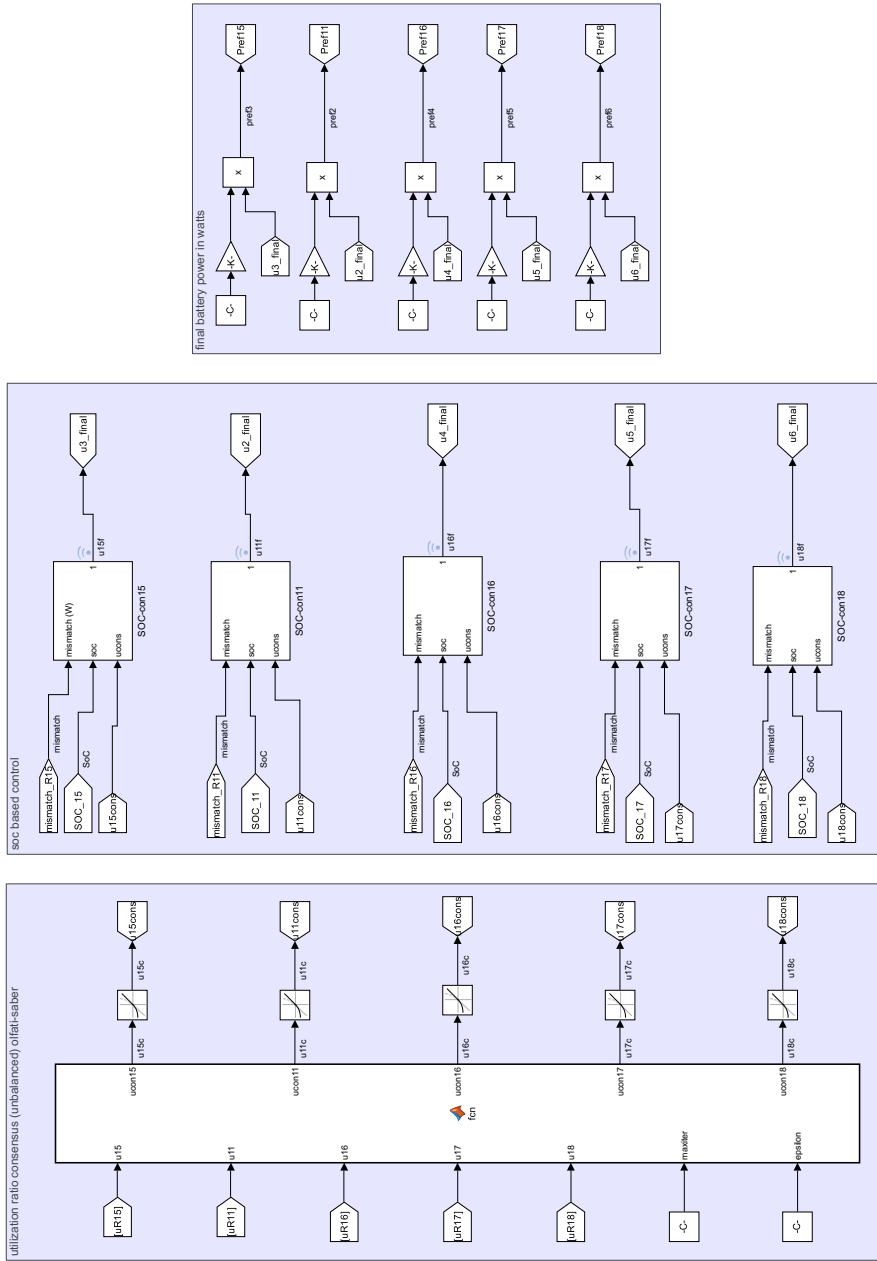


Figure A.1: Overview of the distributed control in Simulink.

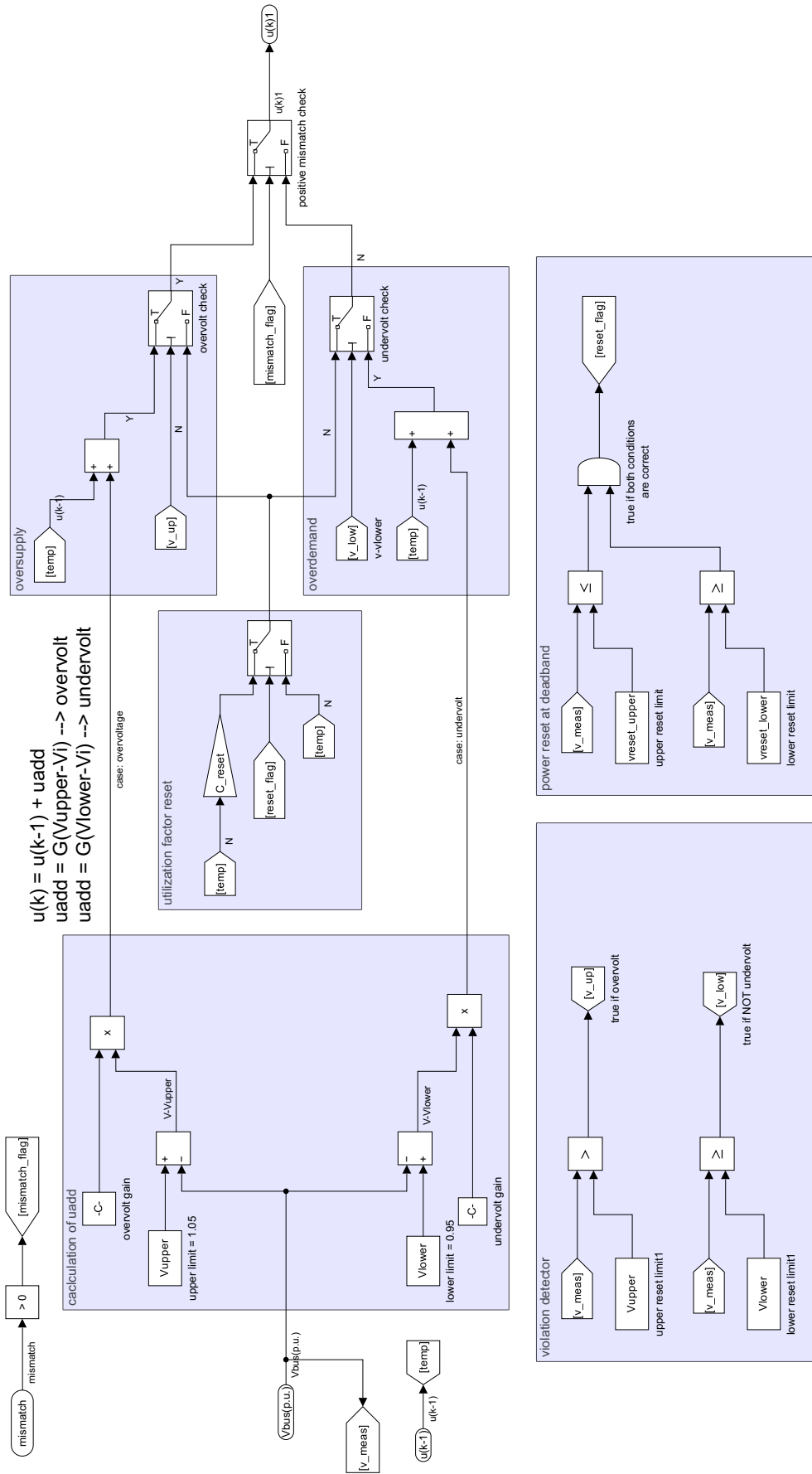


Figure A.2: Simulink block diagram of the local utilization factor computation.

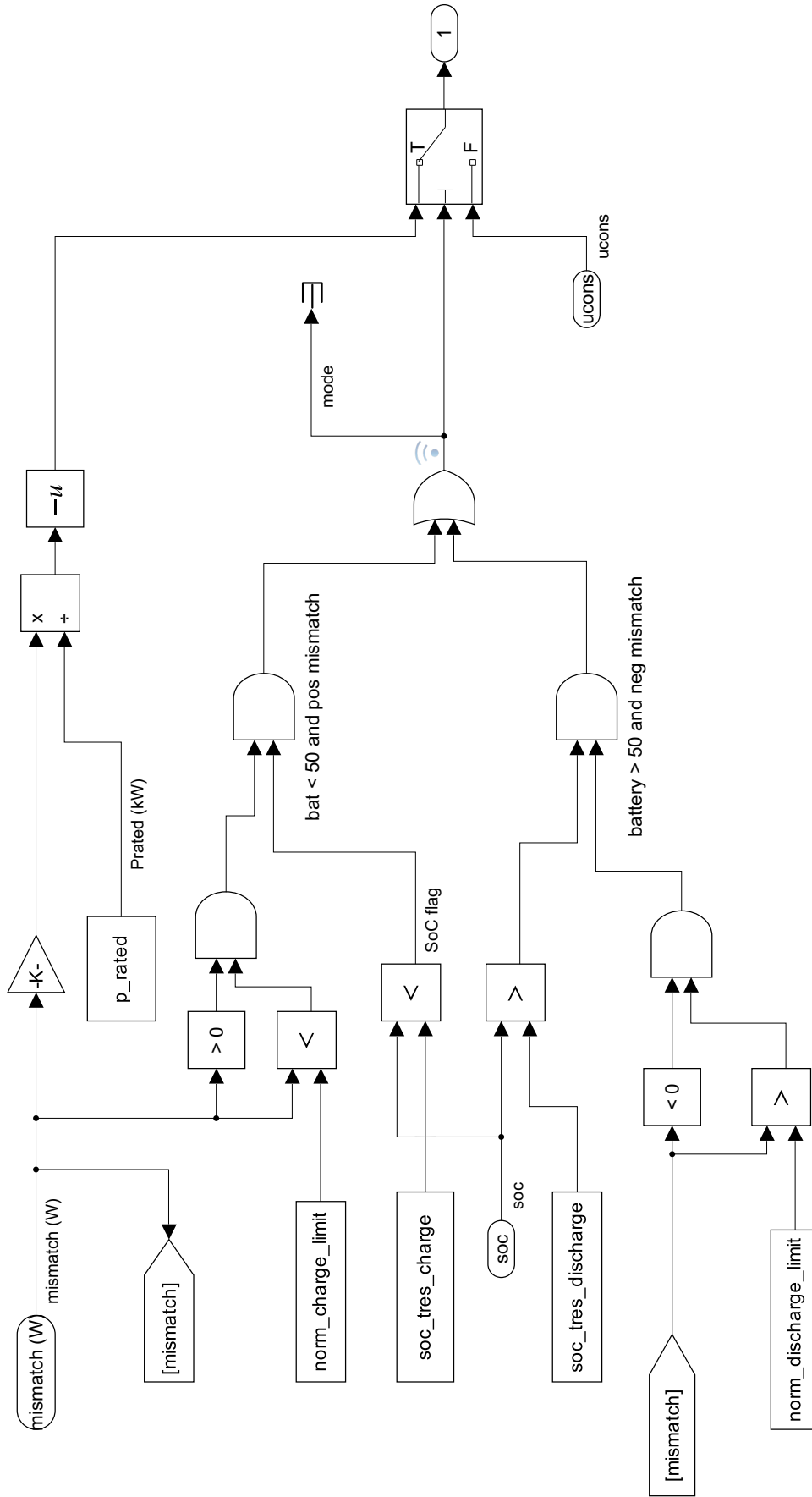


Figure A.3: Simulink block diagram of the final utilization factor computation inside the SOC controller.

B

Simulation Parameters

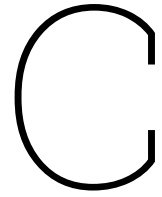
This appendix presents the parameters used when setting up the simulation presented in 4. Parameters for the MV/LV transformer and the network lines are presented in Table B.1, and B.2, respectively.

Table B.1: Transformer specification of the modified CIGRE LV test feeder.

Specification	Value
MV Voltage	20 kV
Short-Circuit Level	100 MVA
X/R	1
MV/LV Transformer rating	500 kVA
Primary Voltage	20 kV
Secondary Voltage	0.4 kV
R _r	0.01 p.u.
X _r	0.04 p.u.

Table B.2: Line parameter of the modified CIGRE LV Network.

Line Name	From Bus	To Bus	Length (km)	R(Ω /km)	X(Ω /km)
Line R1-R2	1	2			
Line R2-R3	2	3			
Line R3-R4	3	4			
Line R4-R5	4	5			
Line R5-R6	5	6		0.549	0.0832
Line R6-R7	6	7			
Line R7-R8	7	8			
Line R8-R9	8	9			
Line R9-R10	9	10	0.08		
Line R3-R11	3	11			
Line R4-R12	4	12			
Line R12-R13	12	13			
Line R13-R14	13	14			
Line R14-R15	14	15		0.822	0.0847
Line R6-R16	6	16			
Line R9-R17	9	17			
Line R10-R18	10	18			



Cell Specification

The battery cell used in this work is presented in detail in this appendix. The cell has a wide range of use from grid applications to transportation solutions. The following datasheet is given by the cell manufacturer.

+ Nanophosphate[®] High Power Lithium Ion Cell

ANR26650*m1-B*



A123's high-performance Nanophosphate[®] lithium iron phosphate (LiFePO₄) battery technology delivers high power and energy density combined with excellent safety performance and extensive life cycling in a lighter weight, more compact package. Our cells have low capacity loss and impedance growth over time as well as high usable energy over a wide state of charge (SOC) range, allowing our systems to meet end-of-life power and energy requirements with minimal pack oversizing.



APPLICATIONS

COMMERCIAL SOLUTIONS

Advanced lead acid replacement batteries for:

- + Datacenter UPS
- + Telecom backup
- + IT backup
- + Autonomously guided vehicles (AGVs)
- + Industrial robotics and material handling equipment
- + Medical devices

GOVERNMENT SOLUTIONS

- + Military vehicles
- + Military power grids
- + Soldier power
- + Directed energy

GRID SOLUTIONS

Versatile, flexible and proven storage solutions for the grid:

- + Frequency regulation
- + Renewables integration
- + Reserve capacity
- + Transmission and distribution

TRANSPORTATION SOLUTIONS

Hybrid, plug-in hybrid and electric vehicle battery systems for:

- + Commercial vehicles
- + Off-highway vehicles
- + Passenger vehicles

ANR26650*m1-B* TECHNICAL DATA

Cell Dimensions	ø26 x 65 mm
Cell Weight	76g
Cell Capacity (nominal/minimum) (0.5C Rate)	2.5/2.4 Ah
Voltage (nominal)	3.3V
Internal Impedance (1kHz AC typical)	6mΩ
Power*	2600 W/kg
Recommended Standard Charge Method	2.5A to 3.6V CCCV, 60 min
Recommended Fast Charge Method to 80% SOC	10A to 3.6V CC, 12 min
Maximum Continuous Discharge	50A
Maximum Pulse Discharge (10 seconds)	120A
Cycle Life at 20A Discharge, 100% DOD	>1,000 cycles
Operating Temperature	-30°C to 55°C
Storage Temperature	-40°C to 60°C

* ~200W as measured by A123 modified HPPC Method @ 23°C, 50% SOC, 10 second discharge